Available online at www.sciencedirect.com

ScienceDirect

journal homepage: www.elsevier.com/locate/he

Review Article

Recent advancements of layered double hydroxide heterojunction composites with engineering approach towards photocatalytic hydrogen production: A review

Areen Sherryna [a], *Muhammad Tahir* [a,b,*], *Walid Nabgan* [a]

[a] *Department of Chemical Engineering, School of Chemical and Energy Engineering, Universiti Teknologi Malaysia, 81310, UTM, Johor Bahru, Johor, Malaysia*

[b] *Chemical and Petroleum Engineering Department, UAE University, P.O. Box 15551, Al Ain, United Arab Emirates*

HIGHLIGHTS

- Current progress in LDH as prominent materials for hydrogen production has reviewed.
- Challenges of pristine LDH and modification for enhancing for H_2 yield are discoursed.
- Constructing Type I, II, III, p-n, Z, S, and R-scheme LDH heterojunction are discussed.
- Fabricating novel hybrid LDH with bandgap engineering are systematically considered.
- Approaches for tuning LDH morphology for high hydrogen efficiency are deliberated.

GRAPHICAL ABSTRACT

ARTICLE INFO

Article history:
Received 22 March 2021
Received in revised form
18 August 2021

ABSTRACT

Photocatalytic hydrogen production has been considered as one of the most promising alternatives for providing clean, sustainable, and renewable energy sources. Tremendous investigation and efforts have been devoted to increase the efficiency of the solar to energy conversion of a photocatalyst. Layered double hydroxide (LDH) received scientific attention

Abbreviations: LDH, Layered Double Hydroxide; CB, Conduction band; VB, Valence band; CBM, Conduction band minimum; VBM, Valence band maximum; UV, Ultraviolet; pDA, Polydopamine; SCA, Semiconductor A; SCB, Semiconductor B; PC I, Photocatalyst I; PC II, Photocatalyst II; NPs, Nanoparticles; IEF, Internal Electric Field; MOF, Metal Organic Framework; SPR, Surface Plasmon Resonances; LBL, Layer-by-layer; SEM, Scanning Electron Microscope; LSV, Linear Sweep Voltammetric; ESA, Electrostatic self-assembly.

* *Corresponding author*. Department of Chemical Engineering, School of Chemical and Energy Engineering, Universiti Teknologi Malaysia, 81310, UTM, Johor Bahru, Johor, Malaysia.
E-mail addresses: m.tahir@utm.my, bttahir@yahoo.com (M. Tahir).

https://doi.org/10.1016/j.ijhydene.2021.10.099

Accepted 12 October 2021
Available online 20 November 2021

Keywords:
Photocatalysis
Hydrogen generation
Layered double hydroxide
Heterojunctions
Hybrid photocatalyst

for its excellent compositional flexibility and controllable morphology, leading to the facile incorporation of the metal species into their layered structure. The unique multi-structure and the tunability of its band gap make LDH more prominent in the field of photocatalysis. This article highlights the recent developments in the fabrication of LDH-based photocatalyst nanocomposites and the engineering approaches for augmenting their photocatalytic hydrogen production efficiency. The thermodynamics and challenges in photocatalytic water splitting are deliberated to understand the pathways to construct efficient semiconductor photocatalysis system. The efficiency enhancement of LDH-based photocatalysts are comprehensively discussed by giving special attention to the heterojunction engineering of type I, type II, p-n junction, Z-scheme, S-scheme, and R-scheme. Fabrication of the hybrid LDH nanocomposites through band gap engineering and metal loading are summarised. The architectural and morphological tuning of LDH-based composite through the construction of the novel core-shell structure and layer-by-layer nanosheets are also demonstrated. Finally, the future recommendations are outlined to provide insights for their development in the photocatalysis field.

Contents

Introduction

The scarcity and the depletion of fossil fuels as the prime energy sources have become a matter of worldwide concern. It was denoted that the utilization of fossil fuel has reached 85% of the total energy demand. The high consumption of fossil fuels will negatively affect the ecological system and economic development [1–4]. The employment of hydrogen energy through photocatalytic water splitting is considered the best alternative to replace fossil fuels [5,6]. Photocatalytic water splitting by scavenging energy from the sunlight using semiconductor materials is a promising hydrogen generation method [7,8]. It has been reported that solar-based photocatalysis could mitigate and abate the long-lived well-mixed greenhouse gases and fight against global warming contributors [9].

The efficiency of photocatalysis has led to the development of various visible-light-active materials. This is because visible light makes up 43% of the total solar radiation [10]. Unfortunately, the scarcities, large band gap, high-cost, low quantum efficiency of this light-active photocatalyst such as TiO_2, CuO, ZnO, IrO_2, WO_3, and CdS limit their activity and photostability for the large-scale hydrogen production [11–14]. CdS photocatalyst has been remarked as an excellent photocatalyst for photocatalytic hydrogen production. The good photochemical properties of CdS having a

high surface crystallinity making CdS highly sought after. However, CdS heavily suffered from photo corrosion due to the oxidation of the sulfide element, limiting their capability as a single photocatalyst in photocatalytic hydrogen generation [15]. The same was reported for the widely studied photocatalyst such as TiO_2. The unique properties, abundancy, and good chemical stability of TiO_2 make it highly favourable in the photocatalysis field [16]. Despite its astounding chemical properties, it is undeniable that TiO_2 suffers from high recombination of photogenerated charges, and thus, modification have to be done on the photocatalyst to improve its efficiency under solar irradiations [17–19]. Different semiconductors exhibit different benefits and properties. For instance, CuO and ZnO are highly preferred in the photocatalysis process due to their abundancy, non-toxic and low-cost materials [20]. However, like TiO_2, they suffered from easy recombination of electron-hole, large band gap, and low light harvesting. Hence, these photocatalysts are typically coupled with other semiconductors forming a heterojunction to improve their photocatalytic efficiency and the separation of photogenerated charges [21,22].

Recently, layered double hydroxide (LDH), also known as anionic clays, garnered the researchers attention as an extensively-studied family of photocatalyst [23]. Besides having a tunable band gap, unique layered structure with high surface area, low cost, and abundant in nature, LDH also possess remarkable photocatalytic and physicochemical properties, which offers a novel route for hydrogen generation [24–28]. Fig. 1 shows the overview of LDH based photocatalysts, the challenges, and improvements made to their efficiency. Many studies have been conducted to increase the efficiency of the LDH-based photocatalyst for photocatalytic hydrogen production. This includes forming the heterojunction by coupling with other visible-light-active photocatalysts, integrating plasmonic material, and modifying the morphology of LDH and hybrid nanocomposites.

Many studies on LDH-based photocatalysts have been conducted by other research groups focusing on the preparation, properties, and their role in various technological fields. Besides, several reviewing articles have been published in the past three years to give perspectives on different aspects of LDH-based photocatalyst. In 2019, Yang et al. published a review on the recent development of LDH-based photocatalyst in photocatalytic CO_2 reduction, focusing on the synthesis and modification strategies [29]. Another review published in the same year by Daud et al. deliberates on the role of hybrid LDH and their recent advances in the photodegradation field [26], while Song et al. focus on the engineering modification of hybrid LDH, narrowing the scope on LDH/g-C_3N_4 composite in photocatalysis applications [30]. Following these contributions, Dewangan et al. reviewed the functional application of LDH for CO_2 conversion, highlighting the fundamental synthesis method and their challenges [31]. On the other hand, the development of LDH-based photocatalyst on the photocatalytic, electrocatalytic, and photoelectrocatalytic application was published by Zhao et al. in 2020 [32]. In the same year, a review on the catalytic properties of POM-intercalated LDH was published by Stamate et al. [33]. Recently, a review article by Wang et al. providing basic insights on the construction of Zn containing LDH was published by giving a fundamental understanding of the

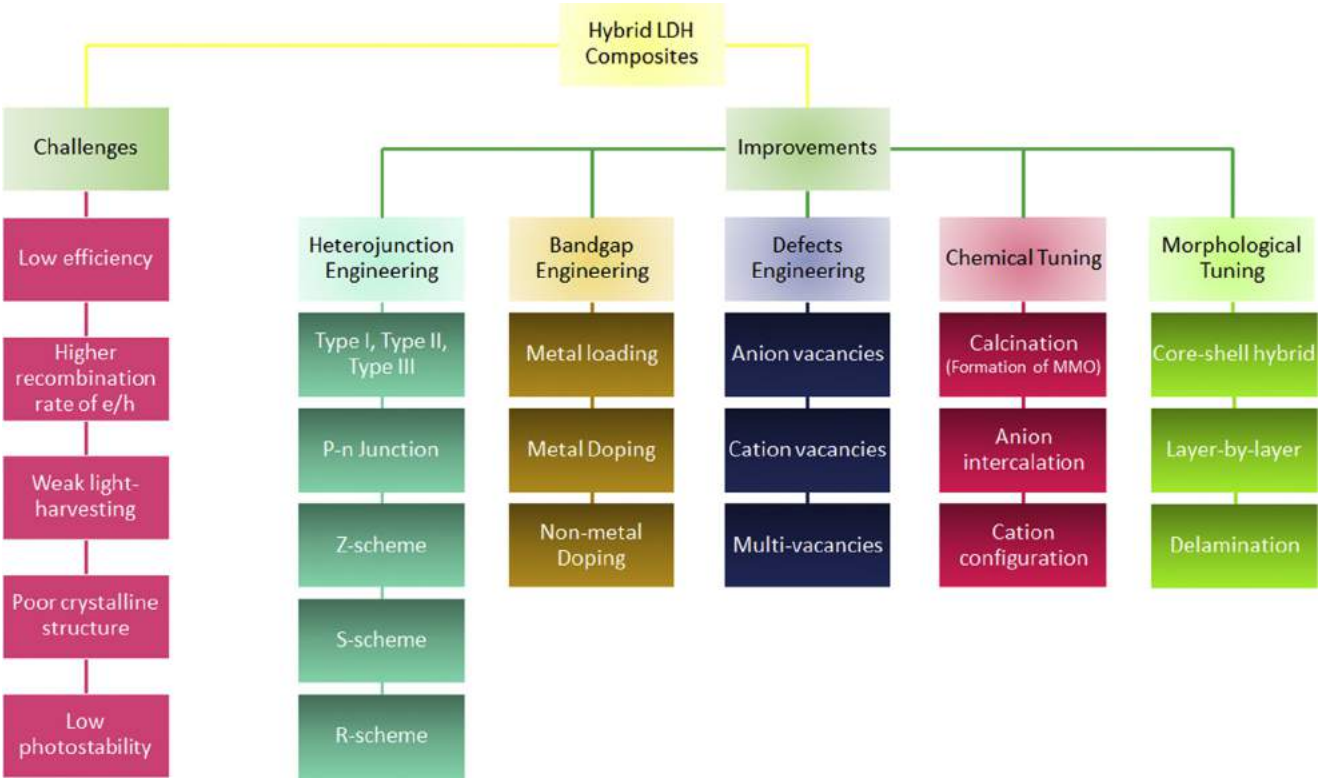

Fig. 1 – The overview of the LDH based photocatalyst, challenges and improvements made to improve its efficiency.

modification strategies in the water treatment field [34]. Additionally, the first review article discussing the engineering application of LDH in the water treatment field through an advanced oxidation process has been published by Yang et al. [35]. Nonetheless, few review articles were published for the past three years that solely focus on the LDH-based photocatalyst and their developments in photocatalytic hydrogen production. Recently, Kaur et al. have published a review detailing the progress of LDH-based photocatalyst in photocatalytic hydrogen production by focusing on the mechanistic approach.

Review studies on LDH-based photocatalyst focusing on their synthesis method and general application on water splitting have been frequently published. Therefore, this review aims to summarise the latest progress, current trends, and developments of hybrid LDH nanocomposites specifically towards hydrogen production, by providing clear explication on the behaviour of LDH in the water reduction reaction through engineering modification. Firstly, the challenges and thermodynamics of photocatalytic water splitting are deliberated. Secondly, the efficiency enhancement of the LDH photocatalyst was comprehensively discussed by giving special attention to the heterojunction engineering of type I, type II, p-n junction, Z-scheme, S-scheme, and R-scheme. Next, the modification and the fabrication of the hybrid LDH nanocomposite through band gap engineering and metal loading are summarised. Finally, architectural and morphological tuning of LDH-based composite through the construction of the novel core-shell structure and layer-by-layer nanosheets are concisely discussed. Herein, LDH composed of unique two-dimensional layered sheets as base materials for photocatalytic water splitting should be given great consideration. Distinct properties of LDH, which differentiate them from the particulate photocatalysts, rendered them a notable place in the photocatalysis field. Hence, this review aspires to give insight into the future development of hybrid LDH photocatalyst in different engineering aspects so that assiduous studies can be performed to ameliorate the role of LDH-based photocatalyst specifically in photocatalytic hydrogen production.

General overview of LDH-based photocatalyst in photocatalytic water splitting

General structure of LDH and its mechanism in water splitting

The unique architectural and morphological structure of LDH have attracted researchers to further explore the functionality and capability of these hydrotalcite-like compounds in photocatalytic water splitting [36]. LDH is a family of 2D clay materials having exceptional compositional flexibility and controllable morphology, making them one of the most promising semiconductors for the photocatalysis process [23,37,38]. LDH is composed of two layers stacking onto each other. Making up a positive layer of LDH is generally referred to as the brucite layer, while the negative layer is known as interlamellar spaces, as shown in Fig. 2. The metal cations will be incorporated into the brucite layer of LDH, while anions will be intercalated at the interlamellar or known as the interlayer of LDH [39]. The general formula for the LDH structure is denoted as in Eq. (1).

$$\left[M^{II}M^{III}{}_{X}(OH)_2\right]^{X+}\cdot\left[\left(A^{n-}{}_{x/n}\right)\cdot mH_2O\right]^{X-} \quad (1)$$

From Eq. (1), M^{II}represents the divalent metal cations having a (+2) charges, while, $M^{III}$is trivalent metal cations with (+3) charges. These metal cations usually will be bonded with

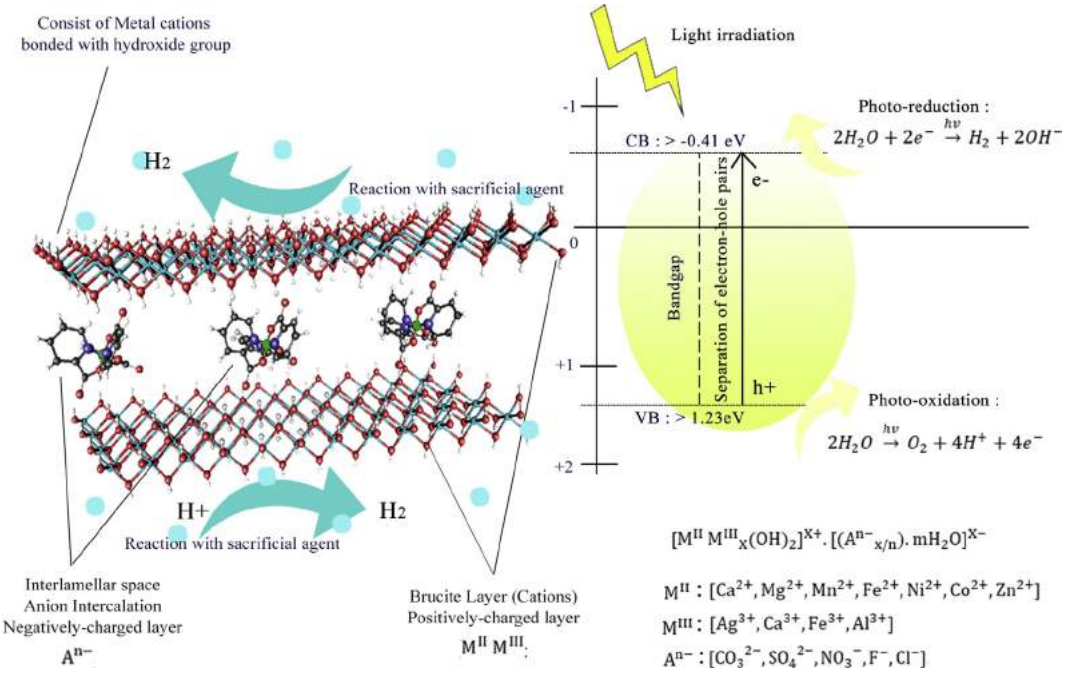

Fig. 2 – Schematic illustration of LDH structure and its mechanism towards photocatalytic hydrogen production [28].

the hydroxide group $(OH)_2$ constituting the backbone of the LDH. The exchangeable cations of M^{II} and M^{III} creates a positive residual charge of layers and usually was stabilised by the anions intercalated at the interlayer of the LDH (A^{n-}) . Hence, the balance of positively- and negatively-charged layers composed by this LDH structure neutralising the overall LDH compounds [40]. Note that LDH naturally consisted of carbonate anions presented at the interlayer gallery. However, this can be exchanged with a different type of active species such as inorganic anions [41], organic acid/base [42], and organic complexes [43]. Besides, the metal cations at the brucite layer of LDH can be tuned with different types of cations pairs. The chemical identity and type of metal cations composed by LDH will influence the optical and chemical properties of LDH. Thus, the type of metals to be incorporated into the LDH structure is significant as different pairs will give a different value of band gap, making LDH uniquely known to have a 'tunable band gap' [28]. Typically, the bonding of the metal cations to the hydroxide group of the LDH primarily are Van Der Waal's and electrostatic forces, while stabilising the structure of LDH compounds are anions at the interlayer bonded with water molecules and connecting the brucite layer through hydrogen bonding [23].

LDH in photocatalytic hydrogen production attained considerable attention due to its positive attributes in the fabrication of the visible light active photocatalyst [44]. Generally, for the LDH based-photocatalyst to be able to undergo a redox reaction in generating hydrogen, several elements needed to be considered. Fundamentally, 1) CB potential of LDH must be more negative than the reduction potential (>−0.41 eV), 2), whereas VB should be more positive than the water oxidation potential (>1.23eV) and, 3) The band gap energy of LDH must larger than the overall Gibbs free energy of water splitting [45–47]. As mentioned earlier, the type of metal cations and anions to be incorporated into LDH should be given attention and must be well considered before fabricating the bimetallic or trimetallic LDH nanocomposites. The basic photocatalytic mechanism of LDH-based photocatalyst is as follows: Under light irradiation, the electron-hole pairs will be formed at the VB of the LDH. The charge separation will occur in which the photogenerated electrons will be transited to the CB of LDH while holes remained at VB. Both the hole at the VB and electrons at CB will undergo oxidation and reduction processes, respectively. The holes will oxidise water into protons and oxygen while electrons at CB will reduce protons into hydrogen [48].

Thermodynamics of water splitting

Thermodynamically, water splitting is an endothermic reaction in which it requires the standard change in Gibbs free energy of 237 kJ/mol to convert water into hydrogen and oxygen. The energy source that meets the Gibbs free energy of the reaction is essential so that the electrons could rearrange, making the redox reaction possible. Temperature, light, band gap, CB, and VB of semiconductors are critical elements in

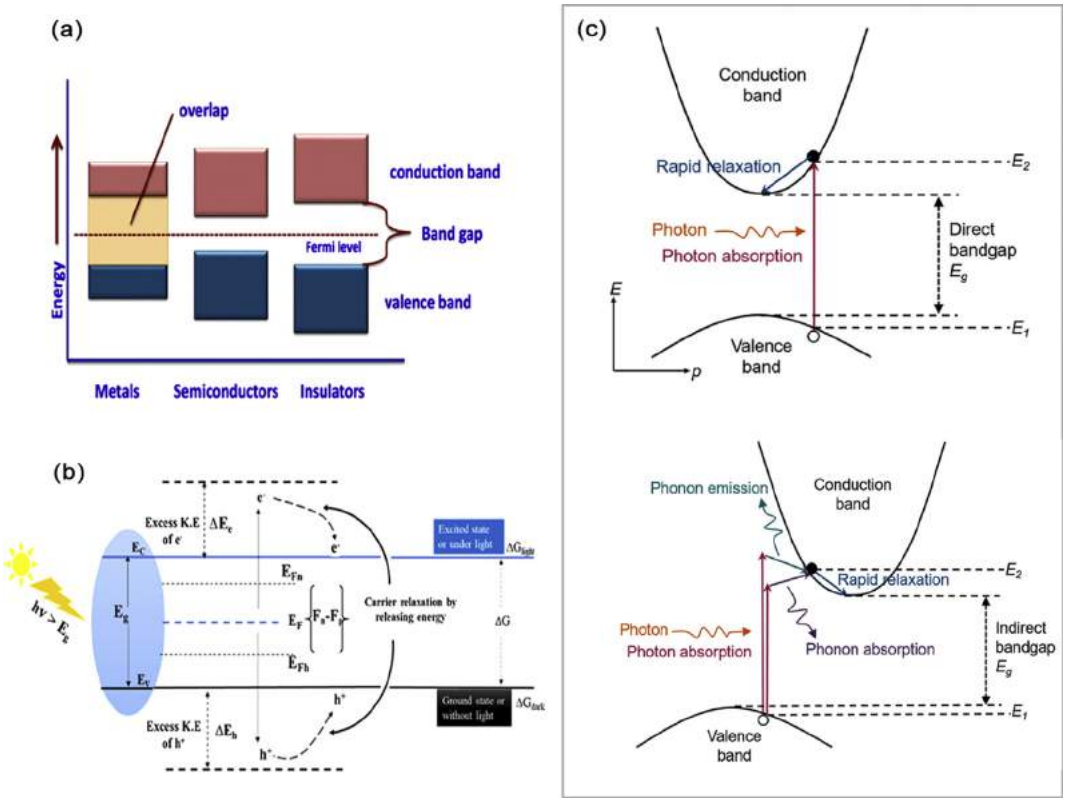

Fig. 3 – (a) Schematic illustration of the band gap, conduction band and valence band of the metals, semiconductors and insulators [54] (b) carrier relaxation under light irradiation [55], (c) Direct (above) and indirect band gap (below) of semiconductor [53].

photocatalysis thermodynamics [17]. Determining the possible photocatalyst for hydrogen generation it is crucial to understand the redox potential for both the reduction and oxidation processes. The water reduction and oxidation potentials should fall within the photocatalyst band gap. The band gap energy (Eg) is the energy level between VB and CB by which in an atom, a different group of electrons occupies the energy levels. Fig. 3 (a) illustrates the band gap energy levels and the position of CB and VB.

The potential photocatalyst should possess these elements in order to be thermodynamically stable; 1) The band gap of 1.23 eV < Eg < 3.26 eV, 2) The band position of bottom CB should be more negative than redox potential, 3) The top of VB should be more positive than the redox potential of water splitting [49]. Under standard conditions, the energy of 2.458 eV is required to generate one hydrogen molecule, while for a full reaction to happen, an energy input of 4.915 eV is required. This is because full water splitting needs four electrons to generate two hydrogen molecules [50,51]. Besides, the energy input of water splitting could be minimized by utilising solar radiation. This is due to that under solar radiation, the full reaction energy can be generated by; 1) one photon of ultraviolet light with a wavelength shorter than 252.3 nm, or 2) two photons with a wavelength shorter than 504.5 nm in the visible spectrum, or 3) four infrared photons of 1.23 eV [46].

The electrons and holes that occupy CB and VB will be disturbed once light with energy > Eg irradiates the semiconductor's surface. Here, the internal equilibrium within the energy level is achieved. The relaxation time within CB is shorter than across the band gap, as shown in Fig. 3 (b). The quasi-equilibrium is the electron's states with internal equilibrium, which means that the electrons and holes population is at equilibrium within the CB and VB energy levels. Eqs. (2) and (3) show the potential of electrons and holes in quasi-fermi levels [52].

$$Fn = Ec + kBT \ln \frac{n}{Nc} \tag{2}$$

$$Fp = Ev + kBT \ln \frac{P}{Nv} \tag{3}$$

$$\Delta G = -|Fn - Fp| = -Eg - kBT \ln \frac{np}{NvNc} \tag{4}$$

The EC and EV are CB minimum and VB maximum energy level positions, kB = Boltzmann constant, Nc and Nv are effective densities of states in CB and VB, n and p are carrier's concentration.

The band gap of semiconductors can be categorised into direct and indirect band gap. As shown in Fig. 3 (c) for the indirect band gap, the valence band maximum (VBM) and conduction band minimum (CBM) contain the same momentum (wave vector) and occur at the same k values. The irradiation of light and the photon absorption and emission can easily excite the electron from VB to CB of the semiconductor. The momentum is conserved without the assistance of the phonons due to the negligibility of the momentum of the absorbed and emitted photon. Contrarily, in the indirect band gap, the states at CBM and VBM of the photocatalyst does not have equal momenta and occur at different k value. The photon absorption must involve either absorption or emission of phonon to conserve the momentum to generate the electron-hole pair. Factors affecting the indirect band gap are due to the interaction of electrons with initial photon and phonon (quantised lattice vibration) to gain energy, increasing and decreasing its momentum. Besides, it was denoted that electron, phonon, and photon involvement proceeds at a lower probability and slower rate in the indirect absorption [53].

Challenges in photocatalytic water splitting

UV-active photocatalysts have shown remarkable progress in photocatalytic water splitting since 1972. However, the solar light that reaches the Earth's surface consists of mainly visible light at wavelengths from 400 to 700 nm, accommodating 43% of the total radiation. The utilization of UV light at 400 nm with 100% quantum efficiency will only make up to 2% of the hydrogen conversion. This explains that even a UV-active photocatalyst with exceptional surface properties could not provide a higher yield of hydrogen. Therefore, visible-active photocatalysts have sought the researchers' attention and have been extensively studied [56]. Some of the critical challenges highlighted in hydrogen photocatalytic water splitting; include 1) low efficiency of the photocatalysts, 2) higher recombination rate of the electrons-holes, 3) weak light-harvesting, 4) low photocatalyst's surface area, 5) high cost, and 6) low abundancy of the materials [57,58].

Additionally, determining the materials that could respond and improve visible light absorption has also been one of the main obstacles in water splitting. Hence, to overcome these limitations, various strategies have been developed to enhance the efficacy of these light-active photocatalysts. Improvements include structural and electronic modification, improving the photocatalyst's morphology, heterojunction formation, noble metal deposition, and doping [58–60]. The photocatalyst low efficiency in hydrogen water splitting is primarily due to the inappropriate band gap energy to fully utilize the solar energy spectrum, the position band of CB and VB to drive the redox reaction, and the redox stability [61]. These limitations lead to the low yield of hydrogen production. In addition, the fast recombination rate of charge carriers is associated with low exciton energy shortening their lifetime. This causes the electron and holes to recombine when they cannot locate the substrates easily [36].

One of the favourable features of LDH photocatalyst, aside from its unique layered structure and tailored design, is its tunable band gap [62,63]. However, the band gap's value must depend on the nature and composition of the metal cations and anions fabricated into the LDH structure. For instance, LDH is comprised of (Zn and Ti; Mg and Al; Zn and Al) having a wide band gap and low light-harvesting efficiency. According to the DRS results done by Zhu et al., the band gap of pure ZnTi LDH approximately 3.35eV is unable to absorb light under 535 and 850 nm. Hence, only a small number of electrons could participate in the photocatalytic reaction under light irradiation, and the rest will quickly be recombined. Some major limitations of LDH photocatalyst are low photoelectronic transition efficiency, inability to absorb visible light, the quick

recombination rate of electron-hole, layer aggregation and poor crystalline structure. Therefore, further studies are needed to enhance their photostability and improve the separation efficiency [64].

A broad absorption spectrum and adequate redox ability are among the significant factors required to design a standard photocatalyst. A narrow band gap for a single photocatalyst helps the absorption and utilization of light with a wide absorption spectrum. However, the photocatalyst should possess a higher CB and lower VB position associated with a large band gap when considering the redox ability. Hence, the formation of the heterojunction is an effective way to conserve the efficiency of the photocatalyst [65]. Constructing a type II heterojunction is considered the best way to improve the separation efficiency and overcome the fast recombination rate between electron-hole pairs. However, this type of heterojunction usually was associated with the weak driving force of charge at the interface, which caused a great challenge for the photocatalysis process. This is because a weaker driving force is not enough to stimulate the charge separation. Therefore, a bridging medium could be used to bridge both semiconductors and overcoming the limitation. Following this, *Meng* et al. have integrated the polydopamine (pDA), a type of polymer, to act as an interface medium to bridge g-C_3N_4 and NiCo-LDH. They discovered that the integration of pDA into g-C_3N_4 and NiCO-LDH leads to improved charge carrier's separation, stability, and light absorption capacity. The adhesive action of pDA could narrow the interface of g-C_3N_4 and NiCo-LDH, besides expediting the electron motions [66].

Another challenge in the heterojunction photocatalyst observed in the Z-scheme system is the use of electron mediators. The use of a redox mediator in the traditional Z-scheme heterojunction system is highly attributed to the backward reaction. Besides, the redox mediator's instability in the system is one of the main drawbacks of this heterojunction system [67,68]. Meanwhile, in the all-solid-state Z-scheme system, the use of noble metal as a solid conductor is non-economical and not commercially applicable. On the other hand, challenges in the S-scheme heterojunction system are mainly on selecting the semiconductors to be coupled. This is because an appropriate selection of the coupled semiconductor will determine the construction of an induced electric field in the S-scheme system, which highly contributes to higher photocatalytic performances. Fig. 4 summarises the challenges of photocatalytic water splitting in a single and hybrid photocatalyst.

Efficiency enhanced through heterojunction formation

Interfacial charge transfer in LDH-based hybrid semiconductors manifest excellent benefits in enhancing the separation efficiency of electrons-holes, reducing the charge's carrier's recombination while increasing their lifetime and improving the overall photocatalytic performances [69–72]. The heterojunction is defined as the interface between two different semiconductors with different band structure positions, which will result in band alignments [73,74]. The coupling of semiconductors with appropriate band potentials could lead to heterojunction formation, an ideal approach to improve photocatalytic performance [75]. Semiconductor interface contact is categorised into type I, type II, type III, Z-scheme, S-scheme, p-n junction, and R-scheme [76–78]. Fig. 5 (a) shows the differences between the main types of

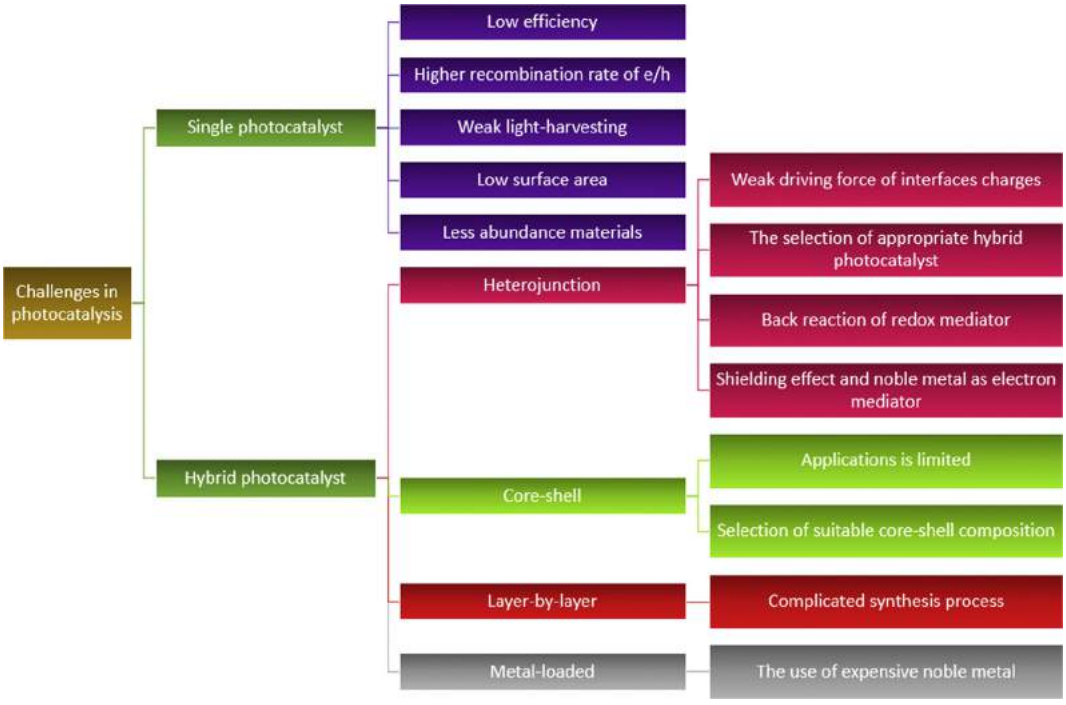

Fig. 4 – Summary of the challenges of the photocatalytic water splitting in a single and hybrid photocatalyst.

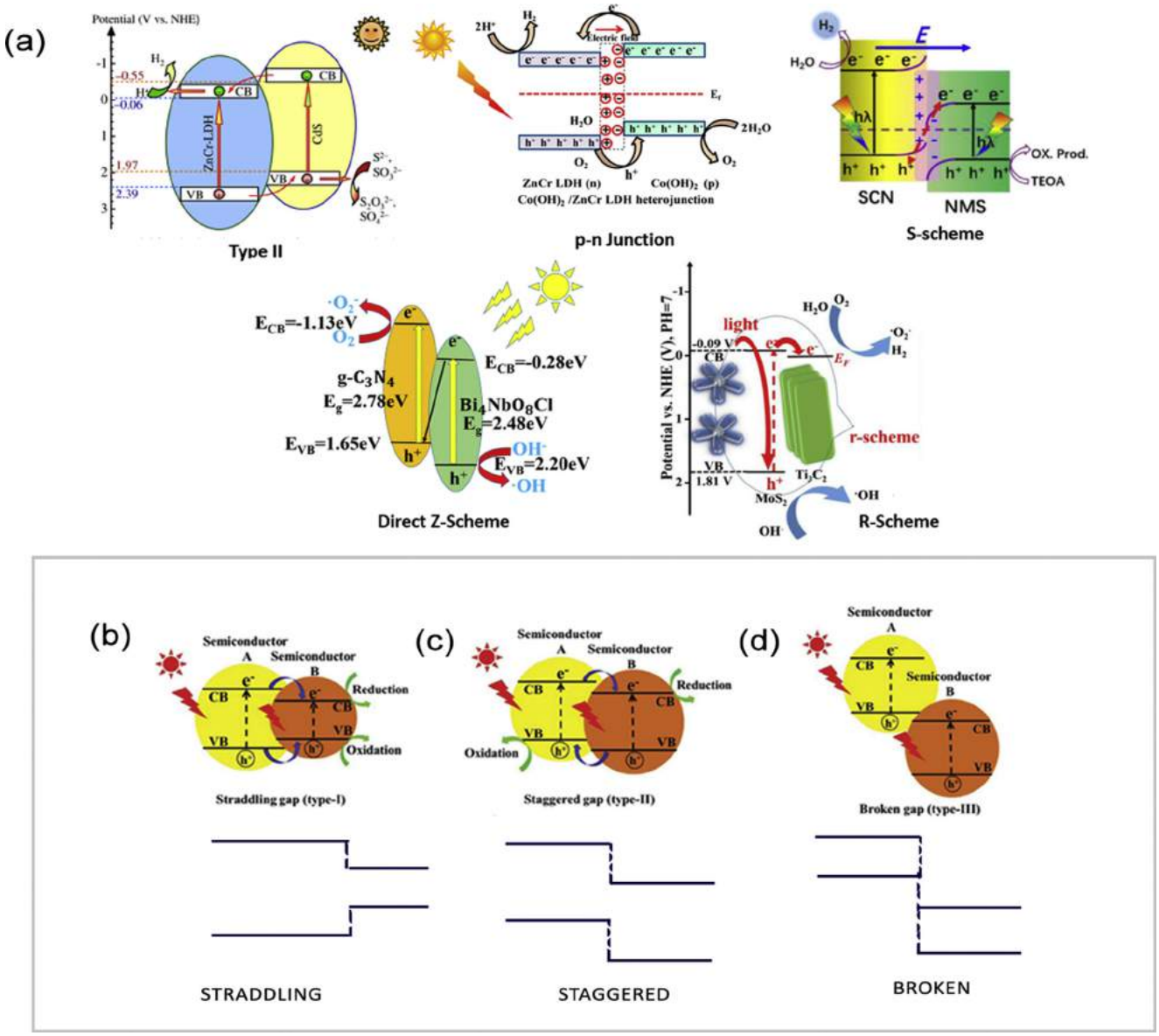

Fig. 5 – (a) Schematic of overall overview in photocatalytic water splitting mechanism through formation of different types of heterojunction (b) schematic illustration of type-I heterojunction with straddling gap (c) type-II heterojunction with staggered gap (d) type-III heterojunction with broken gap [73].

heterojunction formation in terms of electron transfer mechanism and their band structure. The band alignments of type I, II, and III heterojunctions differ from each other with clear distinction of i) type I: straddling gap, ii) type II: staggered gap, and iii) type III: broken gap. The differences in the band alignment depending on the band gap and the band potential of the paired semiconductors. It was believed that hybridising a large band gap semiconductor with a narrow band gap semiconductor could improve the hybrid semiconductor light absorption and increase the separation of the photogenerated charges. The differences of the heterojunction formed based on band alignment will give different charge transfer efficiency depending on the band potential of the paired semiconductors. Different electron transfer mechanisms with different gap types could be observed in each heterojunction type I, type II and type III. Fig. 5(b–c) shows the schematic representation of the 'gap type' of the heterojunction.

Generally, each type of heterojunction system can be identified through different elements such as: (1) the band configuration, (2) the type of assembled semiconductors and, (3) the electron transfer mechanism. In the context of the band configuration, type II heterojunction photocatalyst consisted of a staggered band structure where the CB of reduction photocatalyst and VB of oxidation photocatalyst is located at a lower band potential [79]. Therefore, the transferring of electrons will be from a higher to the lower CB potential, while

holes move from higher to the lower of VB potential to carry out redox reactions. Accordingly, the p-n junction exhibits the same band structure and placement as those of type II [73,80]. On the other hand, the placement of the band potentials in S-scheme and Z-scheme systems are unlike of those in type II and the p-n junction. Contrarily, the CB of reduction photocatalyst in this systems is located at a higher band potential than in oxidation photocatalyst, while VB of reduction photocatalyst is located at a lower band potential than VB of oxidation photocatalyst [81]. Therefore, the electrons will move from a lower CB potential to a higher one to undergo a reduction reaction. The type of coupled semiconductors making up the p-n junction consists of p-type, which commonly denoted as oxidation photocatalyst and n-type referred as a reduction photocatalyst, whereas in the S-scheme system, both oxidation and reduction photocatalyst should be the n-type semiconductors. Additionally, the formation of the positively and negatively charged interfaces in these systems induced an internal electric field that significantly assists in the separation of photogenerated charges [65]. Conversely, in type II and Z-scheme system, with regards to the band potentials, any type of semiconductors can be utilised as an oxidation and reduction photocatalyst. Table 1 summarises the difference between each type of heterojunction systems, while Table 2 summarises the different types of LDH-based photocatalyst heterojunction, including their benefits and drawbacks in photocatalysis.

Table 1 – The differences between each type of heterojunction systems.

	Type II	p-n	Z-scheme	S-scheme	R-scheme
Band structure	Staggered	Staggered	Staggered	Staggered	–
Type of paired semiconductors	any	p-type as oxidation photocatalyst and n-type as reduction photocatalyst	any	n-type as oxidation photocatalyst and reduction photocatalyst	Metal-semiconductor
Band placement	CB of reduction photocatalyst located at lower band potential than CB of oxidation photocatalyst VB of reduction photocatalyst located at higher band potential than VB of oxidation photocatalyst	CB of reduction photocatalyst located at lower band potential than CB of oxidation photocatalyst VB of reduction photocatalyst located at higher band potential than VB of oxidation photocatalyst	CB of reduction photocatalyst located at higher band potential than CB of oxidation photocatalyst VB of reduction photocatalyst located at lower band potential than VB of oxidation photocatalyst	CB of reduction photocatalyst located at higher band potential than CB of oxidation photocatalyst VB of reduction photocatalyst located at lower band potential than VB of oxidation photocatalyst	–
Internal electric field	No	Yes	No	Yes	No
Electrons transfer	Higher to lower CB potential	Higher to lower CB potential	Lower to higher CB potential	Lower to higher CB	From higher Fermi level semiconductor to lower Fermi level metal
Charges recombination at interfaces	No	No	Unused electrons at CB of oxidation photocatalyst recombined with holes at VB of reduction photocatalyst	Unused electron-hole pairs eradicated at the interface	No

Type I heterojunction

In type I heterojunction, the CB and VB position of semiconductor A is higher than in semiconductor B [106]. The electron-hole pairs cannot be separated effectively as they assembled on the same semiconductors. The mechanism of charge migration in the heterojunction type I is primarily dependable on the redox potential and band gap. Typically, in type I, the other semiconductor has a smaller band gap than their pair, in which the semiconductor B (SCB) has a small band gap than semiconductor A (SCA). The migration of the charges are as follows: i) SCA having more negative CB and more positive VB than SCB, ii) More negative CB incited the migration of electrons from CB of SCA to CB of SCB, iii) More positive VB lead to the migration of holes in VB of SCA to VB of SCB. The flow of both electron-hole pairs are in the same direction towards SCB [47,107].

In the study of type I heterojunction, Muhmood et al. has fabricated a hybrid of graphitic carbon nitride with red phosphorus (RPCN) under vacuum conditions and observed a reduction in the structural defects and an improvement in the charges separation [108]. The increased of the stability and enhancement in the photocatalytic performances in the composites photocatalyst is attributed to the novel formation of type I heterojunction, which was analysed through (Mott-Schottky and VB-XPS). It was highlighted that this type I heterojunction hybrid RPCN could degrade the target contaminant in a short duration of time. The mechanism of the electrons migration is represented in Fig. 6 (a), which can be observed that the photo-generated electrons migrate from the CB of graphitic carbon nitride to the CB of red phosphorus while keeping the holes unmoved in the VB. The movement of

Table 2 – Advantages and disadvantages in different types of LDH-based photocatalyst.

LDH based photocatalyst	Heterojunction Type	Hydrogen Production ($\mu mol\ g^{-1}h^{-1}$)	Advantages	Disadvantages	Ref.
CoO/NiCo-LDH	Type II	1500	• Electrons and holes spatially separated by the charge transfer through staggered gap configuration, promoting a higher separation efficiency than type I and type III. • Lower recombination rate of photogenerated charges compared to Z-scheme.	• Weaker driving forces at the interfaces minimising the carriers transfer rate between semiconductors, requiring binding agents to strengthen the contact interfaces. • The charges transfer mechanism through this configuration resulting in poor redox capability as the photoinduced charges carriers accumulated at the band structures. • Redox activities occur at semiconductors with lower band potentials, which suppress their redox ability and lead to the inability to drive some catalytic reactions. • In some system, the shifting of the light-induced electrons to the CB of less active photocatalyst will result in poor photocatalytic performances.	[82]
g-C_3N_4/NiCo-LDH	Type II	1170.1			[66]
CeO_2/CoAl LDH	Type II	6157			[83]
MnCdS@ NiAl-LDH	Type II	7500			[84]
g-C_3N_4/CoAl-LDH 2D/2D	Type II	680.13			[85]
$Zn_xCd_{1-x}S$/CoAl-LDH	Type II	1516			[86]
MgAl-LDH/NiS	Type II	35.8			[87]
$NiTiO_3$/CoAl-LDH	Type II	594			[88]
ZnS–ZnO/ZnAl-LDH	Type II	1599			[89]
gC_3N_4/NiAl-LDH 2D/2D	Type II	3170			[90]
NiCo-LDH/P–CdS	Type II	8665			[91]
g-C_3N_4/ZnTi LDH	Type II	~161.87			[92]
CdS/Ni–Fe-LDH	Type II	469			[93]
g-C_3N_4/NiFe LDH	Type II	744			[94]
CdS-pillared ZnCr-LDH	Type II	374			[95]
CdZnS/ZnCr LDH	Type II	916.20			[96]
CdSe/ZnCr LDH	Type II	2196			[97]
NiAl LDH/g-C_3N_4/Ag_3PO_4	Z-scheme	268	• Able to retain higher redox capabilities and quantum yield than type II, covering a wide range of solar application. • Strong reduction and oxidation reaction are preserved in direct Z-scheme by recombining some of the charge carriers at the interfaces. • Active oxidation and reduction catalytic centres, minimising the backward reactions. • The utilization of a metallic conductor in an all-solid-state Z-scheme system enhances the electron transfer through a synergistic combination of the Schottky barrier and SPR effect.	• Utilization of ion mediator in traditional Z-scheme generate backward reaction suppressing the catalytic efficiency of the photocatalyst. • Absorption of visible light by redox mediators reducing the photoabsorption ability of the photocatalyst. • The use of noble metal as a solid electron mediator is non-economical. • The recombination of photoinduced charge carriers at the interfaces fails to drive catalytic activity at a specific system due to a small number of photogenerated charges are available to undergo a redox reaction.	[98]
WO_{3-x}/Ag/ZnCr- LDH	Z-Scheme	29 375			[99]
MoS_2/NiFe LDH	Z-Scheme	550.9			[100]
MoS_2/CoAl LDH	S-Scheme	17.1	• Unused photogenerated electrons and holes will be eradicated at the interfaces, reserving electrons and holes with strong redox abilities. • Generation of the internal electric field through surfaces contact between two n-type semiconductors effectively speeds up the electrons migration.	• Lack of experimental evidence to support the effective construction of this heterojunction system in various photocatalysis field.	[7]
CoAl-LDH@NiMOF-74	S-Scheme	211			[101]

(*continued on next page*)

Table 2 – (continued)

LDH based photocatalyst	Heterojunction Type	Hydrogen Production ($\mu mol\ g^{-1}h^{-1}$)	Advantages	Disadvantages	Ref.
CdS–NiV LDH	p-n	478.96	• The utilization of p-type and n-type semiconductors induced an internal electric field in the system hasten the charge transfer between the coupled semiconductor. • Internal electric field creates positively and negatively charges junction, optimising the separation of the photoinduced charges. • Higher placement of CB and VB of p-type than n-type semiconductor induce strong redox abilities than those of type II.	• The construction of p-n heterojunction system requires a meticulous selection of coupled semiconductors which each serves as electron donor and acceptor while ensuring each exhibit excellent optical and photochemical properties.	[102]
g-C_3N_4/phosphorylated- NiFe LDH	p-n	1678.6			[103]
NiV LDH@ZIF-67	p-n	280			[11]
Au/$CaFe_2O_4$/CoAl LDH	p-n	379.1			[104]
$Co(OH)_2$/ZnCr LDH	p-n	27 875			[105]

electrons was influenced by the reduction potential by the CB of both the semiconductors, as discussed previously [109]. In this context, the CB band potential of graphitic carbon nitride is more negative than the reduction potential of water, thus leading to the movement of the electrons towards the lower CB band potential of red phosphorus. However, the holes are confined in the VB of red phosphorus and unable to migrate due to red phosphorus having more negative VB than in graphitic carbon nitride. The synthesis representation of RPCN is illustrated in Fig. 6 (b). Recently, Gao et al. have developed a composite of ZnS/ZnIn LDH with the synergy of heterojunction and defects engineering through in situ etching growth process [110]. The hierarchical type I heterojunction hybrid successfully inducing 49.3 μmol $g^{-1}h^{-1}$ hydrogen production. The positive contribution to the construction of ZnS/ZnIn LDH without incorporating ZnS, was hypothetically concluded through the exchange of the anions on the surfaces and in the interlayer of LDH. Fig. 6 (c) illustrates the schematic synthesis process of the construction ZnS on the surface of ZnIn LDH. The introduction of S^{2-} leading to anion exchange with OH^- and CO_3^{2-} of LDH, leading to the formation of seed crystal of Zn–S in the subsurface of ZnIn LDH. It was noted that, good photocatalytic performances was highly attributed to the presence of S vacancies [78,111]. The confinement effect of heteroatoms (In) around Zn within the subsurface and insufficient content of S^{2-} subsequently generates a vertically grown ZnS with rich S defects content, promoting the generation of hydrogen. Besides, the control amount of S^{2-} needed to be given full consideration. This is because excessive amount will lead to the aggregation of ZnS nanosheets, lowering the photocatalytic efficiency. On the other hand optimal amount of S^{2-} contributes to excellent photostability and structural stability. From Fig. 6 (d), it can be observed that the hydrogen production was maintained for three consecutive cycles without any obvious reduction. Furthermore, after three consecutive runs, ZnS/ZnIn LDH does not show any changes in the crystalline structure and still maintaining its flower-like shape implying good structural stability exhibit by the composite. Therefore, it was summarised that the unique hierarchical architecture and the presence of the S vacancies through defects engineering ZnIn LDH bring positive contribution towards the generation of hydrogen. However, insignificant increment of hydrogen generation can be hypothetically scrutinised due to the formation of type I heterojunction. As presented in Fig. 6 (e), the type I band structure does not give significant contribution towards a higher photocatalytic activity owing to their straddling gap structure failed to promote spatial separation of the photogenerated charges [73].

In another study, Zhu et al. reported that type I heterojunction is formed between tricobalt tetroxide with graphitic carbon nitride nanotubes (Co_3O_4/C_3N_4 NTs) under air condition [107]. Photocatalytic hydrogen performance was observed to be higher than its intrinsic counterpart. However, it was disclosed that type II heterojunction exhibits a better photocatalytic performance than in type I. This is because the type II heterojunction system exhibits an optimum band position for the electron-hole separation than in type I. Besides, the band structure of type II provides more efficient electron

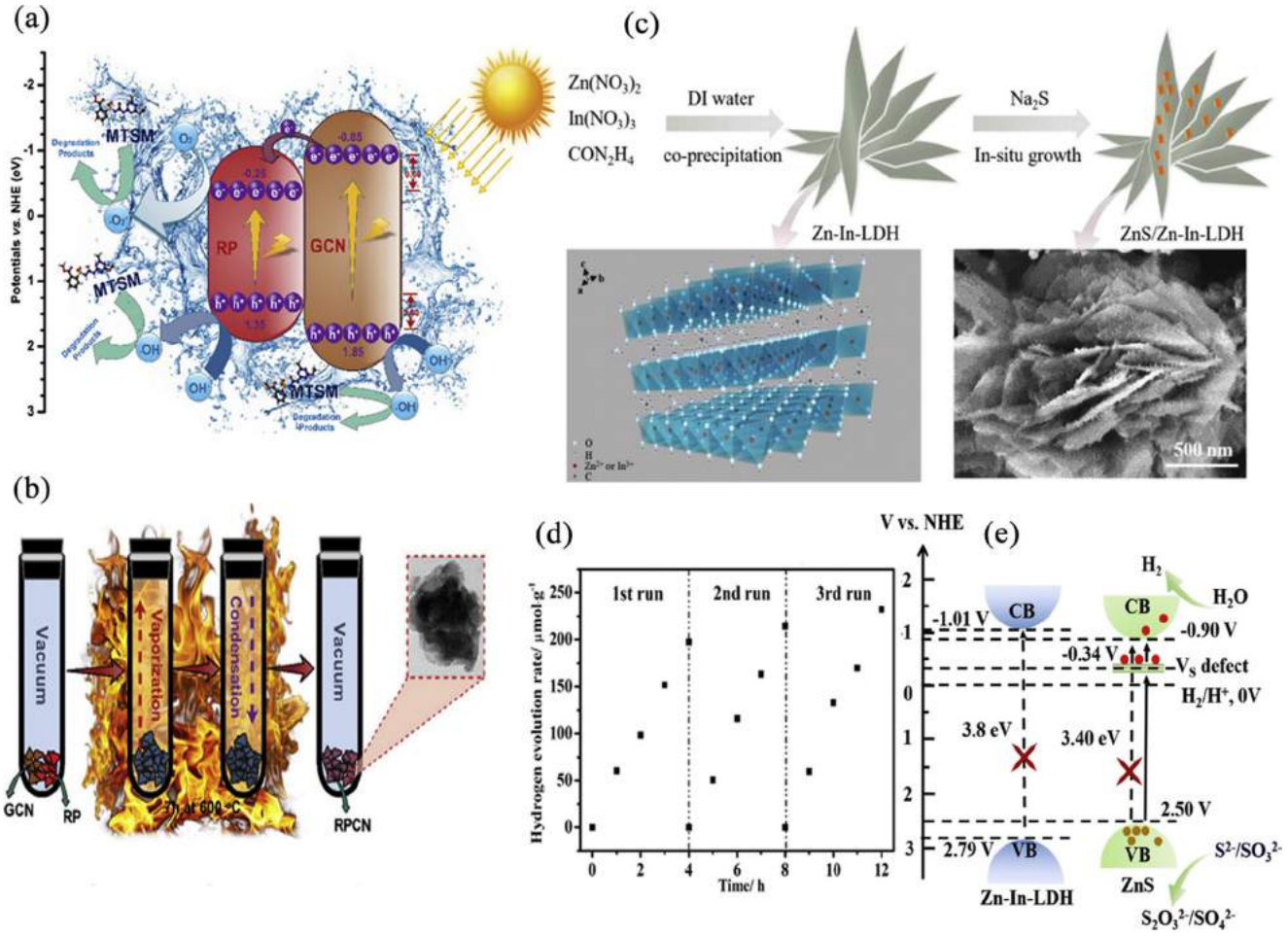

Fig. 6 – (a) Schematic mechanism of red phosphorus with graphitic carbon nitride (b) synthesis representation of RPCN, The Mott-Schottky plot for [108] (c) schematic synthesis process of ZnS/ZnIn LDH through in situ etching growth process (d) Stability test for ZnS/ZnIn LDH for three consecutive cycles (e) photocatalytic charges transfer mechanism in type I heterojunction composite of ZnS/ZnIn LDH [110]. (For interpretation of the references to color in this figure legend, the reader is referred to the Web version of this article.)

transferring which prolong the excitation times and ultimately improved the photocatalytic performance.

Type II heterojunction

The spatially localised charges in type II heterojunction makes it more promising to promote the electrons-holes separation and prolong the lifetime of the charge carriers. The energy gradient present at the interfaces will result in the spatial separation of electrons-holes where the electrons and holes migrate to the different sides of the heterojunction relative to their band potential [106,112]. In type II heterojunction, the transfer of photoexcited electrons flows from SCA to SCB, while holes flow in the opposite direction (SCB to SCA). The more negative CB potential of SCA incites the photoexcited electrons mobility towards the less negative CB potential of SCB. Meanwhile, the more positive VB of SCB leads to the migration of holes towards the less positive VB of SCA. The movement of charges following this pattern leads to spatial separation, directly improving photocatalytic activity [113].

LDH, as a single photocatalyst, has numerous limitations even though it shows a positive photocatalytic accomplishment over the decades. Rapid recombination of the charge carriers and low photochemical energy of LDH-based photocatalyst limit their industrial applicability for photocatalytic hydrogen generation. However, heterojunction formation is considered the best way to overcome this limitation as it could increase the optical absorption range and elevate the photogenic carriers separation and mobility [48]. The synergistic effect of coupling a single-component LDH with other semiconductors with appropriate band potential could boost the photocatalytic activity of LDH. Meanwhile, improving photocatalytic hydrogen generation of LDH-based photocatalyst through type II heterojunction has gained scientific interest. For instance, a very recent study on type II heterojunction constructed by Meng et al. between g-C_3N_4/NiCo-LDH has shown a remarkable improvement in the photocatalytic activity with a hydrogen evolution rate of 1170.1 μmol $g^{-1}h^{-1}$ [66]. The synergistic effects of pDA as an electron mediator with the type II band arrangement spatially improve the

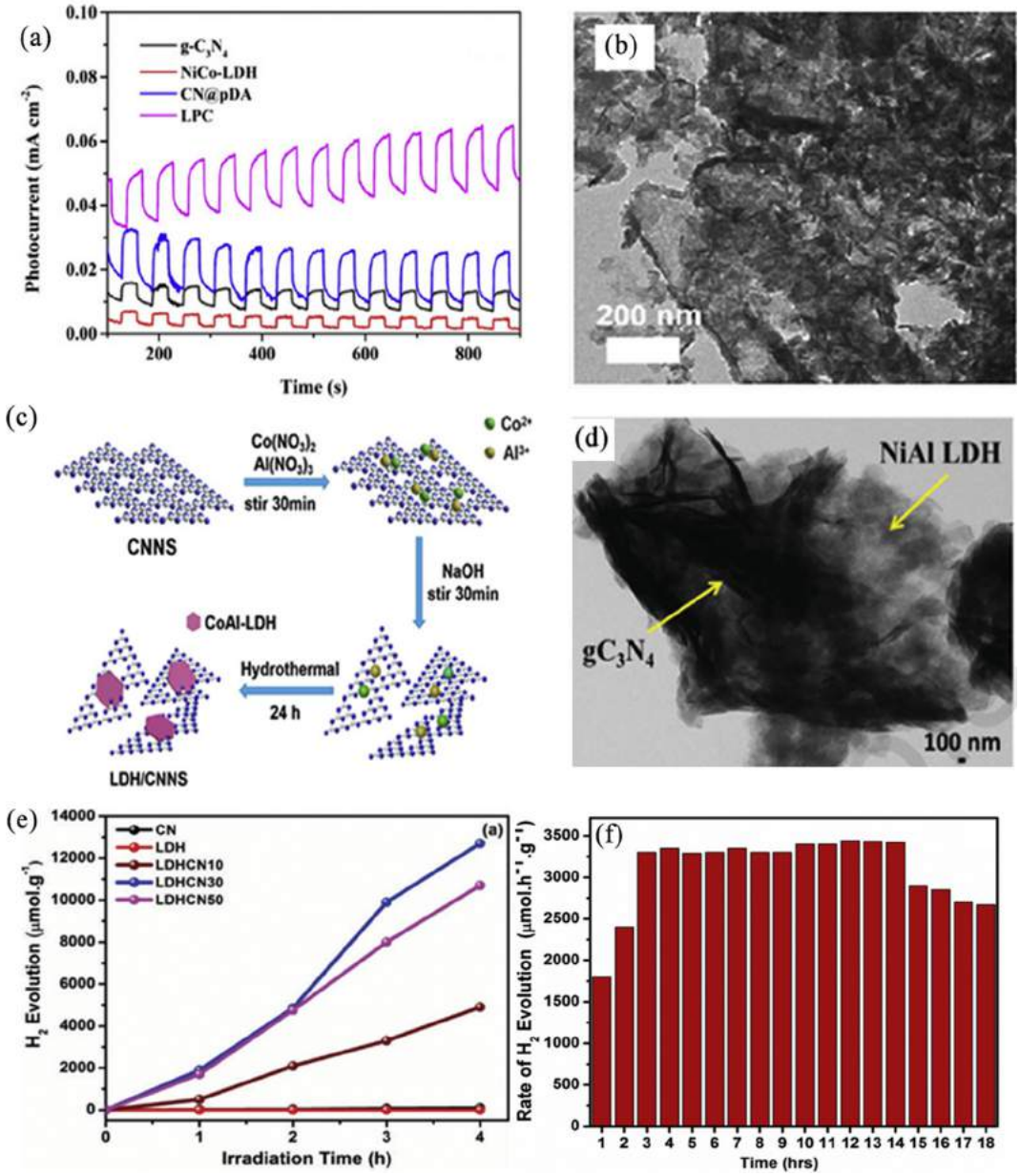

Fig. 7 – (a) Transient photocurrent responses of g-C_3N_4, NiCo-LDH, CN@pDA and LPC (b) TEM image of CoAl-LDH/CNNS [85] (c) synthesis process of CoAl-LDH/CNNS [66] (d) TEM image of g-C_3N_4/NiAl-LDH (e) rate of hydrogen generation of different samples (f) stability test results for 30% g-C_3N_4/NiAl-LDH [90].

electron migration and increase the interfacial contacts between NiCo-LDH/g-C_3N_4. It can be observed from Fig. 7 (a) that the composite of g-C_3N_4@pDA/NiCo-LDH (LPC) exhibits a more robust photocurrent response than their intrinsic counterpart, which indicates an improved separation efficiency. Besides, the composite was observed to maintain its photocatalytic stability under 20 h continuous cycle, which highly attributed to the closer interface contact between the NiCo LDH and g-C_3N_4, inducing a good photo absorption ability. Additionally, enhanced optical properties and the stability of the composite was due to the dispersion of the catalytically active metal of Ni and Co in the LDH [114]. The addition of Co metal acting as a dopant improving the optical properties of the LDH and leads to an improvement in the photochemical properties of the composites [115]. The study of type II heterojunction of NiCo LDH-based composite was extended by Wang et al. [82]. They disclosed that the introduction of NiCo LDH enhanced the charges migration between CoO/NiCo LDH composite. It was highly noted that the bridge linkage of Co atom induced an intimate contact between the semiconductors, accelerating the migration of the photogenerated charges. The transfer of electrons from Co^{2+} of CoO to Co^{3+} of the NiCo LDH promote an optimal separation of the photogenerated charges. Besides, the improvement in the solar activation energy was linked with the types of transition metal instituted into the LDH. The high electron transfer ability in the binary cations of Ni and Co

synergistically contribute to the reduction in the charge transport resistance and promote facile separation. Even though, type II configuration was linked with a weaker driving force to drive the redox reaction, however, the formation of Co–O–Co bond between CoO and NiCo LDH strengthen the interfacial contact and improve the stability of the composite.

Similarly, the study on the type II heterojunction with 2D/2D materials hybrid by Zhang et al. found that strong interfacial interaction between g-C_3N_4/CoAl LDH expedite the spatial separation of the photoinduced charges as well as shorten the charge transmission distance [85]. The TEM morphology and synthesis process of 2D/2D g-C_3N_4/CoAl LDH are illustrated in Fig. 7 (b) and (c). The hydrogen production rate is found to be 680.13 μmol $g^{-1}h^{-1}$ which was 21 times higher than that of pure CoAl LDH. Besides, it was found that the composite exhibit good photoabsorption stability with no apparent decrease in the efficiency up to three cycles. On the other hand, a recent study by Guo et al. reporting an amelioration in the hydrogen production rate of CeO_2/CoAl LDH up to 6157 μmol $g^{-1}h^{-1}$ which is 9 times higher than those reported by Zhang et al. [83]. It was reported that the institution of Co^{2+} leading to a positive impact on the hydrogen evolution rate [116]. However, CoAl LDH was observed to have a poor crystallinity structure, which is one of the factors that cause the lower in photoactivity of most CoAl LDH-based photocatalyst [117]. It was denoted that high crystallinity structure could enhance the photocatalytic activity by expediting the charge transfer to the surface of the photocatalyst and lowering the density of defects which serves as a recombination centre [118]. One way to improve the crystallinity structure of LDH is through the integration with other semiconductors, tuning the morphological structure of the composite. However, in the CeO_2/CoAl LDH type II heterojunction, introducing CeO_2 does not change the crystal structure of CoAl LDH. This infact reduces the specific surface area of the CoAl LDH as observed from the BET analysis. This characteristic nonetheless serving CoAl LDH as a supporting site and prevent particle aggregation by CeO_2. The higher catalytic activity possessed by CeO_2/CoAl LDH was associated with lower interfacial transfer resistance with the strong electrostatic attraction between the two semiconductors. The electron transfer mechanism following type II configuration notably increase the charge carriers transfer efficiency.

In different studies, both Megala et al. and Gil et al. reported that the formation of heterojunction type II could elevate the photocatalytic hydrogen production with the hydrogen yield of 3170 μmol $g^{-1}h^{-1}$ and 1599 μmol $g^{-1}h^{-1}$, respectively [89,90]. Megala et al. highlighted that an appropriate ratio of g-C_3N_4 in the composite of g-C_3N_4/NiAl LDH could generate the highest value hydrogen production reported in the NiAl LDH family. Besides, the construction of type II heterojunction with graphene-based materials was

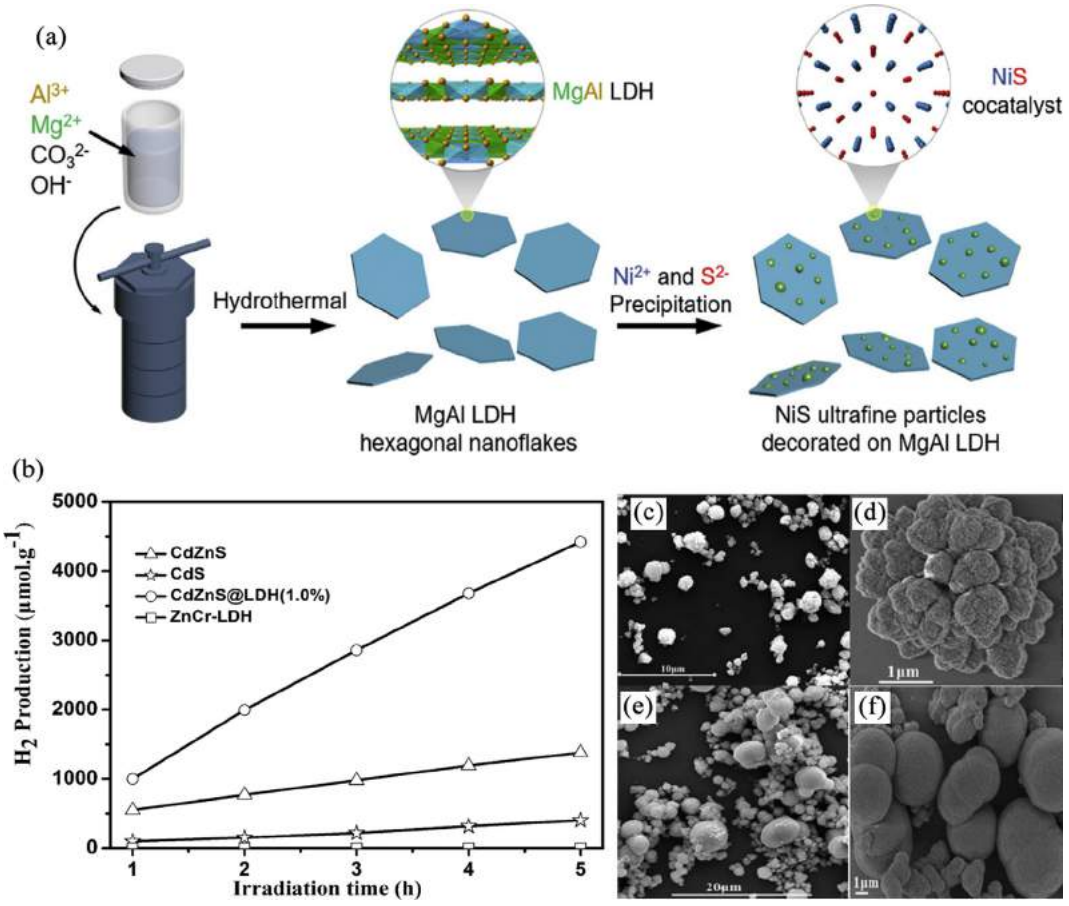

Fig. 8 – (a) Schematic synthesis process of MgAl LDH/NiS hybrid [87] (b) the rate of hydrogen production of CdZnS, CdS, CdZnS@LDH (1%) and ZnCr LDH (c–d) SEM image of CdZnS@LDH (1.0%) (e-f) pristine CdZnS with different magnification [96].

reported to prevent the aggregation of monolayer LDH which could minimise its photocatalytic efficiency [119,120]. Furthermore, it can be observed that the specific surface area of the NiAl LDH was improved from 24.376 to 30.419 m^2g^{-1} after the integration of g-C_3N_4. It is obvious that the surface area of the composite is one of the contributing factors in escalating the photocatalytic hydrogen performance as it provides more reaction sites for water splitting. The TEM image of g-C_3N_4/NiAl LDH is shown in Fig. 7 (d), while the time-dependent hydrogen generation ($\mu mol\ g^{-1}h^{-1}$) is represented in Fig. 7 (e). Under 18 h continuous irradiation, the composite of g-C_3N_4/NiAl-LDH was observed to maintain its photoabsorption stability and a slight reduction in the activity was observed after 18 h irradiation, as shown in Fig. 7 (f). Excellent photoabsorption stability was attributed to a strong 2D/2D (surface-to-surface) contact interface. Besides, the incorporation of divalent metal Ni increases the active catalytic sites and enhances the surface area, contributing to higher photochemical stability [121].

On the other hand, Chen et al. constructed type II MgAl LDH/NiS heterojunction as illustrated in Fig. 8 (a) to study the effect of NiS co-catalyst on the photocatalytic activity of MgAl LDH [87]. Even though the composite displayed a moderate increment in the hydrogen evolution rate compared to other reported LDH-based composite, it was noted to show a positive progression than its intrinsic counterpart. The lower photocatalytic activity of pristine MgAl LDH (2.7 $\mu mol\ g^{-1}h^{-1}$) was improved by forming a heterojunction with NiS escalating the hydrogen generation to 35.8 $\mu mol\ g^{-1}h^{-1}$. The shifting in the solar absorption spectrum considerably indicate an improvement in the photochemical properties of the composites. Note that the development of metal-free heterojunction could be an effective alternative to replace a highly cost noble metal. Additionally, morphological tuning is one of the contributing factors to improve the crystallinity structure of the LDH-based composites. Therefore, the synergistic combination of the morphological tuning with the formation of heterojunction substantially grant the LDH-based composite a notable place in the photocatalysis field. In this context, Yao et al. has developed hierarchical flower-like CdZnS@LDH microstructures through a facile one-pot hydrothermal process [96]. Fig. 8 (b) shows the improvement in the hydrogen evolution rate by the composite of CdZnS@LDH. It was revealed that the introduction of ZnCr LDH nanosheet as a co-catalyst aid in the enhancement of the photocatalytic activity. Besides, it is possible to fabricate a hierarchical photocatalyst of type II heterojunction with reasonable control of the elemental components and the surface charge density of LDH nanosheets. The integration of the ZnCr LDH nanosheet could prevent the agglomeration of the pristine CdZnS. As observed from the SEM image in Fig. 8(c–d), the hierarchical flower-like structure was formed after the institution of ZnCr LDH compared to the agglomerated-stacked structure of pure CdZnS in Fig. 8(e–f). Therefore, the uniform dispersion of ZnCr LDH improves the crystallinity and structural stability of the composite, which directly preserved long-term stability under light irradiation.

Therefore, it can be concluded that the construction of type II heterojunction significantly improves the

Table 3 – Hybrid LDH-based photocatalyst type II heterojunction system and hydrogen generation rate (2019–2021).

LDH based photocatalyst	Heterojunction Type	Light source/incident light	Synthesis Method	Reactor	Sacrificial Agent	Hydrogen Production ($\mu mol\ g^{-1}h^{-1}$)	Ref.
CoO/NiCo-LDH	Type II	100 mW cm^{-2} Xe lamp	–	Quartz reactor	0.1 M Na_2S 0.1 M Na_2SO_3	1500	[82]
NiCo-LDH/P–CdS	Type II	300W Xe lamp, band pass filter (λ = 420 nm)	–	–	Lactic acid	8665	[91]
CeO_2/CoAl LDH	Type II	5 W Xe arc lamp, cut off filter (λ = 420 nm)	–	Quartz reactor	TEOA	6157	[83]
g-C_3N_4/CoAl-LDH 2D/2D	Type II	300 W Xe lamp outfitted with the optical filter AM 1.5	–	Closed Pyrex reactor	TEOA	680.13	[85]
$Zn_xCd1\text{-}_xS$/CoAl-LDH	Type II	5 W LED white light	Ultrasonication	–	Lactic acid	1516	[86]
$NiTiO_3$/CoAl-LDH	Type II	5 W LED light	Phosphating treatment	Quartz reactor	TEOA	594	[88]
MnCdS@ NiAl-LDH	Type II	5 W Xe lamp (λ > 420 nm)	Ultrasonication	Quartz reactor	0.1 M Na_2S and 0.1 M Na_2SO_3	7500	[84]
gC_3N_4/NiAl-LDH 2D/2D	Type II	Quartz Tungsten Halogen lamp	In situ hydrothermal	Quartz reactor	TEOA	3170	[90]
g-C_3N_4/ZnTi LDH	Type II	300 W Xe arc lamp, cutoff filter (λ = 420 nm)	One-step in-situ hydrothermal	–	Methanol	~161.87	[92]
MgAl-LDH/NiS	Type II	300 W Xe-lamp, optical filter (λ = 420 nm)	Hydrothermal and precipitation	Circulation reactor	Methanol	35.8	[87]
ZnS–ZnO/ZnAl-LDH	Type II	Mercury lamp (UV Pen-Ray) (λ = 254 nm)	–	Quartz reactor	Methanol	1599	[89]

photocatalytic activity of all types of LDH-based photocatalyst regardless of the percentage increment. It can be summarised that in type II heterojunction system: 1) the built-in field drives the photogenerated charges to move in the opposite direction, 2) fast electron transfer hasten the redox reaction and the generation of hydrogen, 3) movement of charges following the band configuration assisted its separation and minimising charges recombination [122,123]. Table 3 summarises the hydrogen evolution rate of recently developed type II LDH-based photocatalyst for the past three years. Different types of LDH based-composite has been constructed by integrating different type of binary LDH such as NiCo, MgAl, CoAl, ZnCr, NiAl, and ZnTi. The combination between the divalent and trivalent metal ions in LDH and the configuration of their chemical composition synergistically improve its photoabsorption ability and optimize their electronic structure [124]. Out of the reported LDH-based composite, higher photocatalytic activity can be observed in the Ni-based LDH.

According to Barliarsingh et al. incorporating Ni metal could preserve the crystallinity structure of the LDH and as well improve its surface area [125]. This was in parallel with the stability test done on NiCo-LDH/P–CdS in which excellent structural and photoabsorption stability can be observed with a retained photoactivity after 16 h. It was also proven by Zhao et al. that Ni-containing LDH exhibit the highest crystallinity structure with a substantial reduction of band gap compared to Zn and Mg [126]. As mentioned, CdS highly suffered from photo corrosion due to sulfide oxidation in which S^{2-} readily oxidised by photogenerated holes [127]. Thus, low stability in oxygen-rich solvent limits the role of CdS in photocatalysis despite having good band gap energy [57]. However, constructing a hybrid composite with Ni-based LDH lead to improved properties, enhance its photostability and oxidation stability. The uniform dispersion of active metal Ni subsequently prevents the agglomeration of CdS particles. Furthermore, the incorporation of trivalent metal ions Co and Al was denoted to shift the solar absorption towards the visible spectrum of NiCo LDH and NiAl LDH with a band gap of 2.2 and 2.6 eV, respectively [128]. The intercalated Co_3^{2-} in the interlamellar of LDH serves as holes confinement assisted in the formation of the hydrogen [129]. Therefore, distinct properties manifest by Ni-based LDH is one of the contributing factors leading to an excellent photocatalytic activity and stability observed in NiCo-LDH/P–CdS and MnCdS@NiAl-LDH.

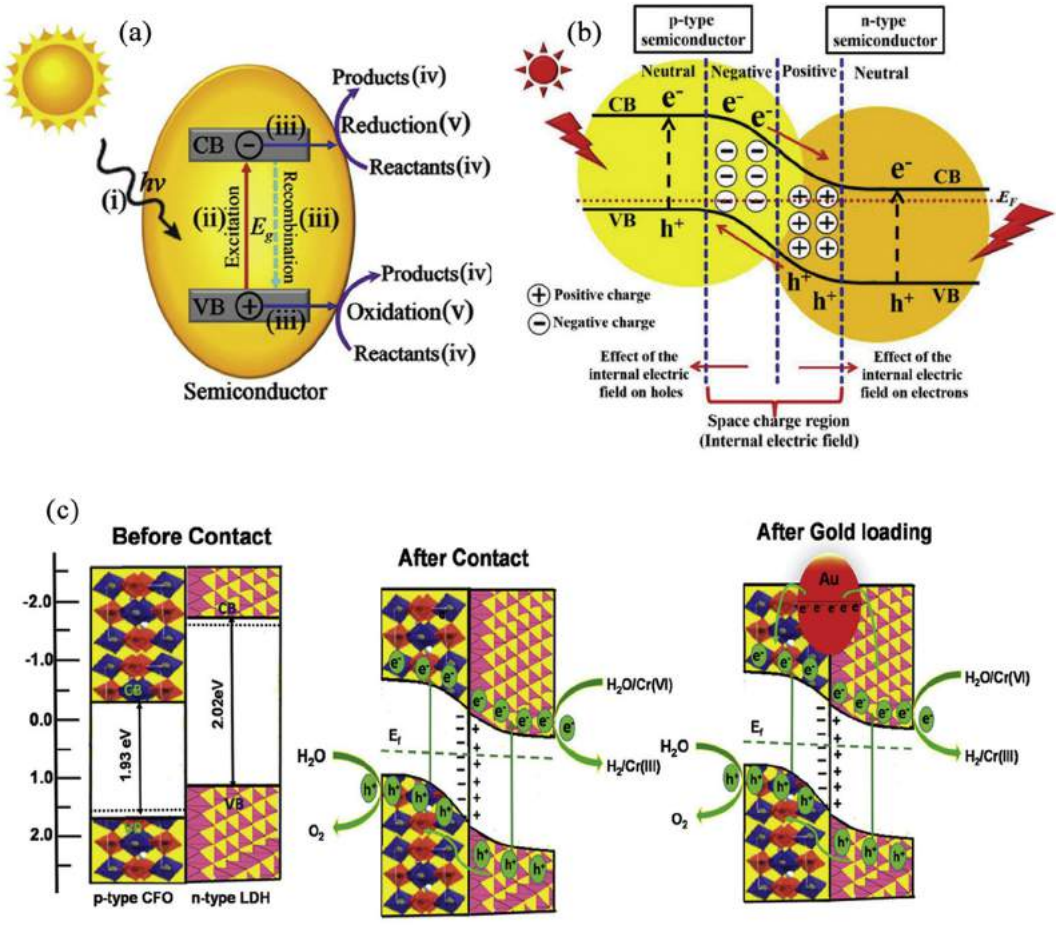

Fig. 9 – Schematic illustration of (a) typical photocatalytic processes on a semiconductor (b) electron–hole separation under the influence of the internal electric field of a p–n heterojunction photocatalyst [73] (c) photocatalytic pathway of charge transfer in Au/$CaFe_2O_4$/CoAl LDH for H_2 and O_2 evolution and Cr(VI) reduction [104].

P-n heterojunction

Tremendous efforts have been devoted to increase the spatial separation of electrons to improve photocatalyst efficiency. One of the most effective methods to improve photocatalytic water splitting overall efficiency is through the formation of the heterojunction [130,131]. The construction of p-n heterojunction can be achieved by integrating p-type and n-type semiconductors. More importantly, the existence of the electric fields at the interface of p-n heterojunction could enhance the photocatalytic activity of the photocatalyst [132]. It was revealed by Guo et al. that the integration of p-type g-C_3N_4 and the n-type $Bi_4Ti_3O_{12}$ heterojunction could suppress the recombination of photogenerated electron-hole pairs, increasing the photodegradation efficiency [133]. The electric field at the interface will assist in separating the electron-hole pairs, resulting in the spatial separation and expediting the photocatalytic performances. The formation of p-n heterojunction was presumed to be distinctly effective than type-II heterojunction due to the synergistic effects between the internal electric field at the interfaces and the methodical band alignment [134].

The schematic illustration of the p-n heterojunction mechanism is shown in Fig. 9. In the p-n heterojunction system, the semiconductors are composed of the p-type (oxidising) and n-type (reducing), which individually consist at different Fermi levels. The photoexcited electron at the n-type semiconductor migrates to the p-type, leaving a positively charged species, while the holes at the p-type semiconductor migrate to the n-type semiconductor leaving a negatively charged species. The region at the p-n interfaces has now become positively and negatively charged. The migration of electrons-holes is continuous until the Fermi level achieved equilibrium [135]. The charged spaced at the interfaces of both the semiconductors is known as the internal electric field. Under light irradiation, the electrons in both p-type and n-type will be excited, generating electron-hole pairs. With the aid of the internal electric field, the photogenerated electrons in the p-type semiconductor will migrate to the CB of the n-type semiconductor, while the holes in the VB of the n-type semiconductor will migrate to the VB of the p-type semiconductor [131]. The migration of the electron-hole in this system leads to the spatial separation of electron-hole pairs and prolonging the exciton lifetime. This system is thermodynamically stable as the CB, and the VB of the p-type semiconductor usually are located higher than those of the n-type semiconductor [73,134,136].

The construction of the p-n heterojunction system in the LDH based photocatalyst has been extensively studied. Even though the selection of LDH in photocatalysis was highly favoured, it was denoted that some of the LDH-based photocatalysts displayed a poor crystalline structure, leading to a low reaction rate in the photocatalytic reaction. Recently, Yang et al. have assembled NiV LDH nanosheet onto hexagonal CdS, constructing p-n heterojunction system [102]. It was believed that the emergence of the internal electric field facilitates the separation of electron-hole pairs in the n-type CdS and p-type NiV LDH escalating the hydrogen generation up to 6.59 times higher than pristine CdS. The integration of NiV LDH does not affect the chemical composition of CdS but improved the stability of the composite. The photo corrosion of CdS was greatly hindered, and the poor crystallinity in

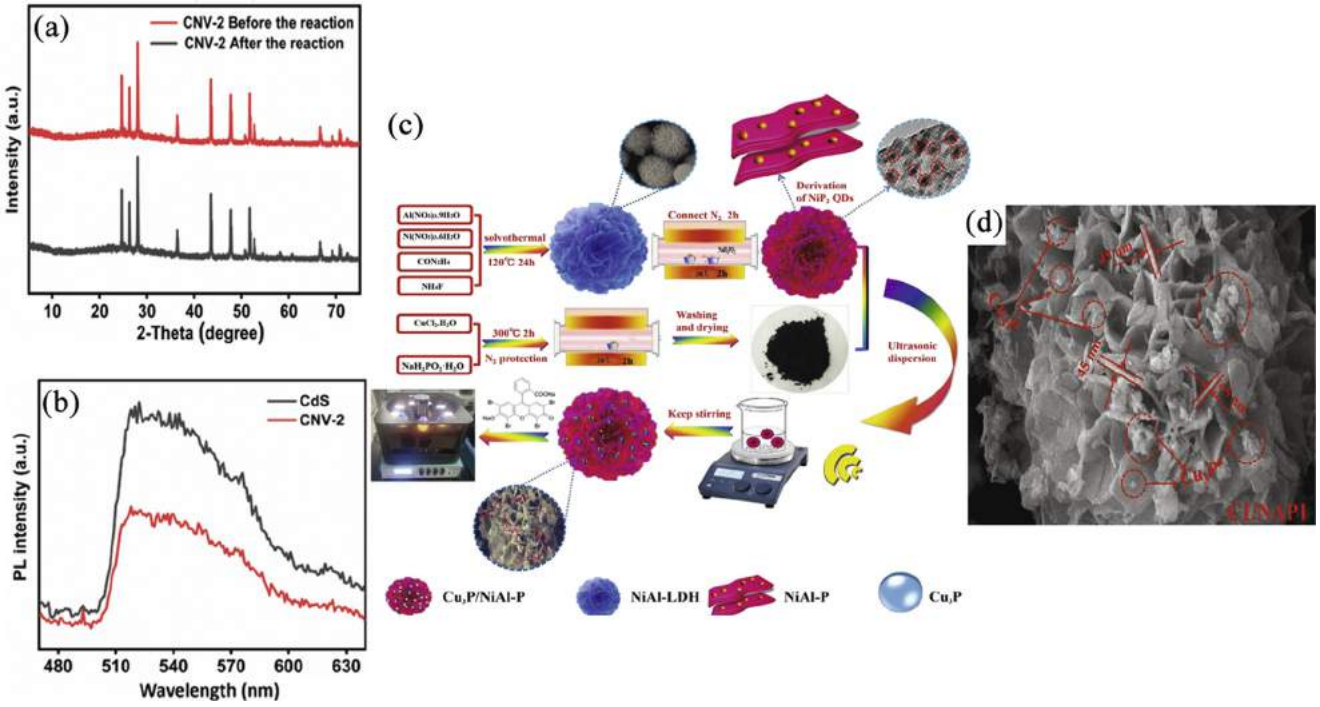

Fig. 10 – (a) XRD pattern of the composite of CdS/NiV LDH before and after the reaction (b) PL spectra of CdS and CdS/NiV-LDH [102] (c) schematic illustration of the synthesis process of NiAl-LDH, NiAl–P, Cu_3P, and Cu_3P/NiAl–P (d) SEM images of Cu_3P/NiAl–P [48].

individual NiV LDH could be overcome by constructing CdS/NiV LDH heterojunction. The large interfacial electric field between the p-n semiconductors facilitates the transfer of electrons and holes to the surface of CdS and NiV LDH [137]. This thereby, inhibits the accumulation of holes at CdS, inherently increase the photostability of CdS/NiV LDH. A sharp diffraction peak of the XRD pattern in Fig. 10 (a) proved that the composite of CdS/NiV LDH retains its crystallographic structure before and after the reaction indicating excellent structural stability. The increased in the crystallinity of the composite leads to more efficient charge migration and minimise the centre for the recombination of photogenerated charges [138]. It was noted that NiV LDH outstandingly serves as a site for the splitting of water to hydrogen, manifesting a more negative zeta potential (−14.0 mV) than CdS (−13.6 mV). PL spectra analysis in Fig. 10 (b) demonstrates a depression in the peak of the composite CdS/NiV LDH, disclosing an exceptional separation efficiency of the photogenerated charges. Additionally, CdS/NiV LDH possesses good optical and photochemical properties with band gap energy of 2.24 eV, favouring its activation under visible light irradiation and higher photoactivity.

On the other hand, p-n heterojunction system has been constructed by integrating binary NiV LDH with a Co-based zeolitic imidazolate framework (ZIF-67) [11]. It was disclosed that hydrogen generation was 9.5 and 5.9 folds higher than pristine NiV LDH and ZIF-67, respectively. However, this LDH-based composite displayed 1.76 folds lower hydrogen production than CdS/NiV LDH. The construction of a large interface between the dodecahedron ZIF-67 and monolayer NiV LDH conspicuously provides a space separation, further enhancing the transfer of charge carriers. Furthermore, the layers aggregation exhibit by NiV LDH could be hindered with the construction of NiV LDH/ZIF-67 due to the higher dispersion and construction of multiphase interphases. Besides, higher photoabsorption ability was highly associated with the activation of ligand adjacent to Co(II) ions in ZIF-67 through coupling with NiV LDH, accelerating the ligand-to-metal charge transfer. It was also noted that the decay lifetime of NiV LDH/ZIF-67 was smaller (0.29 ns) compared to their individual counterpart, indicating an efficient carriers transfer by the composite. The integration of NiV LDH as a co-catalyst forming p-n heterojunction system significantly enhances the stability of the composite and widen the light response range. It was consistent with the XPS analysis before and after the reaction, confirming the excellent chemical stability exhibited by the composite. The presence of transitional element V in NiV LDH also plays significant role in providing more trapping centres and improving the optical properties of the composite [139]. Therefore, the amelioration in the photocatalytic activity observed in NiV LDH/ZIF-67 positively linked with the efficient charges transfer owing to ideal construction of p-n heterojunction system and prominent role plays by NiV LDH.

In a different study, a unique tunable structure of LDH has aspired Yan et al. to derive the NiP_2 QD from NiAl-LDH and integrate it with Cu_3P forming a p-n heterojunction [48]. The preparation of Cu_3P/NiAl−P and its SEM image is illustrated in Fig. 10(c−d). The higher photocatalytic hydrogen production (6783.8 μmol $g^{-1}h^{-1}$) which is 4.5 times that of NiAl-LDH attributed to the well-dispersed point-to-point p-n heterojunction hybrid supported on stereoscopic nanoflower structure. The formation of the 3D structure increased the exposed active sites and enhanced the adsorption of protons. However, it was highlighted that the main contributor to the highly efficient photocatalytic activity is the formation of the p-n junction generating the built-in electric field facilitates the charge migration. Besides, it was reported by Das et al. that the formation of the p-n heterojunction photocatalyst fabricated with noble metal Au showed a high hydrogen generation rate of 379.1 μmol $g^{-1}h^{-1}$ [104]. They developed Au NP loaded on the $CaFe_2O_4$/CoAl LDH and observed the enhancement in terms of the solar conversions and thermodynamically favoured charge migration. The synergistic effects of the built-in internal electric fields with the surface plasmon effect by Au metal improve the rate of hydrogen and oxygen generation.

It was concluded that this heterojunction system exhibits higher efficiency in promoting the transfer of electrons than those of type II, thereby providing higher photocatalytic performances. The additional induced electric field is one of the contributive factor for an excellent acceleration of electron-hole migration across the heterojunction. The construction of LDH-based composite through this system by Sahoo et al. shown to exhibit the most outstanding photocatalytic hydrogen generation. Based on the reported studies, the order of the LDH based p-n junction composite according to their photocatalytic efficiency can be denoted as follows: $Co(OH)_2$/ZnCr LDH > g-C_3N_4/phosphorylated-NiFe LDH > CdS−NiV LDH > Au/$CaFe_2O_4$/CoAl LDH > NiV LDH@ZIF-67. However, the efficiency of the hybrid LDH composite is not solely dependent on the type of heterojunction constructed and the type of paired photocatalyst. Other factors such as the intensity of light, design of the reactor, and the type of sacrificial agents used could also affect the performances of the photocatalysts. Therefore, the efficiency trend observed in the reported LDH based p-n junction composite may be due to the synergy of heterojunction type and the mentioned factors.

Z-scheme heterojunction

The Z-scheme heterojunction system was first introduced by Bard et al. in 1979 in which was inspired by the natural photosynthesis process. The Z-scheme system was then improvised over the years and designed to improve the impediments in the conventional type II heterojunction photocatalyst. Even though the type II heterojunction system has been considered an ideal solution for improving the photoinduced charge separation, weakened driving force has failed to drive a specific reaction in this system. Therefore, the Z-scheme heterojunction system has been perceived as a novel way to ameliorate the separation of photoinduced charges and simultaneously preserve a strong redox ability and driving force [67,81]. Basic principles of Z-scheme photocatalyst typically consisting of a paired semiconductor with one is oxidation photocatalyst while another is reduction photocatalyst. Both of the semiconductors are connected through an appropriate shuttle electron mediator. Oxidation photocatalyst conceptually has a lower VB position with a strong oxidation ability, while reduction photocatalyst is the

Table 4 – LDH-based Z-scheme heterojunction system with their advantages and limitations.

Z-scheme type	LDH-based composite	Hydrogen production	Advantages	Limitations	References
Traditional Z-scheme	–	–	• The accumulation of electrons at CB with higher reduction potential and holes at VB with higher oxidation potential induced strong redox ability. • Redox ion mediator assists the electrons transfer between the semiconductors.	• The existence of a backward reaction decreasing the number of effective electrons and holes. • Not widely applicable as it needs to be constructed in the liquid phase. • The amount of ion redox mediator needed to be optimally controlled to avoid the shielding of electrons. • Absorption of visible light by redox mediators reducing the photoabsorption ability of the photocatalyst. • The utilization of redox ion mediator depends on the pH concentration: o Fe^{3+}/Fe^{2+} promote catalytic reactions under weakly acidic to an alkaline condition. o IO_3^-/I^- promote catalytic reactions under stronger acidic condition.	
All-solid-state Z-scheme	WO_{3-X}/Ag/ZnCr-LDH	29 375	• Exhibit higher redox capabilities, same as traditional and direct Z-scheme. • Hasten the charge transfer between the semiconductors due to the shorter transfer pathway. • Utilization of metallic conductor induced Schottky junction and SPR effects. • Inhibit the backward reaction that commonly occurs in traditional Z-scheme system. • Applicable either in liquid or in gas system.	• Difficult in controlling the position of metal conductor to be assembled between the semiconductors. • The incorrect positioning of the metal conductor leading to them functioning as co-catalyst instead of electron mediator. • Uncontrollable amount of the metal conductor resulting in the electron shielding, lowering the photocatalytic efficiency. • Some of the metal conductors exhibit good photon absorption resulting in competition with the semiconductor for light utilization.	[99]
Direct Z-scheme	MoS_2/NiFe LDH NiAl LDH/g-C_3N_4/Ag_3PO_4	550.9 268	• Promote a spatial separation of photoinduced charges and reduce bulk electron-hole recombination. • Non-effective electrons and holes recombined at VB of reduction photocatalyst, preserving charges with strong redox capabilities. • Does not utilize any mediator to promote charges transfer.	• The recombination of photoinduced charge carriers at the interfaces fails to drive catalytic activity at a specific system due to a small number of photogenerated charges are available to undergo a redox reaction.	[100] [95]

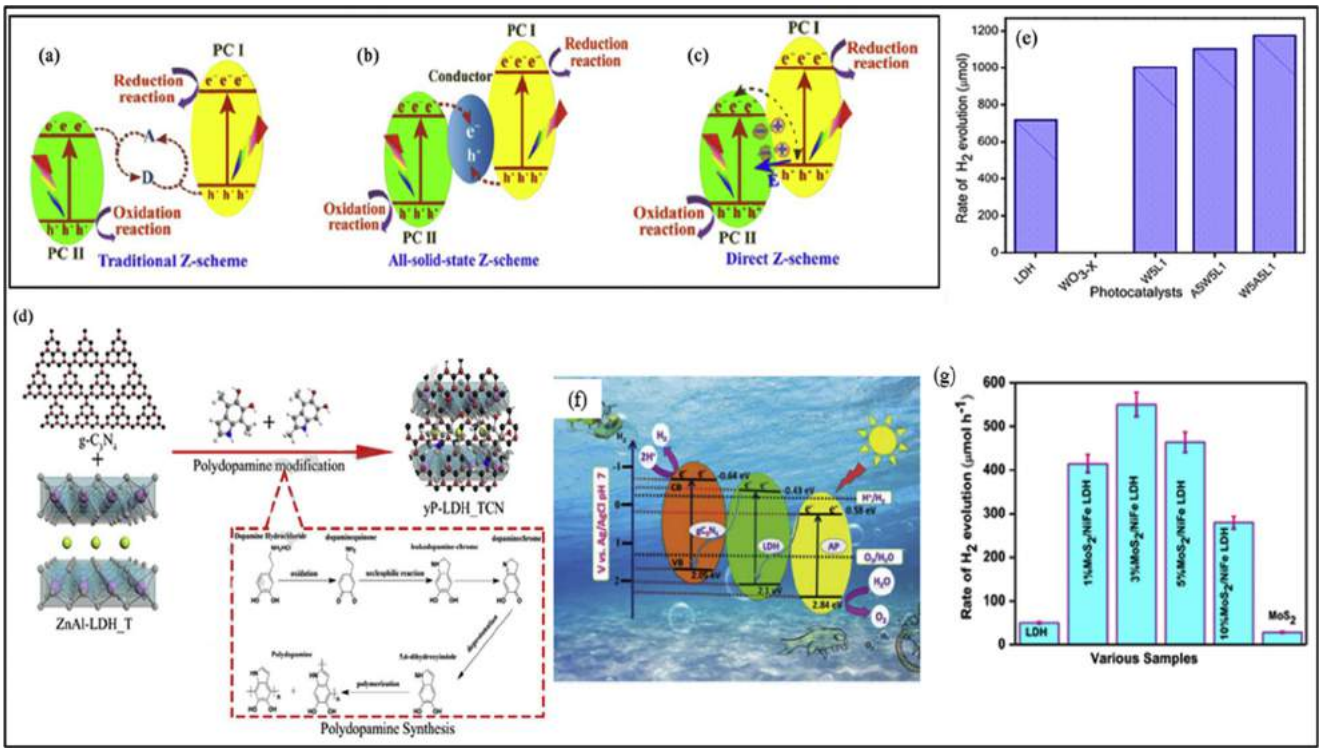

Fig. 11 – (a) Schematic illustration of charge carrier transfer in traditional Z-scheme photocatalysts; A and D stand for electron acceptor and donor, respectively; (b) Schematic illustration of charge carrier transfer in all-solid-state Z-scheme photocatalysts (c) Schematic illustration of charge carrier transfer in direct Z-scheme photocatalysts. E means the electric field [73] (d) Schematic illustration of pDA/g-C_3N_4/ZnAl LDH (yP-LDH_TCN) composites and the structural diagrams of the polydopamine synthesis processes [148] (e) rate of H_2 evolution of pristine ZnCr LDH, WO_3, and WO_3/ZnCr-LDH with different WO_3 ratio [99] (f) mechanism of electron transfer in ternary NiAl LDH/g-C_3N_4/Ag_3PO_4 Z-scheme system [98] (g) rate hydrogen evolution of pristine NiFe LDH, MoS_2, and MoS_2/NiFe LDH with different MoS_2 ratio [63].

one with a higher CB position and exhibits strong reduction ability. These two semiconductors have staggered band structure configurations. Z-scheme heterojunction system can be categorised into three types as denoted in Table 4: (i) traditional Z-scheme photocatalysts, (ii) all-solid-state Z-scheme, and (iii) direct Z-scheme. The type of the Z-scheme heterojunction photocatalyst depends on the type of charge carrier mediator used [140,141]. There are clear distinctions between different types of Z-scheme photocatalyst which can be discussed in terms of working mechanism, the synthetic process, properties, and applications [68,81,140].

In the traditional Z-scheme heterojunction system, the coupling of two semiconductors is basically based on the use of a shuttle redox ion mediator, acting as electron transfer between two semiconductors. Redox mediators or electron shuttles are generally organic molecules that can undergo a reversible oxidation and reduction process [142]. In this context, the shuttle redox mediator acts as a connector consisting of an acceptor and donor pair to aid the photocatalytic process without having the two semiconductors in contact with each other, as illustrated in Fig. 11 (a). For instance, Fe^{3+}/Fe^{2+}, Co^{3+}/Co^{2+}, IO^{3-}/I^-, NO^{3-}/NO^{2-} are the most common redox coupled ion mediators used in the photocatalytic water splitting system. Upon light irradiation, the electrons will be transferred from the O_2 generating photocatalyst to H_2 generating photocatalyst through the mediators where the photogenerated holes in the VB of PC I and electrons in the CB of PC II will be consumed by the electron donor species (D) and electron acceptor species (A) respectively. The reserved electrons in the CB of PCI and holes in the VB of PCII, which possess a strong redox ability, will correspondingly undergo the reduction and oxidation process. The separation of both the oxidation and reduction part ultimately enhanced the photocatalytic activity of the photocatalyst [81]. However, the existence of the back reaction of the redox mediator, light-shielding effect, slow charge carrier transfer rate, and unstable redox mediator are the challenges that minimise their efficiency as the prime system in photocatalysis [67,68].

On the other hand, electron mediators in the all-solid-state Z-scheme are typically in solid form, assisting the migration of electrons from one semiconductor to the other, as shown in Fig. 11 (b). The introduction of a conductor between PC I and PC II is known as Ohmic contact [143]. The all-solid-state Z-scheme system can possess high redox ability and increases the spatial separation of the electron-holes [144]. This system can be considered the best replacement for the traditional Z-scheme system because, without A/D pair, the backward reaction and the shielding effect can be prevented. The photogenerated electrons and holes in CB of PC II and VB of PC I will be recombined and eradicated through the ohmic contact. Therefore, the reserved electrons in the CB of PC I and holes in VB of PC II, holding a powerful redox ability will participate in

the reduction and oxidation process. The mediator provides the pathway for preserving more electrons and holes to undergo redox reaction and leading to a significant increase in the photocatalytic performances. In addition, this system can work both in the gas and liquid phase environment, which extends their applicability from water splitting to solar cells, photodegradation, and CO_2 conversion [140]. However, the main limitation of this heterojunction system is the use of an expensive noble metal as the mediator.

Direct Z-scheme is one of the most advanced heterojunction systems in which the concept was first introduced by Grätzel in 2001 [145]. Since then, the direct Z-scheme heterojunction system has been extensively studied over the years. In this system, the backward reaction and the shielding effects cannot occur due to the absence of the redox mediator. Upon light irradiation, the photogenerated electrons in the CB of PC II will be recombined with holes in the VB of PC I at the heterostructure interface, as shown in Fig. 11 (c). The higher transfer efficiency, powerful oxidative holes, and reductive electrons to undergo redox reaction enhanced the photocatalytic activity [146,147].

In the context of the Z-scheme system in LDH-based photocatalyst, Li et al. fabricated g-C_3N_4/ZnAl-LDH composite by utilising pDA as the redox mediator through polydopamine cross-linking method presented in Fig. 11 (d) [148]. The addition of pDA as an electron transferring medium impressively hasten the electron transfer efficiency. The uniform dispersion of active metal Zn and Al in the calcined ZnAl LDH was denoted to contribute to the strong structural 'memory effect', which benefits its structural reconstruction [149]. Additionally, calcining LDH will convert them into mixed metal oxide due to the removal of −OH groups in the interlamellar space, deactivating its layered structure [150]. On the other hand, rehydrating the calcined LDH will restore its LDH properties and reconstruct its native layered structure due to the unique structural 'memory effect' exhibit by LDH [151]. The calcination process favourably increases the active phase dispersion in LDH, thereby augmenting the energy conversion efficiency in the reconstructed LDH. Additionally, enhanced photocatalytic activity was observed under optimal calcination temperature at 500 °C, which theoretically due to the generation of the active phase, exposing more redox-active sites. The synergy between PdA as electron mediator and calcined ZnAl LDH imparted a prominent role in improving the overall photocatalytic efficiency by providing an additional path for electron transfer and facilitate the separation of photogenerated charges.

The study of all-solid-state Z-scheme heterojunction system was extended by Sahoo et al. by constructing WO_3/ZnCr LDH with the noble metal Ag as an electron mediator [99]. This group so far has reported the highest hydrogen generation in the LDH-based composite Z-scheme systems. As observed in Fig. 11 (e), the hydrogen evolution rate substantially improved up to 29 375 μmol $g^{-1}h^{-1}$. Higher photoactivity observed in this Z-scheme system is primarily due to the outstanding photochemical properties exhibited by WO_3/ZnCr LDH, which can reasonably be explicated as follows. Strong electron conductivity in Ag boosted the mobility of the photoinduced charges and increased the light absorption spectrum, owing to its surface plasmon resonance (SPR) effect [152]. Additionally, the Schottky barrier and SPR effect induced by metallic Ag fundamentally facilitate the transfer of electrons from WO_{3-x} towards ZnCr LDH to be recombined with holes. The formation of Ag—OH bond between Ag NPs and ZnCr LDH favors the construction of Ag as an electron mediator, assisting the flow of charge carriers through the Z-scheme mechanism. The formation of an electron conduction bridge by Ag NPs provides an interior direct channel for an efficient electron transfer, augmenting the excitation energy. Furthermore, the oxygen vacancies in WO_{3-x} significantly provide support for anchoring Ag while serving as carriers trapping site, which could reduce the reaction activation energy for the photocatalysis process [153]. On the other hand, ZnCr LDH was given attention due to its high quantum efficiency and excellent photoabsorption ability as a stand-alone catalyst [154]. It was noted that the increase of the oxygen vacancies was observed after hybridizing WO_{3-x} with ZnCr LDH, effectively enhances its electrical conductivity and hindered the recombination of photogenerated charges. The trivalent Cr ion was reported to be the most active than other trivalent metal ions, which plays a vital role in shifting the absorption range towards the visible spectrum [155]. The presence of metal-to-metal charge transfer in ZnCr LDH through oxo-bridged bimetallic linkage positively contributes to the enhancement of the photoabsorption ability [105]. Therefore, the coupling of WO_{3-x} with ZnCr LDH through Ag as an electron channeling bridge not only hasten the electron transfer in the Z-scheme system but synergistically boost the photocatalytic activity of the composites.

A very recent work by Megala et al. on the formation of direct Z-scheme in the NiAl LDH/g-C_3N_4/Ag_3PO_4 revealed a dual functionality exhibited by the ternary photocatalyst in accelerating the generation of hydrogen and oxygen [98]. The study on the wettability of the composite, disclosing good hydrophilicity properties exhibit by NiAl LDH/g-C_3N_4/Ag_3PO_4 observed through the measured water contact angle. It was denoted that surface wettability is highly linked with the catalytic activity of the materials [156]. In this context, materials with hydrophilic properties were reported to exhibit higher photocatalytic performances. Additionally, the formation of multi-heterojunction in NiAl LDH/g-C_3N_4/Ag_3PO_4 could greatly enhance the absorption spectrum and efficiently constrain the separation resistance thereby, extending the carriers lifetime. In this dual Z-scheme system, Ag_3PO_4 serves as an oxidation site in generating oxygen owing to more positive VB, while g-C_3N_4 with more negative CB serves as a reduction site in generating hydrogen. On the other hand, NiAl LDH sandwiched between g-C_3N_4/Ag_3PO_4 acting as carrier transfer in facilitating the charges transmission. The mechanism of electron transfer in ternary NiAl LDH/g-C_3N_4/Ag_3PO_4 Z-scheme system is demonstrated in Fig. 11 (f). The production of hydrogen in this unique dual Z-scheme system was reported to be 268 μmol $g^{-1}h^{-1}$ while oxygen evolution is 4330 μmol $g^{-1}h^{-1}$.

In another study, Nayak et al. reported the formation of the Z-scheme heterojunction system enhancing the photocatalytic hydrogen evolution of MoS_2/NiFe LDH to 550.9 μmol $g^{-1}h^{-1}$ which is 10.9 times higher than pure bimetallic NiFe-LDH [100], as shown in Fig. 11 (g). Through the Z-scheme heterojunction system, the remaining electrons in the CB of MoS_2 with a robust reduction ability participate in the reduction of H^+ to H_2 leading to enhanced photocatalytic activity. Z-scheme system with Ag as electron transferring medium also was reported by Chen et al. in the photocatalytic reduction of Cr(VI) and observed a good photocatalytic stability without

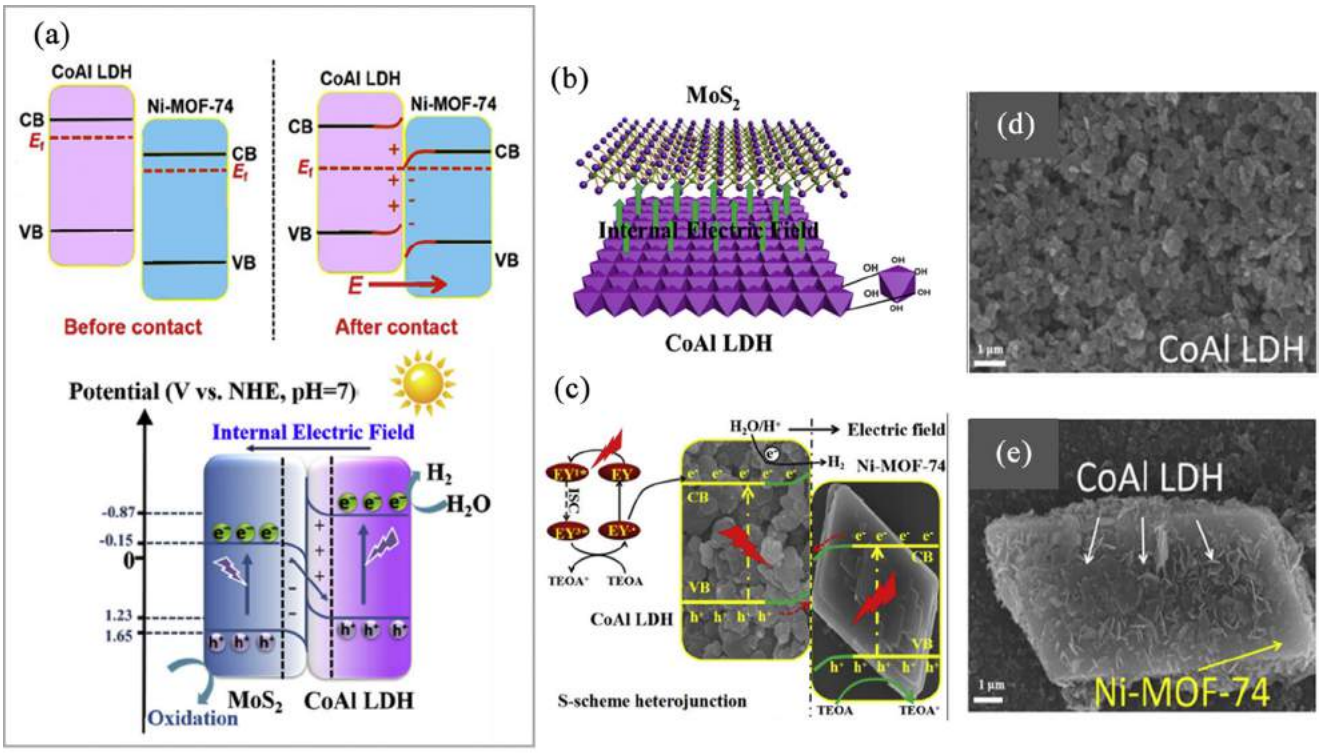

Fig. 12 – Schematic illustration of (a) S-scheme band structures before/after contact and mechanism (b) internal electric field diagram of the MoS_2/CoAl LDH [7] (c) mechanism of S-scheme electron migration of CoAl LDH@Ni-MOF-74 hybrid [101] (d) SEM image of CoAl LDH (e) CoAl LDH/Ni-MOF-74 [101].

decrease in the efficiency after 5 cycles [63]. The construction of Z-scheme system can be seen as the novel alternative to substitute type II heterojunction system as this system demonstrated strong redox ability and accord more catalytic active center than conventional type II system.

S-scheme heterojunction

The step scheme, known as S-scheme, was first proposed by Fu and co-workers in 2018 to overcome the shortcomings in the Z-scheme and type II heterojunction system. S-scheme system typically constituted of two n-type semiconductors depicted as oxidation photocatalyst and reduction photocatalyst, respectively, relative to their band structure [157]. In this system, reduction photocatalyst was assigned to those having more negative conduction band, which predominantly served in the production of solar fuels such as the generation of hydrogen. On the other hand, the holes in oxidation photocatalyst plays a significant role in the oxidation reaction commonly serves in the photodegradation process [65]. S-scheme heterojunction has the same staggered band structures as those of type II heterojunction. However, in the S-scheme system, the potential band's energies were bent to provide an easy transfer of electrons at the interface driven by the interfacial internal electric field (IEF) [7]. As discussed, type II heterojunction exhibits weak redox ability due to the accumulation of photogenerated electrons and holes in the CB of oxidation photocatalyst and VB of reduction photocatalyst [158]. Contrarily, in the S-scheme system, the useful electrons at CB of reduction photocatalyst and holes at VB of oxidation photocatalyst will be reserved, while the unused electrons and holes will be recombined and eradicated at the interface, thereby enhancing the redox ability [159].

The critical point in the S-scheme transfer route system is that the semiconductor consisting of lower CB and VB positions of oxidation photocatalyst) should be paired with those of higher CB and VB positions of reduction photocatalyst). As depicted in Fig. 12 (a), once contact is formed, the electrons from the reduction photocatalyst will disperse to oxidation photocatalyst, creating an electron depletion and accumulation layer near the interface of reduction and oxidation photocatalyst, generating a negatively and positively charge interface. The formation of the IEF flowing from reduction photocatalyst to oxidation photocatalyst will facilitate the electrons flow against the field. Generally, a material that manifests a larger work function will have a lower Fermi level. In this context, when reduction and oxidation photocatalyst forming an intimate contact, there will be upward shifting in the Fermi level of oxidation photocatalyst and downward shifting in the Fermi level of reduction photocatalyst, aligning the Fermi level of both semiconductors. The bending of the potential band energy substantially eliminates those unused electrons and holes in CB of oxidation photocatalyst and VB of reduction photocatalyst. Therefore, the remaining electrons

at CB of reduction photocatalyst and holes in VB of oxidation photocatalyst will participate in the redox reaction and maintained a strong redox ability [101,159–161].

The effectiveness of the S-scheme system in expediting the photocatalytic performances of LDH-based photocatalyst is still lack of experimental evidence. Not many studies have been reported on this system, supporting their efficacy on photocatalytic hydrogen production. However, a very recent study on the LDH-based S-scheme system by Tao et al. provide insights on designing and fabricating novel S-scheme heterojunction photocatalysts [7]. The construction of MoS_2/CoAl LDH via hydrothermal method positively improves the hydrogen generation up to 17.1 μmol $g^{-1}h^{-1}$. Even though the hydrogen production is not considerably high like those reported in type II and Z-scheme, however, the fundamental concept of this IEF-induced heterojunction system is a primary notion to improve the photocatalysis process. In this study, the selection of paired semiconductors is vital to establish the S-scheme electrons flow. CoAl LDH has been selected as a primary photocatalyst due to its higher CB -0.75 eV and VB of 1.35 eV. Besides, the constitutional Co-active sites in CoAl LDH inherently linked with excellent photocatalytic properties [62,117]. On the other hand, propitious features in 2D MoS_2 with matched band potential (EB = 0.12 eV, VB = 1.78 eV) for constructing S-scheme heterojunction system denotes them as the best candidate for the photocatalytic study [162]. A minimized charge-transfer resistance observed in the composite of MoS_2/CoAl LDH, leading to an efficient flow of electrons following the S-scheme system. As shown in Fig. 12 (b), the IEF pointing from CoAl LDH (smaller work function) to MoS_2 (higher work function), suggesting the flow of electrons from CoAl LDH to MoS_2. This hastens the transfer of charge carriers, directly improving the photoabsorption stability due to a lengthen carriers lifetime. Aside from the excellent electron transferring system exhibit by this hybrid composite, they also possesses a unique architectural structure. The carnation-like structure of the 3D hierarchical MoS_2/CoAl LDH with multi-dimensional domains inhibits the particle aggregation by nanosphere MoS_2 [88]. Besides, the amorphous structure of CoAl LDH provides a large number of catalytic active sites due to the exposure of unsaturated surface atoms [163]. Therefore,

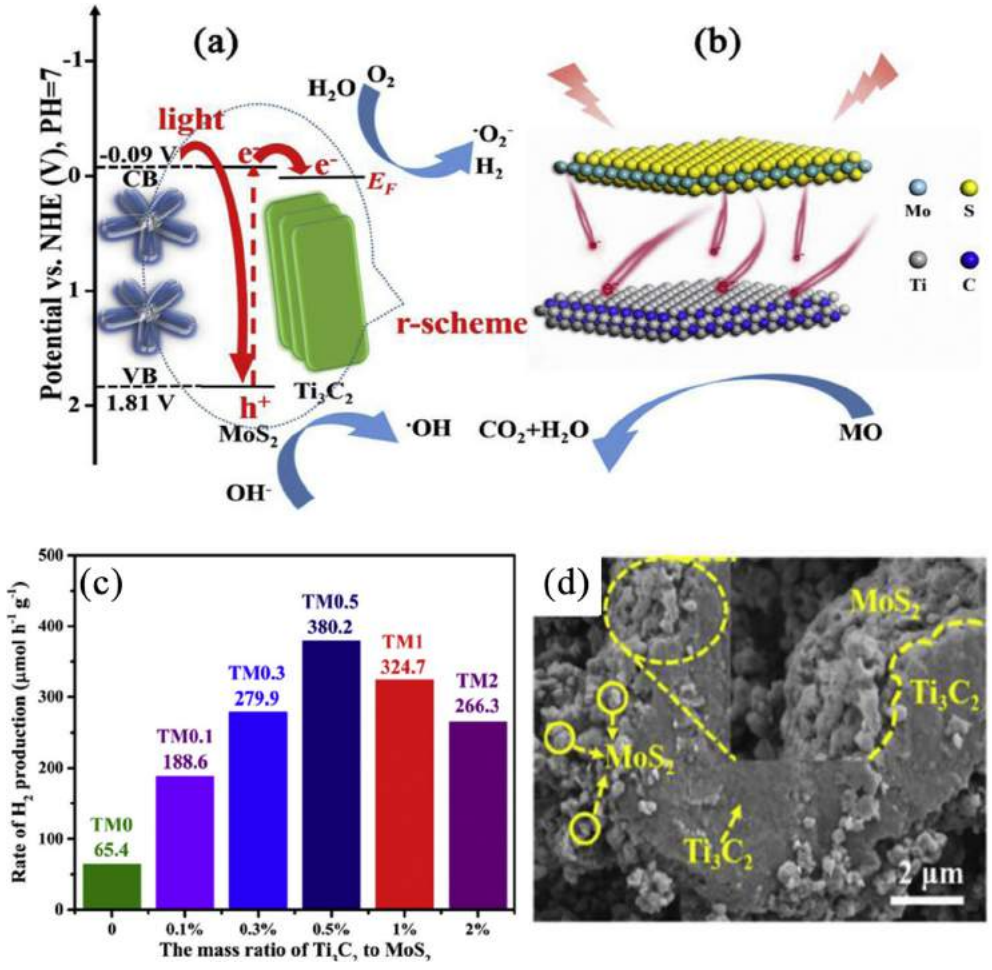

Fig. 13 – (a) Energy level structure diagram of MoS_2 and Ti_3C_2 (b) schematic illustration of photo-induced electron transfer process at the heterojunction interface (c) rate of hydrogen evolution with different mass ratio of Ti_3C_2 to MoS_2 (d) SEM image of 0.5% MoS_2/Ti_3C_2 [165].

distinct properties of this hybrid photocatalyst favourably contribute to the enhancement of photocatalytic activity.

In different studies, the same LDH precursor has been used to construct an S-scheme heterojunction system with metal-organic frameworks Ni-MOF-74 [101]. This hybrid Ni-MOF-74/CoAl LDH revealed a 12.3 fold higher hydrogen production than the composite of MoS_2/CoAl LDH and 6.2 times greater than pristine CoAl LDH. Excellent structural diversity and properties to develop highly controllable nanostructures as carriers nominate MOF as the best selection catalyst to be coupled with CoAl LDH. Furthermore, it is undeniable that the formation of IEF notably induced a strong interfacial contact and facilitate the flow of charge carriers between the semiconductors, as shown in Fig. 12 (c). A dodecahedron hexahedron structure of Ni-MOF-74 provides strong structural supports for assembling CoAl LDH. Pristine CoAl LDH exhibit a serious aggregation as designated in Fig. 12 (d), limiting the construction of photocatalyst with higher photoabsorption stability. However, hybridizing Ni-MOF-74 with CoAl LDH notably annihilates the agglomeration of CoAl LDH nanolayer as observed through the SEM image in Fig. 12 (e). Ni-MOF-74/CoAl LDH not only possess excellent architectural structure to induce high redox activities, however, homogeneous dispersion of transition metal atom in this composite greatly enhanced their solar absorption. It was disclosed that the photoactivity of this hybrid composite predominantly depends on the CoAl LDH. In this context, CoAl LDH plays a primary role in maximizing visible light absorption to carry out the catalytic reaction. Hence, the type of metal constituted into LDH is significant not only to ensure the tunability of the band potential to match the S-scheme system, but to obtain good optical properties. The divalent metal ion Co in LDH-based photocatalyst evidently improve the conductivity and optical absorption due to the role of Co as a highly active transition metal [164]. At the same time, trivalent metal Al acting as a co-catalyst to support the catalytic reaction. High dispersion of Co^{2+} assembled with $Al^{3+,}$ and their interaction in the LDH layers synergistically enhances the catalyst stability and improve the solar absorption [25].

R-scheme heterojunction

R-scheme a new type of heterojunction first proposed by Yao et al. in 2020. The R-scheme heterojunction is favourable to improve the aggregation and electron transferring from the conduction band of the first semiconductor to the active sites of the second semiconductor. This directly facilitates the separation of the photogenerated charges. In the R-scheme heterojunction system, Yao and co-workers have fabricated the Ti_3C_2 MXene with MoS_2 nanosheets through hydrothermal reaction and observed the mechanism of the charge transfer in this system. It was ascribed that the Ti_3C_2 MXene having rich in oxidised surface groups, will favour a strong interface contact heterojunction with the coupled semiconductors. Similarly, like in the S-scheme system, the selection of the suitable semiconductor to be coupled is the most significant element in constructing this R-scheme system. It was denoted that the intense physical and electronic coupling effect enhanced the transferring of the charge carriers and provided a spatial separation. They disclosed that the mechanism of the photodegradation in the R-scheme system is obtained through trapping experiments. As illustrated in Fig. 13(a–b), under light irradiation, the electrons will be excited to the conduction band of MoS_2. The migration of electrons was observed from the CB of MoS_2 to active sites of Ti_3C_2 by a close-contact heterojunction. This is due to the highly active Fermi level in Ti_3C_2 than the CB potential of MoS_2. The enhancement of the photodegradation and photocatalytic hydrogen production by 0.5% MoS_2/Ti_3C_2 was observed through this system in which the sample reaches an optimum MO degradation of 97.4% after 30 min irradiation and hydrogen evolution rate of 380.2 μmol h^{-1} g^{-1} under visible irradiation [165]. Fig. 13 (c) depicts hydrogen production rate with 0.5% MoS_2/Ti_3C_2 exhibit the highest. Even though the R-scheme heterojunction system has shown a great improvement in photocatalytic activity, there are not many literatures focusing on this heterojunction type, especially in photocatalytic hydrogen production. Besides, this type also depicts similar carriers mobility as those in metal-semiconductor configuration. Therefore, the theoretical concept of this R-scheme system needed to be studied in-depth to reveal the distinct characteristics that could ameliorate the photocatalytic performances.

Novel Hybrid-LDH nanocomposite

Metal loaded LDH precursor

One of the limitations exhibited by a single photocatalyst is the inability to trap the electrons, increasing the ability for the charge's recombination. The formation of surface defects through metal loading can optimize solar absorption and improve electron-holes separation efficiency [166,167]. The metal loading could effectively improve the photocatalytic activity's performances by forming the Schottky barrier and surface plasmon resonances (SPR) [47,168]. The metals work function value (ϕ) is the energy required to transfer an electron from Fermi level into the vacuum (the higher ϕ, the lower Fermi level energy), influencing the photocatalyst efficiency. It was denoted that the formation of the Schottky barrier from the metal loading positively affects the photocatalytic activity of the composite [169]. The Schottky barrier could improve the separation of the electron-hole pairs and inhibits the recombination of the photoinduced charges [170]. Schottky barrier is the junction formed at the interface between the metal and the semiconductor, which acts as an electron trapping site. Additionally, the metal loading on the semiconductor produces a visible light-activated photocatalyst system with a plasmonic effect [171]. The loading of noble metal on the photocatalyst has been regarded as an effective method to expedite the charge separation and prolonging the lifetime of the photoinduced charges. The primary noble metal such as Ag, Au, and Pt contains a remarkable optical property especially the unique localised SPR properties, making them special [172]. Additionally, two metals can also be loaded onto a semiconductor, whereby each of the metal serves a different function. For instance, one metal act as an electron trapping site while another will provide the SPR effect by absorbing the visible light [47].

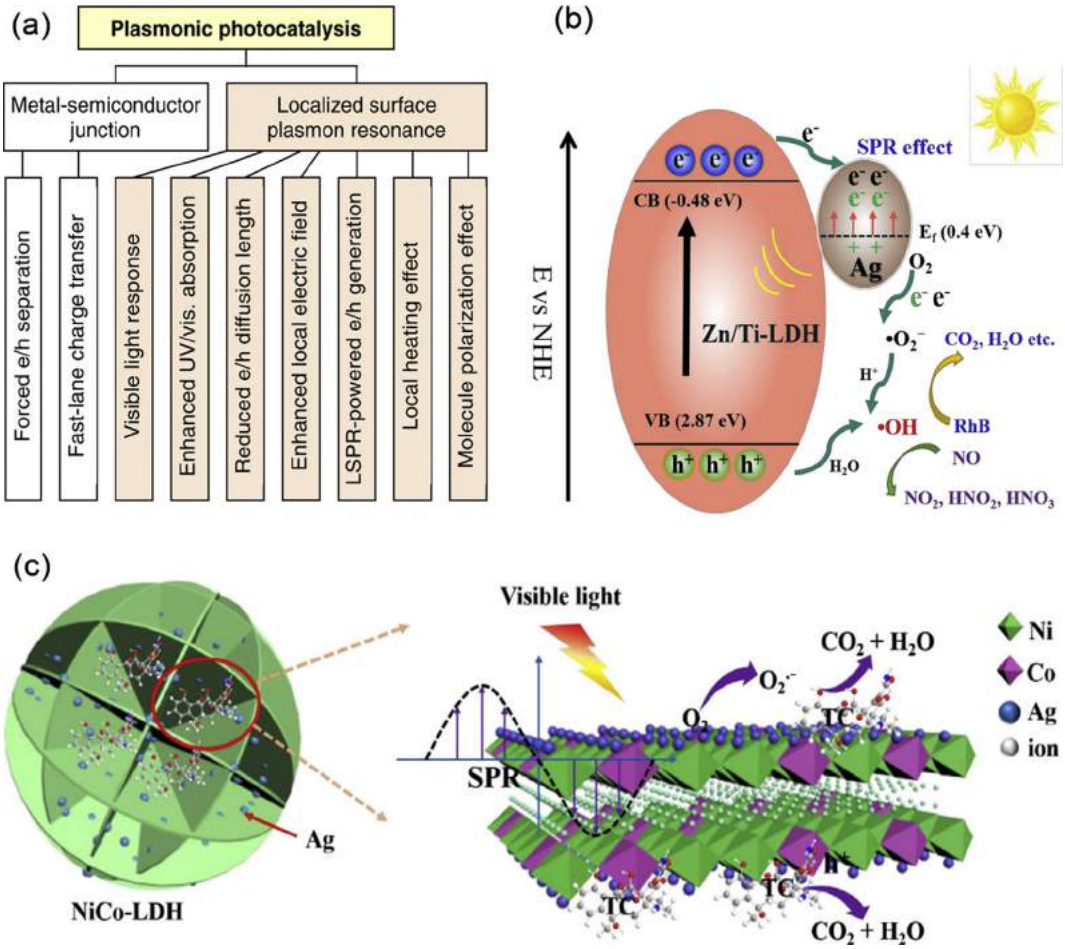

Fig. 14 – (a) Advantages of Schottky junction and SPR effects on plasmonic photocatalysis [176] (b) schematic diagram of photocatalytic mechanism of Ag loaded ZnTi LDH for the degradation of NO and RhB [64] (c) photocatalytic mechanism of Ag/NiCo-LDH [179].

Plasmonic material which is attributed to the surface plasmonic resonance and Schottky barrier, are two primary elements when designing a metal loading semiconductor [173]. The advantages of Schottky junction and SPR effects on plasmonic photocatalysis is denoted in Fig. 14 (a). Schottky barriers are formed when a noble metal and semiconductor in closed contact. There is a built-in internal electric field in a region between the semiconductor-metal interfaces. The emergence of the internal electric field facilitates the migration of electrons and holes in different directions once it emerges near the Schottky junction [174]. Additionally, the metal region will be served as electron trapping to provide more active sites for the photoreactions [175]. Hence, the Schottky barrier could suppress the electron-hole recombination and prolong the lifetime of the photoinduced charges. Another notable feature exhibited by the noble metal is the localised surface plasmon resonance, representing the strong oscillation of the metal's free electrons in phase with the varying electric field of the incident light [176]. SPR could improve and broaden the light absorption spectrum towards visible light, especially in the low band gap photocatalyst. Besides, SPR aid in prolonging the exciton time, expedites the redox reaction rate and the mass transfer. In the photocatalysis system, noble metals received considerable attention mainly due to the induced SPR absorption and Schottky barrier [176]. For instance, Li et al. disclosed the synergistic effect between the noble metal such as Ag, Au, Pt, and Pd with the semiconductor metal oxide (TiO_2@ZnO) [177]. It was observed that all the hybrid noble metal-metal oxide photocatalyst shows a positive result. However, the incorporation of Ag and Au on the TiO_2@ZnO photocatalyst has shown an astounding result compared to other noble metals in which the light absorption was shifted to the highest extend.

Generally, pristine LDH exhibits weak solar to energy conversion, limiting their role as a prime photocatalyst for the water-splitting process. In order to improve the solar conversion efficiency of the LDH based photocatalyst, Zhu et al. fabricated a noble metal-modified LDH by loading Ag on the surface of the ZnTi LDH with different percentage loading (0, 1, 2, and 3 wt %)) [64]. The mechanism of electron transferring and trapping is denoted in Fig. 14 (b). Based on the UV–vis diffuse reflectance spectrum, the addition of Ag on the surface of the ZnTi LDH successfully shifted the absorption spectrum from the UV region to the Visible region (500–600)

nm. It was firmly believed that the SPR effect of the Ag NP could amplify the absorption of the visible light resulting in the remarkable photocatalytic degradation of RhB and NO. In another study, Tonda et al. decorated Ag NP with NiAl-LDH/g-C_3N_4 photocatalyst through in situ hydrothermal methods [178]. The synergistic combination of Ag with NiAl-LDH/g-C_3N_4 resulting in an exceptional photocatalytic activity than pure g-C_3N_4 and pristine NiAl-LDH. The results demonstrated the significance of Ag NP in promoting the electron transfer and facilitate the separation. Similarly, Wang et al. reported that the incorporation of Ag NP into NiCo-LDH enhanced photocatalytic performances. The lower PL intensity was observed in Ag/NiCo-LDH photocatalyst, which indicates an excellent electrical conductivity and induced SPR effect highly attributed to the facile separation of electron-hole pairs [179].

A very recent report by Zhu et al. on the synergistic interaction of Ru with MgAl-LDH revealed that the introduction of metal support promotes high photocatalytic activity and selectivity [180]. Note that the selection of semiconductor support is significant for the metal dispersion and stabilizer. The use of Ru species with suitable semiconductor support could maximize the atom efficiency, and the Ru coordination can be tuned to expose the base sites at the surface, preventing the addition of extra bases. In different studies, Carja et al. have developed a series Au loaded LDH to study the effects of noble metal loading on the photocatalytic hydrogen performances of bimetallic Au/ZnAl LDH and trimetallic Au/ZnCeAl LDH [181]. It was revealed that the presence of the third element Ce, is responsible for the higher catalytic activity of the LDH-based composite. The composite of Au/ZnCeAl LDH successfully generates 1.35 fold higher hydrogen than the composite of Au/ZnAl LDH with the same percentage loading of Au. However, both composite shows a positive hydrogen increment than without the incorporation of Au. It was pointed out that the size of Au NP could affect the catalytic performances of the composites. This is because larger Au NP could lead to a lower number of joint active sites between Au and the support, resulting in lower photocatalytic efficiency. Besides, it was also remarked that the lower the specific surface area of Au NP, the lower the photocatalytic hydrogen efficiency of the composites. On the other hand, Au loading on the composite $CaFe_2O_4$/CoAl LDH by Das et al. revealed a higher hydrogen generation than those reported by Carja et al. It was disclosed that the hydrogen generation by Au@$CaFe_2O_4$/CoAl LDH soaring up to 379.1 μmol $g^{-1}h^{-1}$. Higher photocatalytic efficiency was attributable to the confinement effects induced by Au NP, assisting the transport of electrons. The negative shifting in the binding energy of Au observed through the XPS spectra highly indicate that the electrons were transferred from the surface of Au to the heterojunction surface, promoting photocatalytic activity. It was noticed that Au deposition resulted in a well-maintained crystal structure of the composite. Besides, it was further noted that the good interaction between CoAl LDH and Au, preventing the sintering of the metal and hexagonal structure of LDH, provide strong support for Au deposition.

Additional studies by Wang et al. on the decomposition of formaldehyde using Pt/NiFe-LDH/rGO revealed that the hierarchical honeycomblike structures could efficiently degrade the formaldehyde. This is associated with the better dispersion of NiFe LDH with rGO and the addition of noble metal Pt enhancing the photocatalytic performances [182]. Even though the use of noble metal in photocatalysis has proven to show an outstanding photocatalytic performance, the scarcity and high cost of the noble metal limit their industrial commerciality [183]. Therefore, studies have been conducted

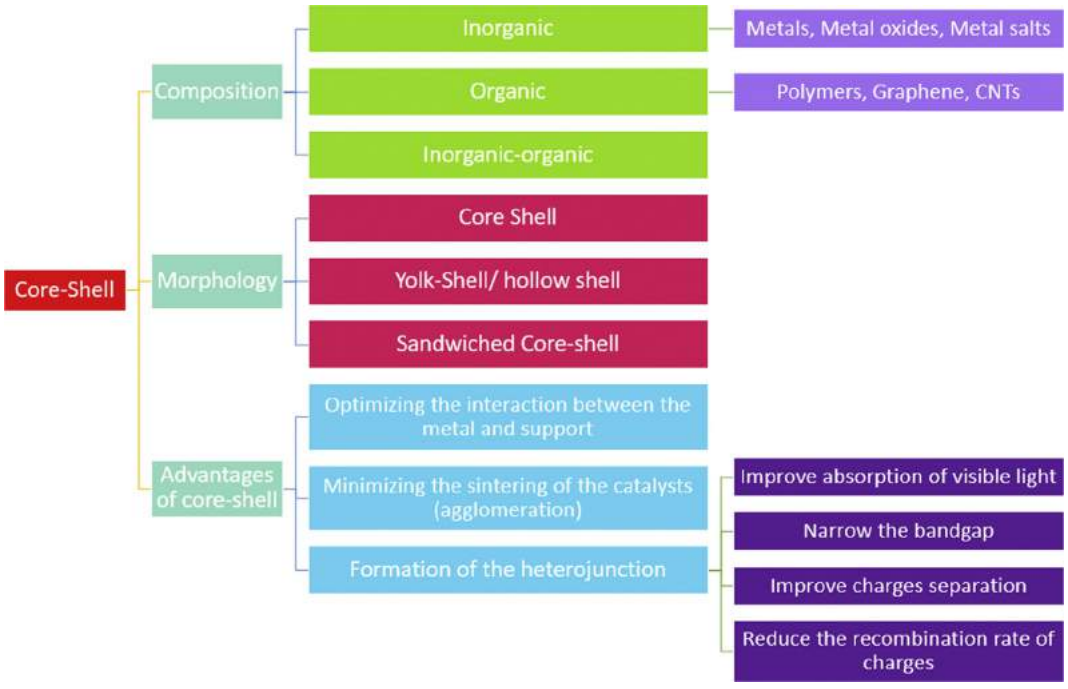

Fig. 15 – Overview of core-shell photocatalyst in terms of the composition, morphology and its advantages.

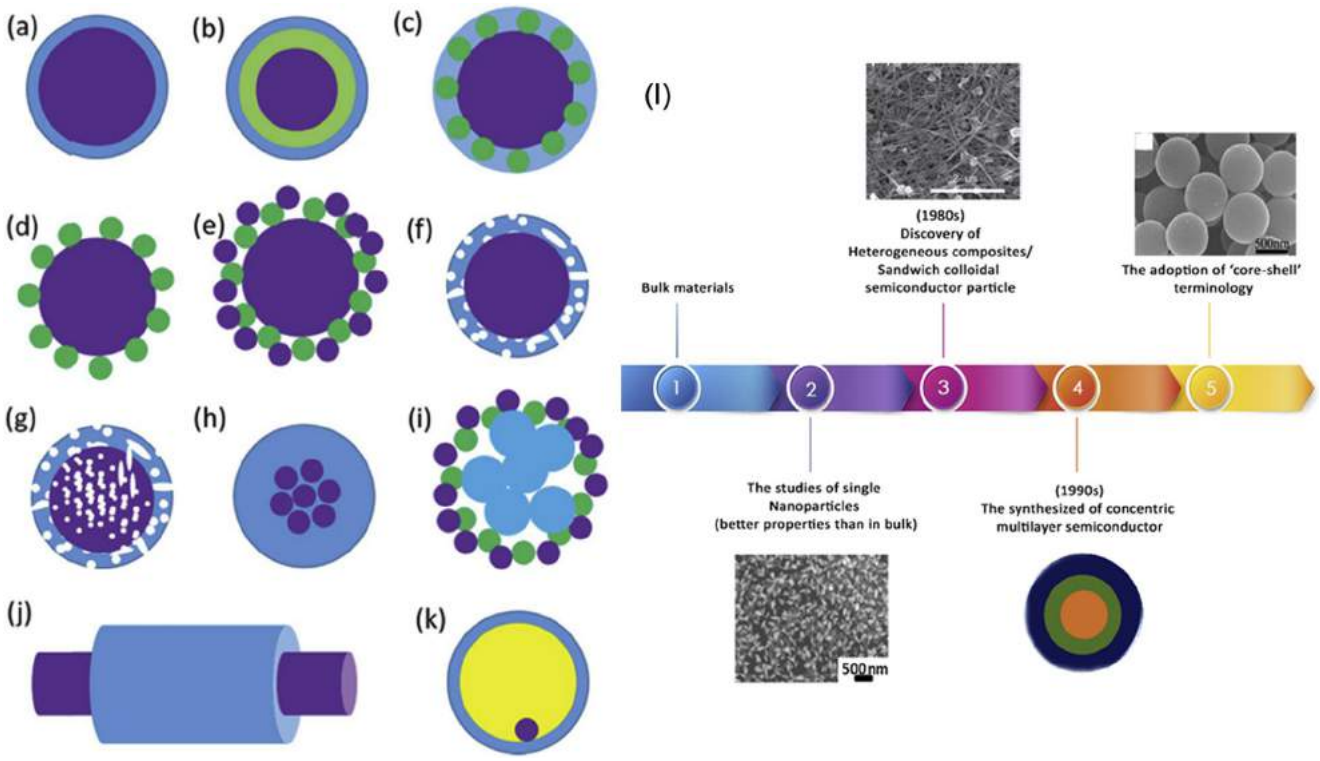

Fig. 16 – Various morphological designs of core-shell nanostructures (a) core as a single sphere, (b) core with multiple concentric shells, (c) shell incorporated with smaller spheres, (d) shell in the form of identical smaller spheres, and (e) shell in the form of different spheres, (f) solid core and porous shell, (g) core–shell both porous, (h) multiple spherical cores, (i) multiple cores covered by shell formed by several small spheres, (j) core–shell fiber, and (k) yolk–shell morphology shows a movable core within a hollow shell [200] (l) chronological development of the single photocatalyst to the core-shell structure.

to replace the noble metal with the same functioning low-cost metal. Some promising noble-free metal features the same characteristics as noble metals, including Cr, Mn, Fe, Co, and Ni. The utilization of MXene from the family of MAX phases successfully induced an excellent photocatalytic activity and even superior to those by the noble metals [184,185]. Besides, employing noble free metal such as Mn has also shown a positive contribution in augmenting the photocatalytic activity of LDH-based composite. For instance, Mendoza et al. have developed a noble free metal Mn–Zn/Al LDH to study 4-chlorophenol photodegradation [186]. They have remarked that the incorporation of metallic Mn inducing an excellent photocatalytic activity. However, they also disclosed that 1% maximum of Mn content could be incorporated onto the LDH photocatalyst. Additionally, increasing the Mn content by more than 1% is not possible in this case as the instability of Mn to form an oxide [187]. However, with an appropriate content of Mn, the LDH crystalline structure could be preserved, and the physicochemical and photocatalytic properties are improved. Therefore, after scrutinizing the available literature, it was apparent that the studies of metal loading LDH in photocatalytic hydrogen production are minimal. However, it was noticed that the composite of Au@$CaFe_2O_4$/CoAl LDH by Das et al. yields the best catalytic activity. It was mainly due to the incorporation of noble metal Au expediting the transfer of electrons in the composite. Besides, LSV analysis confirming that CB of LDH can easily trap the hot electron from Au NP thus facilitating water splitting reaction.

Novel core-shell nanocomposite

Hybrid core-shell photocatalyst shows a constructive development over decades due to its significant advantages. The fabrication of core-shell nanostructure could improve the physicochemical properties and functionality of the photocatalyst [188]. Compared to the single element photocatalyst, the development of hybrid core-shell structure depicts the revamped advancement of the composite materials in terms of unique chemical composition, optical performances, and electronic properties. Core-shell nanomaterials offer great functionality in various fields such as photocatalysis, energy storage, optoelectronics, and bionanotechnology. Fig. 15 depicts the overview of the development in the core-shell nanomaterials.

The fabrication of the core-shell nanocomposites could optimize the contact efficiency in between the metal and support, minimising sintering effects (agglomeration) of nanoparticles. In this context, the photochemical efficiency will be greatly enhanced through the unique combination of morphological contact and heterojunction. It was highly

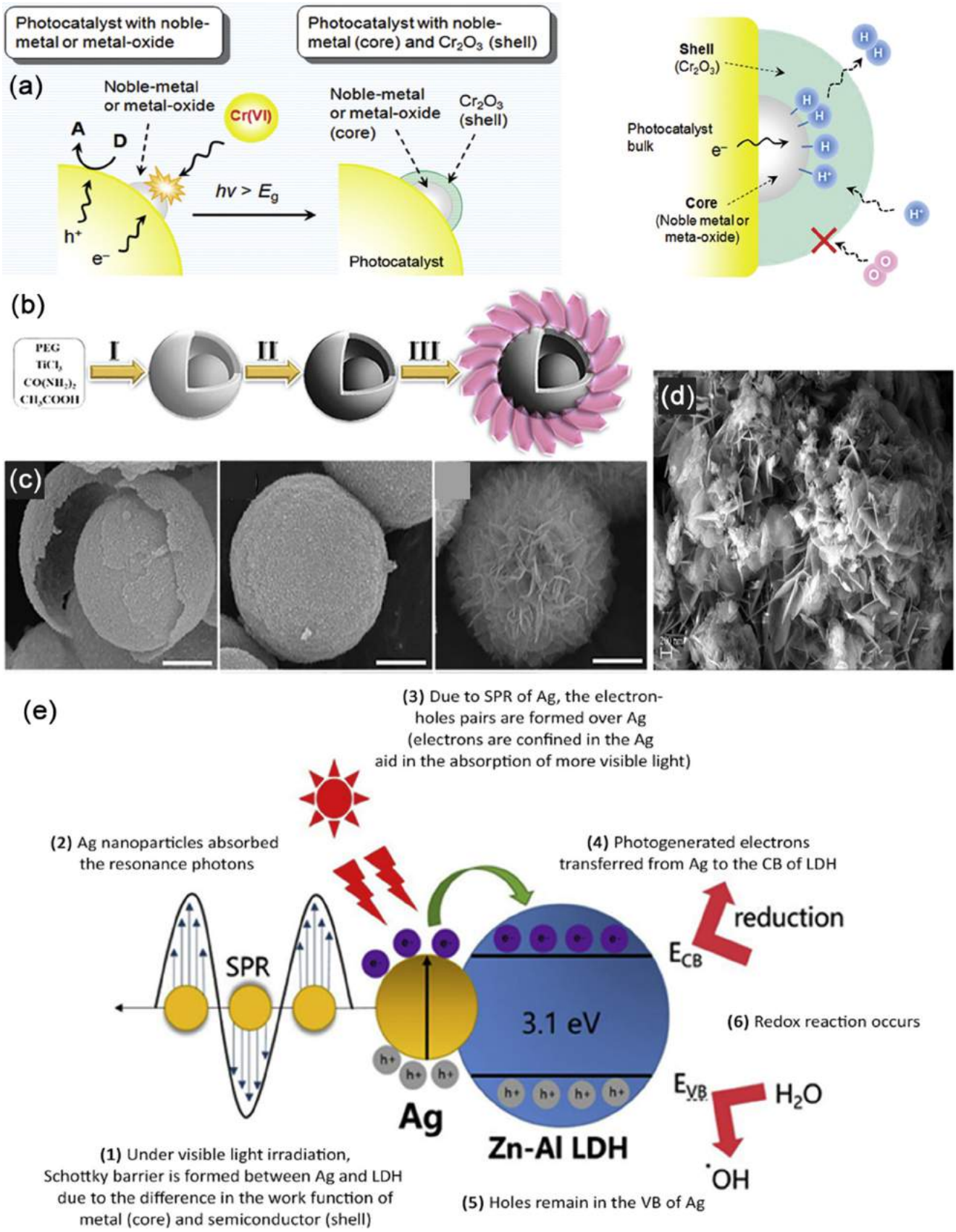

Fig. 17 – (a) Schematic illustration of H_2 evolution on noble metal/metal oxide core and Cr_2O_3 shell structured nanoparticles [213] (b) Overall flowchart for the fabrication of 3D York-Shell TiO_{2-x}/LDH architecture (c) SEM images of the 3D York-Shell TiO_{2-x}/LDH [208] (d) SEM image of the core-shell Ag/ZnAl LDH (e) schematic illustration of the Ag/ZnAl LDH core-shell photocatalytic mechanism [211].

noted that the formation of the interface between the core and the shell could narrow the band gap [189], enhance the absorption of visible light, provide a transfer pathway for the photogenerated charges [190], and reduce the recombination rate of the electrons-holes [191]. Core-shell semiconductors theoretically are nanoscales assemblies with the difference in the chemical composition between the shell and the core region [192].

Core-shell nanocomposites were mainly fabricated into a spherical form [193] and nanorods/nanowires [188,194]. However, according to Gosh et al., the advancement in the core-shell nanostructure's fabrication technique has led to the development of various architectural designs and shapes of the core-shell nanocomposites. Fig. 16(a–k) illustrated the various morphological designs of the core-shell nanostructure. Chronologically, the core-shell hybrid photocatalyst construction started with the blooming of the single nanoparticle semiconductors, having a better photochemical property than their bulk counterparts. The evolution of the nanoparticles in the late 1980s led to the discovery of heterogeneous or composite semiconductors with better efficiency than preceding single nanoparticle semiconductors. Later in the 1990s, researchers synthesized a multilayer semiconductor with an improved optical and electronic properties leading to the adoption of "core-shell" terminology [195]. Since then, the core-shell hybrid semiconductors have been tremendously studied, and many improvements have been made to this class of semiconductors to improve their performances, especially in photocatalytic water splitting [196–199]. Fig. 16 (l) shows the chronological development of the single nanoparticle photocatalyst to the core-shell structure.

Core-shell nanoparticles are divided into two types, which were differentiated based on the band offset. Typically, in the type-I core-shell nanoparticles, the electrons-holes are confined in the cores. As a result, the shell having higher CB and lower VB energy than that of the core. There is an opposite difference in the band energy of either the shell or the core. In contrast, the type-II core-shell structures have both the VB and CB energy in the core higher or lower than those of the shell. Hence, the electrons and the holes are separated between the core and the shell. This makes type-II core-shell nanoparticles fundamentally favoured due to increased separation between the charge carriers and the exciton lifetime [201]. In terms of the synthesis of the core-shell structure, different methods have been developed over the years. However, "bottom-up" techniques are substantially favoured even though the fabricated designed can be achieved through the "top-down" method. In the bottom-up method, the core and the shell can be synthesized in a stepwise or one-pot fashion that combines several steps into one. The materials are synthesized from their basic units, which depends on their intrinsic chemical properties, allowing optimal control over their shape and size [191,202].

The core-shell structure is typically composed of metal cores such as Zn, Cu, Au, Ag, Pt, Pd, Ni, and Fe wrapped with semiconductor metal oxides as the shell such as ZnO, TiO_2, SnO_2, Cu_2O, Fe_2O_3, and SiO_2. However, the fabricated core and the shell can also be composed of different materials such as organics, inorganics, and inorganic-organic [203]. The synergistic combination of core-shell nanoarchitecture promotes a higher photocatalytic efficiency, improves their optical properties and photostability [200]. Note that the thickness of the core-shell structure significantly affects the photocatalytic performances in which it controls the effective band gap through quantum confinement effects [201]. The thickness of the designed photocatalyst's core-shell structure influences their optical, electrical, and photocatalytic properties, directly affecting their photocatalytic water splitting performances [204]. Niu et al. fabricated a hybrid Ta_3N_5@PANI core-shell photocatalyst and observed that the polyaniline's shell thickness (PANI) dramatically affects the hydrogen production yield. They disclosed that the monolayer of the shell photocatalyst (PANI) could improve the separation of photoinduced charges and provide a better electron transfer between the shell and the core of Ta_3N_5 [205]. Fig. 17 (a) illustrated the H_2 evolution on noble metal/metal oxide core and Cr_2O_3 shell structured nanoparticles.

Hybrid core-shell LDH structures usually exhibit superior photocatalytic performances than their intrinsic structures [206,207]. LDH suffered from difficult adjustments over their structural, architectural, and morphological properties, minimising their photocatalytic solar conversion efficiency. Therefore, finding a suitable electron acceptor and developing a core-shell LDH photocatalyst are the critical factors in escalating the charge separation and photocatalytic performances [208]. Recently, Wang et al. constructed a hybrid core-shell (CoO/NiCo-LDH) in the form of a core-shell nanowire. They observed that the electrons from the core (CoO) could efficiently be transferred to the shell (NiCo-LDH) nanosheet due to the effective interface between both CoO and NiCo-LDH [82]. This resulting in higher separation efficiency and prolong the charge carriers lifetime. The electrons are confined on the surface of NiCo-LDH and then undergoing a reduction reaction to generate 1500 $\mu mol\ g^{-1}h^{-1}$ of hydrogen yield. In another study, Ziarati et al. developed another type of core-shell photocatalyst by integrating TiO_2 with CoAl-LDH forming an oxygen vacancy "yolk-shell" structure [208]. The fabrication of yolk-shell LDH structure assembled by sequential solvothermal, hydrogen treatment, and hydrothermal preparation steps revealed a high photoreduction efficiency without a noble metal co-catalyst. The void space is shown in Fig. 17 (b) and (c) could be served as a nanoreactor resulting in effective diffusion of any solvents or substrates into the porous surfaces. The unique architecture of this 3D mesoporous yolk-shell with oxygen vacancy could enhance the photostability, absorption of the light spectrum and increase the solar energy conversion. The oxygen vacancies (Vo) in metal oxides could improve the electron donor density and electrical conductivity, acting as an electron acceptor to reduce the recombination rate of the photoinduced charges [209].

The fabrication of the metal core and semiconductor shell nanocomposites provides significant advantages as it could improve the stability against the aggregation, increase the corrosion resistance of the nanocomposites and eliminate unwanted dissolution in practical reactions. Furthermore, the noble metal core could act as electron trapping and increase the lifetime of the photoinduced charges, which directly enhance the overall photocatalytic efficiency [177,210]. For instance, Li et al. designed an inorganic metal core (Ag) with

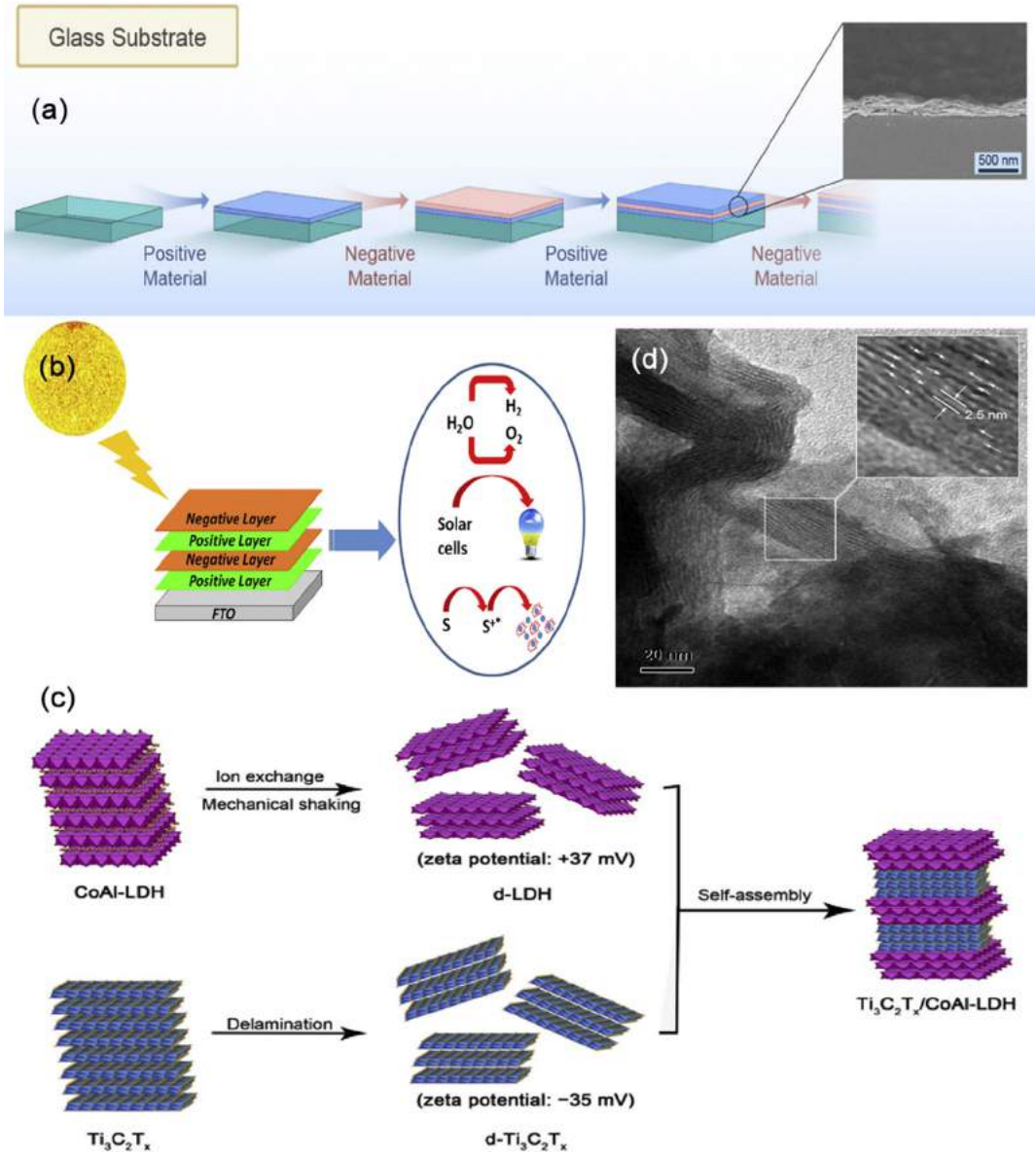

Fig. 18 – Schematic illustration of (a) LBL assembly on the glass substrates [220] (b) LBL assembled photocatalysts for the solar energy conversion [221] (c) the synthesis process of the LBL multi-sheet of Ti_2C_2T/CoAl LDH [223] (d) HRTEM image of CdS/ZnCr-LDH (white arrows indicate the CdS pillars between the host sheets) [95].

an inorganic semiconductor shell (ZnAl LDH) to study the photocatalytic activity of the hybrid nanocomposites [211]. They disclosed that the enhancement of the photocatalytic activity was primarily attributed to the formation of the Schottky barrier between the noble metal Ag and ZnAl LDH and the surface plasmon resonance effect of the Ag nanoparticles. The SEM image of Ag/ZnAl LDH is represented in Fig. 17 (d), and the mechanism of the electrons transfer pathway was illustrated as in Fig. 17 (e). Recently, Yang et al. studied the formation of direct Z-scheme heterojunction in a metal-oxide-semiconductor core-shell structure of CoAl-LDH with Cerium oxide [212]. It was highlighted that the built-in electric field across the CeO_2 and the LDH assist the efficient migration of the charge carriers in the Z-scheme heterojunction, improving the overall photocatalytic efficiency. The development of the Z-scheme core-shell nanostructures was proven to improve physical and chemical stability, increase more exposed actives sites, and provide a spatial separation.

It can be disclosed that the fabrication of core-shell LDH-based composite needed comprehensive studies to address their efficiency in photocatalytic hydrogen production. Additionally, there is a lack of studies that focus on improving the photocatalytic activity in LDH-based composite through morphological and architectural tuning. However, the construction of hybrid core-shell CoO/NiCo-LDH by Wang et al. gain scientific interest due to the high photocatalytic activity exhibit by the composite. This unique hybrid composite does

not only induced a higher crystallinity structure and purity but possesses a large surface area. Furthermore, the deposition of NiCo LDH as a shell wrapping the CoO provides abundant catalytic active sites for enhancing the redox reaction. Besides, the dispersion of active metal Ni and Co on LDH is responsible for excellent solar utilization and outstanding photocatalytic hydrogen production.

Self-assembly layer-by-layer LDH nanosheets

Layer-by-layer (LBL) is the technique for the fabrication of LDH nanosheet film, in which the sheets are stacked together to form a multilayer film. LBL assembly has attracted fundamental and technological viewpoints due to its simplicity and low-cost equipment, providing a photoactive surface for film fabrication [214]. Besides, the film thickness can be controlled at molecular and nanometric scales through LBL assembly. Generally, the LDH film will be deposited onto various substrates and other surface materials to form a hybrid LDH. After delamination, positively-charged LDH nanosheets can be a good model system in the LBL assembly to construct various nanocomposites [215].

The assembly of LBL is based on several types of driving forces. This includes electrostatic force [216], covalent bonding [217], hydrogen bonding [218], coordination bonding [219] and charge interaction. Most of the studies reported on the LDH LBL were based on the electrostatic driving force assembly known as electrostatic self-assembly (ESA). The basic principles for the ESA LBL for the LDH, schematically illustrated as in Fig. 18(a–c); 1) The solid substrate is immersed into the solutions containing anionic polymer; 2) The negatively-charged polymer is adsorbed to the surfaces of the positively-charged substrate due to the strong electric field; 3) The substrate coated with the anionic polymer is then exposed to the positively-charged exfoliated LDH nanosheet; 4) The layer is formed when the substrate's charges become saturated, resulting in the charge compensation; 5) Adsorption ends when the charge of the substrate is reversed [220,221]. Some of the polyanionic charged species usually act as a building block for the LBL assembly of LDH includes poly (styrenesulfonate) (PSS) [216], poly (vinylsulfate) (PVS) and polyacrylic acid (PAA) [222].

In the context of the development in LDH hybrid through LBL assembly, Gunjakar et al. first developed LBL-ordered nanohybrids composed of two inorganic 2D nanosheets, a positively charged ZnCr-LDH with negatively charged layered titanate nanosheets [154]. They observed the improvement in terms of chemical stability and visible light absorption. Note that the highly porous hybrid structure could be formed from the ESA between the two inorganic nanosheets in which the porosity can be controlled by tuning the ratio of both individual components. Even though this LBL-hybrid structure exhibits remarkable optical properties, yet the hydrogen production yield is still low. This might be due to the low photocatalytic activity observed in ZnCr-LDH, as reported by Zhang et al. [97]. However, in terms of morphological improvement, this composite structure exhibit more efficient structural organisation. The formation of mesoporous LBL structure of LDH significantly contributes to a higher photocatalytic activity. It was denoted that materials with mesoporous structure exhibit large surface area and high surface pore, which provide more adsorption and active sites for the photocatalytic reaction [60]. Besides, assembling two sheet-like crystals layer-by-layer contributes to many exposed catalytic active sites and effectively promotes the catalytic reaction. The more ordered hybrid structure facilitates the transfer of electron-hole towards the catalytic site thereby, increasing the separation efficiency. Furthermore, the difference in the surface charges of layered titanate and LDH enable them to form a strong electronic coupling and improve the physical contact. Additionally, increasing the strong electronic contact between the semiconductors promotes spatial separation and inhibit the recombination of the photoinduced charges.

In another study, LDH has been developed into a CdS-pillared ZnCr-LDH nanohybrid. This is done by assembling the CdS nanoparticles into the interlayer of ZnCr-LDH through ESA [95]. It was observed that the pillared nanohybrids exhibit an increase in the surface area ($86\ m^2\ g^{-1}$) compared to its pristine structure ($33\ m^2\ g^{-1}$) and forming 'the house-of-cards type stacking, correspond to those reported by Gunjakar et al. as shown in Fig. 18 (d). This highly mesoporous nanohybrid having an astounding photocatalytic activity with the generation of hydrogen of 374 $\mu mol\ g^{-1}h^{-1}$. It was highly suggested that the construction of the hybrid LDH through LBL assembly could improve the hybrid photocatalyst morphology, increase the solar light conversion, and enhance the photocatalytic of hydrogen generation. However, selecting suitable assembling substrates and paired semiconductors should be taken into account to ensure the high efficiency of the hybrid photocatalyst. The study of LDH hybrid LBL opens new routes in promoting a higher photocatalytic activity through morphological and structural tuning. The unique formation between the positively-charged and negatively-charged semiconductors layers facilitate a strong electronic contact. This subsequently fosters the transfer of photoinduced charges between the semiconductors. Therefore, it can be summarised that constructing a layer-by-layer LDH through ESA, could generate a unique house-of-cards-type structure with good light-harvesting ability, high porosity structure and provide good electronic contact between the semiconductors.

Conclusion and future recommendations

The depletion and the scarcity of fossil fuels have become major concerns as their utilization has reached almost the maximum of global energy demand. Photocatalytic hydrogen production by layered double hydroxide has been considered as one of the best alternatives to provide sustainable and renewable energy sources. It was highly denoted that enormous efforts have been directed to develop a highly efficient LDH-based photocatalyst. It was revealed that higher photocatalytic efficiency is not only dependent on the heterojunction type but also the synergy between light intensity, design of photoreactor, and sacrificial reagents used. Nevertheless, the type of heterojunction constructed could play a significant role in expediting the performances of LDH based composites. For instance, Z-scheme heterojunction system

inducing strong redox capabilities compared to those of type II might be the leading attribution for the increased in photocatalytic activity. From the thermodynamics viewpoint, the construction of Z-scheme system could preserve the electrons/holes with higher redox potential by sacrificing the non-effective electron-hole pairs. These electron-hole pairs will be eradicated at the VB of reducing photocatalyst and CB of oxidation photocatalyst thus, inducing a stronger redox reaction. Besides, the synergistic integration inherently improve the overall photocatalytic efficiency through the following aspects: 1) the presence of oxygen vacancies hinder the recombination of photogenerated charges and improve electrical conductivity, 2) trivalent metal ion of LDH, promotes the shifting of the absorption range towards the visible spectrum, 3) enhancement in photostability associated with the metal-to-metal charge transfer in LDH, 4) higher quantum efficiency of individual LDH (e.h., ZnCr LDH), and 5) the presence of electron mediator e.g., Ag, facilitating the electron transfer and synergistically boost the photocatalytic activity of the composites.

Additionally, the review presented describes the main challenges in photocatalytic water splitting, the hydrogen production mechanism, thermodynamics analysis, and different modifications made on the LDH-based photocatalyst to improve its efficiency. The summary of literature about the modification and future approaches has been presented as follow:

- The formation of heterojunction has been denoted as one of the best ways to overcome the limitations manifested by the pristine LDH. Integrating LDH-based photocatalyst with other metal semiconductors could improve the solar absorption spectrum, expedite the spatial separation of the charge carriers, and boost photocatalytic activity. The selection of the hybrid semiconductor should be given more attention. Details such as the band potential, energy level, work function, band gap width, structural diversity, and the photocatalyst type should be considered when designing a heterojunction system photocatalyst. The mentioned elements positively affect the photocatalytic efficiency also the type of heterojunction that will be constructed.
- The temperature, light, band gap, CB and VB are the critical elements in favouring the water-splitting reaction. It is highly noted that understanding the fundamental of a redox reaction is significant in the photocatalysis field. For a reaction to be thermodynamically stable, the water reduction and oxidation potential should fall within the photocatalyst band gap. The efficiency of the photocatalyst greatly affected by its band gap energy. Therefore, the band gap should be within $1.23\ eV < Eg < 3.26\ eV$ in fabricating a thermodynamically favoured photocatalyst. Besides, the reduction and oxidation potential should not exceed the range of the band gap.
- Core-shell nanomaterials offer great functionality in various fields, and the construction of core-shell nanoarchitecture could optimize the photochemical efficiency of LDH-based photocatalysts. However, the progress towards the application of core-shell structure in LDH-based photocatalyst for photocatalytic hydrogen generation is still limited. The effectiveness of core-shell structure in promoting a higher photocatalytic hydrogen generation is still vague. Thus, more studies needed to be conducted to study the catalytic properties of the core-shell structure. The interconnection between the morphology of the core-shell structure and their effects on photocatalytic performances also needed to be further explored. Besides, while designing the core-shell nanostructures, aspects needed to be considered are the composition and heterojunction formation between the shell and the core, the morphology of the LDH hybrid nanostructure, and the shell's thickness which will positively affect the photocatalytic of hydrogen production.
- Metal-loaded LDH is associated with the formation of the Schottky barrier and surface plasmon effect. The integration of plasmonic materials onto the LDH based photocatalyst could enhance photocatalytic hydrogen production. The Schottky barrier serves as an electron trapping site to augment the photo-induced charges migration and prolong the exciton time. Meanwhile, SPR effect by the noble metal aid in shifting the solar absorption towards the visible spectrum. Despite the advantages of the noble metal and its role in boosting photocatalytic performances, the high prices and scarcity of the materials limiting its application and commerciality. Thus, a rigorous investigation is needed on the noble-free metal that exhibits the same functionality as the noble metal but is more affordable and abundant. Employing MXenes from the family of MAX phase to substitute the noble metals should be given full consideration. MXenes have been reported to exhibit great functionality over various technological applications due to their noble metal-like characteristics. They are highly sought after due to their abundancy, cost-affordability and excellent optical properties. Besides, higher conductivity and unique compositional configuration in MXenes could substantially drive the solar absorption towards the visible spectrum. They could also serve as electron trapping sites, thus maximizing the separation and inhibiting the recombination of photogenerated charges in LDH-based composite.

Besides, future perspectives on LDH photocatalyst has been deliberated to render them a notable place in photocatalytic hydrogen production.

- Maintaining a higher crystallinity and broken the aggregation in the LDH nanosheet is still a major challenge. Controlling the compositional constitution of the divalent and trivalent metal ions in the LDH photocatalyst was observed to enhance its crystallinity structure. Different synthesis techniques were reported to develop LDH with different crystallinity structure. Future development on the synthesis procedure that could provide LDH with a higher crystallinity structure should be given attention. Furthermore, theoretical and analytical analysis on characterizing the crystal structure of LDH should be deeply studied. This is to give fundamental explication on the crystallography of LDH, which could be beneficial for enhancing their structural properties.

- Theoretical understanding of the photocatalytic mechanism of LDH is still indistinct with less computational analysis supporting the inter-relation between the changes in the coordination of the hydroxide layers, compositional factors of divalent and trivalent ions and the electronic band structure upon photocatalysis.
- LDH containing active transitional species such as Ni, Cu, Co and Cr shows excellent photostability and higher photoactivity over other metals institutions. Therefore, future investigation based on the theoretical modelling should be given attention to studying the effect of each metal constitutions not only on bimetallic and trimetallic LDH, but attention should be focused on constructing tetrametallic LDH with how configuring each metal elements affecting the lattice of LDH, the chemical ordering and stability. Besides, the diffusion mechanism of the intercalated ions at the interlayer, their interaction with the brucite layers in LDH and their effects on catalytic reaction should be elucidated through more computational evidence.

Declaration of competing interest

The authors declare that they have no known competing financial interests or personal relationships that could have appeared to influence the work reported in this paper.

Acknowledgements

The authors would like to extend their most profound appreciation to Ministry of Higher Education (MOHE), Malaysia for this work financial support under Fundamental Research (FRGS, R.J130000.7851.5F384).

REFERENCES

[1] Yan T, Liu H, Jin Z. g-C_3N_4/α-Fe_2O_3 supported Zero-dimensional Co_3S_4 nanoparticles form S-scheme heterojunction photocatalyst for efficient hydrogen production. Energy Fuels 2020;35(1):856–67.
[2] Sun W, Meng X, Xu C, Yang J, Liang X, Dong Y, Dong C, Ding Y. Amorphous CoO coupled carbon dots as a spongy porous bifunctional catalyst for efficient photocatalytic water oxidation and CO_2 reduction. Chin J Catal 2020;41(12):1826–36.
[3] Jiang X, Gong H, Liu Q, Song M, Huang C. In situ construction of NiSe/$Mn_{0.5}Cd_{0.5}S$ composites for enhanced photocatalytic hydrogen production under visible light. Appl Catal B 2020;268:118439–49.
[4] Umer M, Tahir M, Usman Azam M, Tasleem S, Abbas T, Muhammad A. Synergistic effects of single/multi-walls carbon nanotubes in TiO_2 and process optimization using response surface methodology for photo-catalytic H_2 evolution. J Environ Chem Eng 2019;7(5):103361–73.
[5] Zhao Y, Lu Y, Chen L, Wei X, Zhu J, Zheng Y. Redox dual-cocatalyst-modified CdS double-heterojunction photocatalysts for efficient hydrogen production. ACS Appl Mater Interfaces 2020;12(41):46073–83.
[6] Zhao J, Fu B, Li X, Ge Z, Ma B, Chen Y. Construction of the Ni_2P/MoP heterostructure as a high-performance cocatalyst for visible-light-driven hydrogen production. ACS Appl Energy Mater 2020;3(11):10910–9.
[7] Tao J, Yu X, Liu Q, Liu G, Tang H. Internal electric field induced S-scheme heterojunction MoS_2/CoAl LDH for enhanced photocatalytic hydrogen evolution. J Colloid Interface Sci 2021;585:470–9.
[8] Tasleem S, Tahir M, Zakaria ZY. Fabricating structured 2D Ti_3AlC_2 MAX dispersed TiO_2 heterostructure with Ni_2P as a cocatalyst for efficient photocatalytic H_2 production. J Alloys Compd 2020;842:155752–70.
[9] de_Richter R, Caillol S. Fighting global warming: the potential of photocatalysis against CO_2, CH_4, N_2O, CFCs, tropospheric O_3, BC and other major contributors to climate change. J Photochem Photobiol, C 2011;12(1):1–19.
[10] Zhang D, Cao W, Mao B, Liu Y, Li F, Dong W, Jiang T, Yong Y-C, Shi W. Efficient 0D/2D heterostructured photocatalysts with Zn-$AgIn_5S_8$ quantum dots embedded in ultrathin NiS nanosheets for hydrogen production. Ind Eng Chem Res 2020;59(37):16249–57.
[11] Wang G, Li Y, Xu L, Jin Z, Wang Y. Facile synthesis of difunctional NiV LDH@ZIF-67 p-n junction: serve as prominent photocatalyst for hydrogen evolution and supercapacitor electrode as well. Renew Energy 2020;162:535–49.
[12] Ombaka LM, Curti M, McGettrick JD, Davies ML, Bahnemann DW. Nitrogen/carbon-coated Zero-valent copper as highly efficient Co-catalysts for TiO_2 applied in photocatalytic and photoelectrocatalytic hydrogen production. ACS Appl Mater Interfaces 2020;12(27):30365–80.
[13] Zhang L, Li L, Sun X, Liu P, Yang D, Zhao X. ZnO-layered double Hydroxide@Graphitic carbon nitride composite for consecutive adsorption and photodegradation of dyes under UV and visible lights. Materials 2016;9(11):1–16.
[14] Jing D, Guo L. Efficient hydrogen production by a composite CdS/mesoporous Zirconium titanium phosphate photocatalyst under visible light. J Phys Chem C 2007;111:13437–41.
[15] Bao N, Shen L, Takata T, Domen K. Self-templated synthesis of nanoporous CdS nanostructures for highly efficient photocatalytic hydrogen production under visible light. Chem Mater 2008;20:110–7.
[16] Umer M, Tahir M, Azam MU, Jaffar MM. Metals free MWCNTs@TiO_2@MMT heterojunction composite with MMT as a mediator for fast charges separation towards visible light driven photocatalytic hydrogen evolution. Appl Surf Sci 2019;463:747–57.
[17] Shehzad N, Tahir M, Johari K, Murugesan T, Hussain M. A critical review on TiO_2 based photocatalytic CO_2 reduction system: strategies to improve efficiency. J CO_2 Util 2018;26:98–122.
[18] Kandiel TA, Dillert R, Robben L, Bahnemann DW. Photonic efficiency and mechanism of photocatalytic molecular hydrogen production over platinized titanium dioxide from aqueous methanol solutions. Catal Today 2011;161(1):196–201.
[19] Azam MU, Tahir M, Umer M, Jaffar MM, Nawawi MGM. Engineering approach to enhance photocatalytic water splitting for dynamic H_2 production using La_2O_3/TiO_2 nanocatalyst in a monolith photoreactor. Appl Surf Sci 2019;484:1089–101.
[20] Chen W-T, Jovic V, Sun-Waterhouse D, Idriss H, Waterhouse GIN. The role of CuO in promoting photocatalytic hydrogen production over TiO_2. Int J Hydrogen Energy 2013;38(35):15036–48.

[21] Harish S, Archana J, Sabarinathan M, Navaneethan M, Nisha KD, Ponnusamy S, Muthamizhchelvan C, Ikeda H, Aswal DK, Hayakawa Y. Controlled structural and compositional characteristic of visible light active ZnO/CuO photocatalyst for the degradation of organic pollutant. Appl Surf Sci 2017;418:103–12.
[22] Tahir M. La-modified TiO_2/carbon nanotubes assembly nanocomposite for efficient photocatalytic hydrogen evolution from glycerol-water mixture. Int J Hydrogen Energy 2019;44(7):3711–25.
[23] Rives V, Ulibarri MaA. Layered double hydroxides (LDH) intercalated with metal coordination compounds and oxometalates. Coord Chem Rev 1998;181:61–120.
[24] Li X, Yu J, Jaroniec M. Hierarchical photocatalysts. Chem Soc Rev 2016;45(9):2603–36.
[25] Li C, Wei M, Evans DG, Duan X. Layered double hydroxide-based nanomaterials as highly efficient catalysts and adsorbents. Small 2014;10(22):4469–86.
[26] Wu Y, Wang H, Sun Y, Xiao T, Tu W, Yuan X, Zeng G, Li S, Chew JW. Photogenerated charge transfer via interfacial internal electric field for significantly improved photocatalysis in direct Z-scheme oxygen-doped carbon nitrogen/CoAl-layered double hydroxide heterojunction. Appl Catal B 2018;227:530–40.
[27] Silva CuG, Bouizi Ys, Fornés V, García H. Layered double hydroxides as highly efficient photocatalysts for visible light oxygen generation from water. J Am Chem Soc Photocatalysts for Oxygen Generation 2009;131:13833–9.
[28] Zhang G, Zhang X, Meng Y, Pan G, Ni Z, Xia S. Layered double hydroxides-based photocatalysts and visible-light driven photodegradation of organic pollutants: a review. Chem Eng J 2020;392:123684.
[29] Yang Z-z, Wei J-j, Zeng G-m, Zhang H-q, Tan X-f, Ma C, Li X-c, Li Z-h, Zhang C. A review on strategies to LDH-based materials to improve adsorption capacity and photoreduction efficiency for CO_2. Coord Chem Rev 2019;386:154–82.
[30] Song B, Zeng Z, Zeng G, Gong J, Xiao R, Ye S, Chen M, Lai C, Xu P, Tang X. Powerful combination of g-C_3N4 and LDHs for enhanced photocatalytic performance: a review of strategy, synthesis, and applications. Adv Colloid Interface Sci 2019;272:101999.
[31] Dewangan N, Hui WM, Jayaprakash S, Bawah A-R, Poerjoto AJ, Jie T, Jangam A, Hidajat K, Kawi S. Recent progress on layered double hydroxide (LDH) derived metal-based catalysts for CO_2 conversion to valuable chemicals. Catal Today 2020;356:490–513.
[32] Zhao G, Zou J, Chen X, Yu J, Jiao F. Layered double hydroxides materials for photo(electro-) catalytic applications. Chem Eng J 2020;397:125407.
[33] Stamate Pavel, Zavoianu Marcu. Highlights on the catalytic properties of polyoxometalate-intercalated layered double hydroxides: a review. Catalysts 2020;10(1).
[34] Wang L, Zhu Z, Wang F, Qi Y, Zhang W, Wang C. State-of-the-art and prospects of Zn-containing layered double hydroxides (Zn-LDH)-based materials for photocatalytic water remediation. Chemosphere 2021;278:130367.
[35] Yang Z-z, Zhang C, Zeng G-m, Tan X-f, Wang H, Huang D-l, Yang K-h, Wei J-j, Ma C, Nie K. Design and engineering of layered double hydroxide based catalysts for water depollution by advanced oxidation processes: a review. J Mater Chem A 2020;8(8):4141–73.
[36] Cao Y, Jin S, Zheng D, Lin C. Facile fabrication of ZnAl layered double hydroxide film co-intercalated with vanadates and laurates by one-step post modification. Colloids Interface Sci Commun 2021;40:100351.
[37] Mohapatra L, Patra D. Multifunctional hybrid materials based on layered double hydroxide towards photocatalysis. In: Pandikumar A, Jothivenkatachalam K, editors. Photocatalytic functional materials for environmental remediation. John Wiley & Sons, Inc.; 2019. p. 215–41.
[38] Mishra G, Dash B, Pandey S. Layered double hydroxides: a brief review from fundamentals to application as evolving biomaterials. Appl Clay Sci 2018;153:172–86.
[39] Yan K, Wu G, Jin W. Recent advances in the synthesis of layered, double-hydroxide-based materials and their applications in hydrogen and oxygen evolution. Energy Technol 2016;4(3):354–68.
[40] Mallakpour S, Hatami M, Hussain CM. Recent innovations in functionalized layered double hydroxides: fabrication, characterization, and industrial applications. Adv Colloid Interface Sci 2020;283:102216.
[41] Bini M, Ambrogi V, Donnadio A, Di Michele A, Ricci P, Nocchetti M. Layered double hydroxides intercalated with fluoride and methacrylate anions as multifunctional filler of acrylic resins for dental composites. Appl Clay Sci 2020;197:105796.
[42] Tran HN, Lin C-C, Chao H-P. Amino acids-intercalated Mg/Al layered double hydroxides as dual-electronic adsorbent for effective removal of cationic and oxyanionic metal ions. Separ Purif Technol 2018;192:36–45.
[43] Rives V, del Arco M, Martín C. Intercalation of drugs in layered double hydroxides and their controlled release: a review. Appl Clay Sci 2014;88–89:239–69.
[44] Shakeel M, Arif M, Yasin G, Li B, Khan HD. Layered by layered Ni-Mn-LDH/g-C_3N_4 nanohybrid for multi-purpose photo/electrocatalysis: morphology controlled strategy for effective charge carriers separation. Appl Catal B 2019;242:485–98.
[45] Etacheri V, Di Valentin C, Schneider J, Bahnemann D, Pillai SC. Visible-light activation of TiO_2 photocatalysts: advances in theory and experiments. J Photochem Photobiol, C 2015;25:1–29.
[46] Acar C, Dincer I, Zamfirescu C. A review on selected heterogeneous photocatalysts for hydrogen production. Int J Energy Res 2014;38(15):1903–20.
[47] Tahir M, Tasleem S, Tahir B. Recent development in band engineering of binary semiconductor materials for solar driven photocatalytic hydrogen production. Int J Hydrogen Energy 2020;45(32):15985–6038.
[48] Yan X, Jin Z. Interface engineering: NiAl-LDH in-situ derived NiP_2 quantum dots and Cu_3P nanoparticles ingeniously constructed p-n heterojunction for photocatalytic hydrogen evolution. Chem Eng J 2020:127682.
[49] Colón G. Towards the hydrogen production by photocatalysis. Appl Catal A-Gen 2016;518:48–59.
[50] Zamfirescu C, Naterer GF, Dincer I. Photo-electro-chemical chlorination of cuprous chloride with hydrochloric acid for hydrogen production. Int J Hydrogen Energy 2012;37(12):9529–36.
[51] Zamfirescu C, Dincer I, Naterer GF. Analysis of a photochemical water splitting reactor with supramolecular catalysts and a proton exchange membrane. Int J Hydrogen Energy 2011;36(17):11273–81.
[52] Liu B, Zhao X, Terashima C, Fujishima A, Nakata K. Thermodynamic and kinetic analysis of heterogeneous photocatalysis for semiconductor systems. Phys Chem Chem Phys 2014;16(19):8751–60.
[53] Wang Q, Domen K. Particulate photocatalysts for light-driven water splitting: mechanisms, challenges, and design strategies. Chem Rev 2020;120(2):919–85.
[54] Karthikeyan C, Arunachalam P, Ramachandran K, Al-Mayouf AM, Karuppuchamy S. Recent advances in semiconductor metal oxides with enhanced methods for solar photocatalytic applications. J Alloys Compd 2020;828:154281–96.

[55] Anpo M. Photocatalytic reduction of CO_2 with H_2O on highly dispersed Ti-oxide catalysts as a model of artificial photosynthesis. J of CO_2 Utilization 2013;1:8–17.
[56] Bae SW, Ji SM, Hong SJ, Jang JW, Lee JS. Photocatalytic overall water splitting with dual-bed system under visible light irradiation. Int J Hydrogen Energy 2009;34(8):3243–9.
[57] Liu G, Kolodziej C, Jin R, Qi S, Lou Y, Chen J, Jiang D, Zhao Y, Burda C. MoS_2-Stratified CdS-$Cu_{2-x}S$ core-shell nanorods for highly efficient photocatalytic hydrogen production. ACS Nano 2020;14(5):5468–79.
[58] Naldoni A, Altomare M, Zoppellaro G, Liu N, Kment S, Zboril R, Schmuki P. Photocatalysis with reduced TiO_2: from black TiO_2 to cocatalyst-free hydrogen production. ACS Catal 2019;9(1):345–64.
[59] Lin L, Ou H, Zhang Y, Wang X. Tri-s-triazine-Based crystalline graphitic carbon nitrides for highly efficient hydrogen evolution photocatalysis. ACS Catal 2016;6(6):3921–31.
[60] Ding J, Hong B, Luo Z, Sun S, Bao J, Gao C. Mesoporous monoclinic $CaIn_2S_4$ with surface nanostructure: an efficient photocatalyst for hydrogen production under visible light. J Phys Chem C 2014;118(48):27690–7.
[61] Acar C, Dincer I, Naterer GF. Review of photocatalytic water-splitting methods for sustainable hydrogen production. Int J Energy Res 2016;40(11):1449–73.
[62] Das S, parida K. Superior photocatalytic performance of CoAl LDH in the race of metal incorporated LDH: a comparison study. Mater Today: Proceedings 2021;35:275–80.
[63] Chen C, Zeng H, Xiong J, Xu S, An D. Z-scheme AgBr@Ag/CoAl layered double hydroxide heterojunction for superior photocatalytic Cr(VI) reduction under visible light. Appl Clay Sci 2020;192.
[64] Zhu Y, Zhu R, Zhu G, Wang M, Chen Y, Zhu J, Xi Y, He H. Plasmonic Ag coated Zn/Ti-LDH with excellent photocatalytic activity. Appl Surf Sci 2018;433:458–67.
[65] Xu Q, Zhang L, Cheng B, Fan J, Yu J. S-scheme heterojunction photocatalyst. Inside Chem 2020;6(7):1543–59.
[66] Meng F, Qin Y, Lu J, Lin X, Meng M, Sun G, Yan Y. Biomimetic design and synthesis of visible-light-driven g-C_3N_4 nanotube @polydopamine/NiCo-layered double hydroxides composite photocatalysts for improved photocatalytic hydrogen evolution activity. J Colloid Interface Sci 2021;584:464–73.
[67] Jia Y, Li S, Gao J, Zhu G, Zhang F, Shi X, Huang Y, Liu C. Highly efficient (BiO)2CO3-BiO2-x-graphene photocatalysts: Z-Scheme photocatalytic mechanism for their enhanced photocatalytic removal of NO. Appl Catal B 2019;240:241–52.
[68] Palanivel B, Mani A. Conversion of a type-II to a Z-scheme heterojunction by intercalation of a 0D electron mediator between the integrative $NiFe_2O_4$/g-C_3N_4 composite nanoparticles: boosting the radical production for photo-fenton degradation. ACS Omega 2020;5(31):19747–59.
[69] Li X, Zhang J, Zhang S, Xu S, Wu X, Chang J, He Z. Hexagonal boron nitride composite photocatalysts for hydrogen production. J Alloys Compd 2020:158153–65.
[70] Guo X, Peng Y, Liu G, Xie G, Guo Y, Zhang Y, Yu J. An efficient $ZnIn_2S_4$@$CuInS_2$ core–shell p–n heterojunction to boost visible-light photocatalytic hydrogen evolution. J Phys Chem C 2020;124(11):5934–43.
[71] Mohapatra L, Parida K. A review of solar and visible light active oxo-bridged materials for energy and environment. Catal Sci Technol 2017;7(11):2153–64.
[72] Zhao Y, Jia X, Waterhouse GIN, Wu L-Z, Tung C-H, O'Hare D, Zhang T. Layered double hydroxide nanostructured photocatalysts for renewable energy production. Adv Energy Mater 2016;6(6):1501974.
[73] Low J, Yu J, Jaroniec M, Wageh S, Al-Ghamdi AA. Heterojunction photocatalysts. Adv Mater 2017;29(20):1601694.
[74] Vinodgopal K, Kamat PV. Enhanced rates of photocatalytic degradation of an azo dye using SnOfiiO_2 coupled semiconductor thin films. Environ Sci Technol 1995;29:841–5.
[75] Huang D, Yan X, Yan M, Zeng G, Zhou C, Wan J, Cheng M, Xue W. Graphitic carbon nitride-based heterojunction photoactive nanocomposites: applications and mechanism insight. ACS Appl Mater Interfaces 2018;10(25):21035–55.
[76] Tahir M, Tasleem S, Tahir B. Recent development in band engineering of binary semiconductor materials for solar driven photocatalytic hydrogen production. Int J Hydrogen Energy 2020;45(32):15985–6038.
[77] Tasleem Sehar, Tahir Muhammad, Khalifa WA. Current trends in structural development and modification strategies for metal-organic frameworks (MOFs) towards photocatalytic H_2 production: a review. Int J Hydrogen Energy 2021;46:14148–89.
[78] Tasleem S, Tahir M. Recent progress in structural development and band engineering of perovskites materials for photocatalytic solar hydrogen production: a review. Int J Hydrogen Energy 2020;45(38):19078–111.
[79] San Martín S, Rivero MJ, Ortiz I. Unravelling the mechanisms that drive the performance of photocatalytic hydrogen production. Catalysts 2020;10(8).
[80] Kumar S, Yadav N, Kumar P, Ganguli AK. Design and comparative studies of Z-scheme and type II based heterostructures of $NaNbO_3$/CuInS2/in_2S_3 for efficient photoelectrochemical applications. Inorg Chem 2018;57(24):15112–22.
[81] Xu Q, Zhang L, Yu J, Wageh S, Al-Ghamdi AA, Jaroniec M. Direct Z-scheme photocatalysts: principles, synthesis, and applications. Mater Today 2018;21(10):1042–63.
[82] Wang Y, Guo S, Xin X, Zhang Y, Wang B, Tang S, Li X. Effective interface contact on the hierarchical 1D/2D CoO/NiCo-LDH heterojunction for boosting photocatalytic hydrogen evolution. Appl Surf Sci 2021:149108.
[83] Guo X, Fan Z, Wang Y, Jin Z. CeO_2 nanoparticles dispersed on CoAl-LDH hexagonal nanosheets as 0D/2D binary composite for enhanced photocatalytic hydrogen evolution. Surf. Interfaces 2021;24:101105.
[84] Wang Y, Hao X, Wang G, Jin Z. Rational design of a core–shell-shaped flowerlike $Mn_{0.05}Cd_{0.95}S$@NiAl-LDH structure for efficient hydrogen evolution. Catal Lett 2020;151(3):634–47.
[85] Zhang J, Zhu Q, Wang L, Nasir M, Cho S-H, Zhang J. g-C_3N_4/CoAl-LDH 2D/2D hybrid heterojunction for boosting photocatalytic hydrogen evolution. Int J Hydrogen Energy 2020;45(41):21331–40.
[86] Li H, Hao X, Liu Y, Li Y, Jin Z. $Zn_xCd_{1-x}S$ nanoparticles dispersed on CoAl-layered double hydroxide in 2D heterostructure for enhanced photocatalytic hydrogen evolution. J Colloid Interface Sci 2020;572:62–73. 2020.
[87] Chen J, Wang C, Zhang Y, Guo Z, Luo Y, Mao C-J. Engineering ultrafine NiS cocatalysts as active sites to boost photocatalytic hydrogen production of MgAl layered double hydroxide. Appl Surf Sci 2020;506:144999.
[88] Li Y, Wang G, Wang Y, Jin Z. Phosphating 2D CoAl LDH anchored on 3D self-assembled $NiTiO_3$ hollow rods for efficient hydrogen evolution. Catal Sci Technol 2020;10(9):2931–47.
[89] Gil JJ, Aguilar-Martínez O, Piña-Pérez Y, Pérez-Hernández R, Santolalla-Vargas CE, Gómez R, Tzompantzi F. Efficient

ZnS–ZnO/ZnAl-LDH composite for H_2 production by photocatalysis. Renew Energy 2020;145:124–32.
[90] Megala S, Sathish M, Harish S, Navaneethan M, Sohila S, Liang B, Ramesh R. Enhancement of photocatalytic H_2 evolution from water splitting by construction of two dimensional gC_3N_4/NiAl layered double hydroxides. Appl Surf Sci 2020;509:144656.
[91] Li S, Wang L, Li Y, Zhang L, Wang A, Xiao N, Gao Y, Li N, Song W, Ge L, Liu J. Novel photocatalyst incorporating Ni-Co layered double hydroxides with Pdoped CdS for enhancing photocatalytic activity towards hydrogen evolution. Appl Catal B 2019;254:145–55. 2019.
[92] Sun D, Chi D, Yang Z, Xing Z, Yin J, Li Z, Zhu Q, Zhou W. Mesoporous g-C_3N_4/Zn–Ti LDH laminated van der Waals heterojunction nanosheets as remarkable visible-light-driven photocatalysts. Int J Hydrogen Energy 2019;44(31):16348–58.
[93] Zhou H, Song Y, Liu Y, Li H, Li W, Chang Z. Fabrication of CdS/Ni Fe LDH heterostructure for improved photocatalytic hydrogen evolution from aqueous methanol solution. Int J Hydrogen Energy 2018;43(31):14328–36.
[94] Nayak S, Mohapatra L, Parida K. Visible light-driven novel g-C_3N_4/NiFe-LDH composite photocatalyst with enhanced photocatalytic activity towards water oxidation and reduction reaction. J Mater Chem A 2015;3(36):18622–35.
[95] Zhang G, Lin B, Yang W, Jiang S, Yao Q, Chen Y, Gao B. Highly efficient photocatalytic hydrogen generation by incorporating CdS into ZnCr-layered double hydroxide interlayer. RSC Adv 2015;5(8):5823–9.
[96] Yao L, Wei D, Yan D, Hu C. ZnCr layered double hydroxide (LDH) nanosheets assisted formation of hierarchical flower-like CdZnS@LDH microstructures with improved visible-light-driven H_2 production. Chem Asian J 2015;10(3):630–8.
[97] Zhang G, Lin B, Qiu Y, He L, Chen Y, Gao B. Highly efficient visible-light-driven photocatalytic hydrogen generation by immobilizing CdSe nanocrystals on ZnCr-layered double hydroxide nanosheets. Int J Hydrogen Energy 2015;40(14):4758–65.
[98] Megala S, Ravi P, Maadeswaran P, Navaneethan M, Sathish M, Ramesh R. The construction of a dual direct Z-scheme NiAl LDH/g-C_3N_4/Ag_3PO_4 nanocomposite for enhanced photocatalytic oxygen and hydrogen evolution. Nanoscale Adv 2021;3(7):2075–88.
[99] Sahoo DP, Patnaik S, Parida K. Construction of a Z-scheme dictated WO_{3-X}/Ag/ZnCr LDH synergistically visible light-induced photocatalyst towards tetracycline degradation and H_2 evolution. ACS Omega 2019;4(12):14721–41.
[100] Nayak S, Swain G, Parida K. Enhanced photocatalytic activities of RhB degradation and H_2 evolution from in situ formation of the electrostatic heterostructure MoS_2/NiFe LDH nanocomposite through the Z-scheme mechanism via p-n heterojunctions. ACS Appl Mater Interfaces 2019;11(23):20923–42.
[101] Jin Z, Li Y, Ma Q. CoAl LDH@Ni-MOF-74 S-scheme heterojunction for efficient hydrogen evolution. Transactions of Tianjin University; 2020.
[102] Yang M, Wang K, Li Y, Yang K, Jin Z. Pristine hexagonal CdS assembled with NiV LDH nanosheet formed p-n heterojunction for efficient photocatalytic hydrogen evolution. Appl Surf Sci 2021:149212.
[103] He J-Y, Zhang D, Wang X-J, Zhao J, Li Y-P, Liu Y, Li F-T. Phosphorylation of NiAl-layered double hydroxide nanosheets as a novel cocatalyst for photocatalytic hydrogen evolution. Int J Hydrogen Energy 2021;46(36):18977–87.
[104] Das S, Patnaik S, Parida KM. Fabrication of a Au-loaded $CaFe_2O_4$/CoAl LDH p–n junction based architecture with stoichiometric H_2 & O_2 generation and Cr(vi) reduction under visible light. Inorg Chem Front 2019;6(1):94–109.
[105] Sahoo DP, Nayak S, Reddy KH, Martha S, Parida K. Fabrication of a $Co(OH)_2$/ZnCr LDH "p-n" heterojunction photocatalyst with enhanced separation of charge carriers for efficient visible-light-driven H_2 and O_2 evolution. Inorg Chem 2018;57(7):3840–54.
[106] Zhou H, Qu Y, Zeid T, Duan X. Towards highly efficient photocatalysts using semiconductor nanoarchitectures. Energy Environ Sci 2012;5(5):6732.
[107] Zhu Y, Wan T, Wen X, Chu D, Jiang Y. Tunable Type I and II heterojunction of CoO_x nanoparticles confined in g-C_3N_4 nanotubes for photocatalytic hydrogen production. Appl Catal B 2019;244:814–22.
[108] Muhmood T, Xia M, Lei W, Wang F. Under vacuum synthesis of type-I heterojunction between red phosphorus and graphene like carbon nitride with enhanced catalytic, electrochemical and charge separation ability for photodegradation of an acute toxicity category-III compound. Appl Catal B 2018;238:568–75.
[109] Xiao M, Luo B, Wang S, Wang L. Solar energy conversion on g-C_3N_4 photocatalyst: light harvesting, charge separation, and surface kinetics. J Energy Chem 2018;27(4):1111–23.
[110] Gao F, Lei R, Huang X, Yuan J, Jiang C, Feng W, Zhang L, Liu P. In situ etching growth of defective ZnS nanosheets anchored vertically on layered-double-hydroxide microflowers for accelerated photocatalytic activity. Appl Catal B 2021;292:120187–99.
[111] Yu K, Huang HB, Zeng XY, Xu JY, Yu XT, Liu HX, Cao HL, Lu J, Cao R. CdZnS nanorods with rich sulphur vacancies for highly efficient photocatalytic hydrogen production. Chem Commun 2020;56(56):7765–8.
[112] Wang H, Zhang L, Chen Z, Hu J, Li S, Wang Z, Liu J, Wang X. Semiconductor heterojunction photocatalysts: design, construction, and photocatalytic performances. Chem Soc Rev 2014;43(15):5234–44.
[113] Moniz SJA, Shevlin SA, Martin DJ, Guo Z-X, Tang J. Visible-light driven heterojunction photocatalysts for water splitting – a critical review. Energy Environ Sci 2015;8(3):731–59.
[114] Baliarsingh N, Parida KM, Pradhan GC. Effects of Co, Ni, Cu, and Zn on photophysical and photocatalytic properties of carbonate intercalated MII/Cr LDHs for enhanced photodegradation of methyl orange. Ind Eng Chem Res 2014;53(10):3834–41.
[115] Lu Y, Lin Y, Wang D, Wang L, Xie T, Jiang T. A high performance cobalt-doped ZnO visible light photocatalyst and its photogenerated charge transfer properties. Nano Res 2011;4(11):1144–52.
[116] Sun K, Shen J, Liu Q, Tang H, Zhang M, Zulfiqar S, Lei C. Synergistic effect of Co(II)-hole and Pt-electron cocatalysts for enhanced photocatalytic hydrogen evolution performance of P-doped g-C_3N_4. Chin J Catal 2020;41(1):72–81.
[117] Wang S, Huang Z, Li R, Zheng X, Lu F, He T. Template-assisted synthesis of NiP@CoAl-LDH nanotube arrays with superior electrochemical performance for supercapacitors. Electrochim Acta 2016;204:160–8.
[118] Cen W, Xiong T, Tang C, Yuan S, Dong F. Effects of morphology and crystallinity on the photocatalytic activity of $(BiO)_2CO_3$Nano/microstructures. Ind Eng Chem Res 2014;53(39):15002–11.
[119] Liang J, Wei Y, Yao Y, Zheng X, Shen J, He G, Chen H. Constructing high-efficiency photocatalyst for degrading ciprofloxacin: three-dimensional visible light driven graphene based NiAlFe LDH. J Colloid Interface Sci 2019;540:237–46.

[120] Miao MY, Feng JT, Jin Q, He YF, Liu YN, Du YY, Zhang N, Li DQ. Hybrid Ni–Al layered double hydroxide/graphene composite supported gold nanoparticles for aerobic selective oxidation of benzyl alcohol. RSC Adv 2015;5(45):36066–74.
[121] Xu Y, Xu R. Nickel-based cocatalysts for photocatalytic hydrogen production. Appl Surf Sci 2015;351:779–93.
[122] Harrison S, Hayne M. Photoelectrolysis using type-II semiconductor heterojunctions. Sci Rep 2017;7(1):11638.
[123] Wang Y, Wang Q, Zhan X, Wang F, Safdar M, He J. Visible light driven type II heterostructures and their enhanced photocatalysis properties: a review. Nanoscale 2013;5(18):8326–39.
[124] Khan R, Mehran MT, Baig MM, Sarfraz B, Naqvi SR, Niazi MBK, Khan MZ, Khoja AH. 3D hierarchical heterostructured LSTN@NiMn-layered double hydroxide as a bifunctional water splitting electrocatalyst for hydrogen production. Fuel 2021;285.
[125] Baliarsingh N, Mohapatra L, Parida K. Design and development of a visible light harvesting Ni–Zn/Cr–CO_3^{2-} LDH system for hydrogen evolution. J Mater Chem A 2013;1(13).
[126] Zhao Y, Chen P, Zhang B, Su DS, Zhang S, Tian L, Lu J, Li Z, Cao X, Wang B, Wei M, Evans DG, Duan X. Highly dispersed TiO_6 units in a layered double hydroxide for water splitting. Chemistry 2012;18(38):11949–58.
[127] Ning X, Li J, Yang B, Zhen W, Li Z, Tian B, Lu G. Inhibition of photocorrosion of CdS via assembling with thin film TiO_2 and removing formed oxygen by artificial gill for visible light overall water splitting. Appl Catal B 2017;212:129–39.
[128] Miao Y-f, Guo R-t, Gu J-w, Liu Y-z, Wu G-l, Duan C-p, Zhang X-d, Pan W-g. Fabrication of β-In_2S_3/NiAl-LDH heterojunction photocatalyst with enhanced separation of charge carriers for efficient CO_2 photocatalytic reduction. Appl Surf Sci 2020;527:146792.
[129] Mancipe S, Tzompantzi F, Gómez R. Synthesis of CdS/MgAl layered double hydroxides for hydrogen production from methanol-water decomposition. Appl Clay Sci 2017;136:67–74.
[130] Ju P, Wang P, Li B, Fan H, Ai S, Zhang D, Wang Y. A novel calcined Bi_2WO_6/$BiVO_4$ heterojunction photocatalyst with highly enhanced photocatalytic activity. Chem Eng J 2014;236:430–7.
[131] Jiang D, Chen L, Zhu J, Chen M, Shi W, Xie J. Novel p-n heterojunction photocatalyst constructed by porous graphite-like C_3N_4 and nanostructured BiOI: facile synthesis and enhanced photocatalytic activity. Dalton Trans 2013;42(44):15726–34.
[132] Ge M, Cao C, Li S, Zhang S, Deng S, Huang J, Li Q, Zhang K, Al-Deyab SS, Lai Y. Enhanced photocatalytic performances of n-TiO_2 nanotubes by uniform creation of p-n heterojunctions with p-Bi_2O_3 quantum dots. Nanoscale 2015;7(27):11552–60.
[133] Guo Y, Li J, Gao Z, Zhu X, Liu Y, Wei Z, Zhao W, Sun C. A simple and effective method for fabricating novel p–n heterojunction photocatalyst g-C_3N_4/$Bi_4Ti_3O_{12}$ and its photocatalytic performances. Appl Catal B 2016;192:57–71.
[134] Yu J, Wang W, Cheng B. Synthesis and enhanced photocatalytic activity of a hierarchical porous flowerlike p-n junction NiO/TiO_2 photocatalyst. Chem Asian J 2010;5(12):2499–506.
[135] Li L, Xu J, Zhao S, Mao M, Li X. Construction of p-n type heterojunction for effective photo-generated electron separation and visible light hydrogen evolution. Int J Hydrogen Energy 2021;46(2):1934–44.
[136] Wang L, Ge J, Wang A, Deng M, Wang X, Bai S, Li R, Jiang J, Zhang Q, Luo Y, Xiong Y. Designing p-type semiconductor-metal hybrid structures for improved photocatalysis. Angew Chem Int Ed Engl 2014;53(20):5107–11.
[137] Toe CY, Scott J, Amal R, Ng YH. Recent advances in suppressing the photocorrosion of cuprous oxide for photocatalytic and photoelectrochemical energy conversion. J Photochem Photobiol, C 2019;40:191–211.
[138] Weng B, Qi M-Y, Han C, Tang Z-R, Xu Y-J. Photocorrosion inhibition of semiconductor-based photocatalysts: basic principle, current development, and future perspective. ACS Catal 2019;9(5):4642–87.
[139] Varma R, Yadav M, Tiwari K, Makani N, Gupta S, Kothari DC, Miotello A, Patel N. Roles of vanadium and nitrogen in photocatalytic activity of VN-codoped TiO_2 photocatalyst. Photochem Photobiol 2018;94(5):955–64.
[140] Zhou P, Yu J, Jaroniec M. All-solid-state Z-scheme photocatalytic systems. Adv Mater 2014;26(29):4920–35.
[141] Li H, Tu W, Zhou Y, Zou Z. Z-scheme photocatalytic systems for promoting photocatalytic performance: recent progress and future challenges. Adv Sci (Weinh) 2016;3(11):1500389.
[142] Zhou M, Yang J, Wang H, Jin T, Hassett DJ, Gu T. Bioelectrochemistry of microbial fuel cells and their potential applications in bioenergy. Bioenergy Res: Adv and Appl 2014:131–52.
[143] Kochuveedu ST, Jang YH, Kim DH. A study on the mechanism for the interaction of light with noble metal-metal oxide semiconductor nanostructures for various photophysical applications. Chem Soc Rev 2013;42(21):8467–93.
[144] Wang W, Wang X, Gan L, Ji X, Wu Z, Zhang R. All-solid-state Z-scheme BiVO4–$Bi_6O_6(OH)_3(NO_3)_3$ heterostructure with prolonging electron-hole lifetime for enhanced photocatalytic hydrogen and oxygen evolution. J Mater Sci Technol 2021;77:117–25.
[145] Grätzel M. Photoelectrochemical cells. Nature 2001;414:338–44.
[146] Lv B, Feng X, Lu L, Xia L, Yang Y, Wang X, Zou X, Wang H, Zhang F. Facile synthesis of g-C_3N_4/TiO_2/CQDs/Au Z-scheme heterojunction composites for solar-driven efficient photocatalytic hydrogen. Diam Relat Mater 2021;111.
[147] Wang R, Ye C, Wang H, Jiang F. Z-scheme $LaCoO_3$/g-C_3N_4 for efficient full-spectrum light-simulated solar photocatalytic hydrogen generation. ACS Omega 2020;5(47):30373–82.
[148] Li X, Yu Z, Shao L, Zeng H, Liu Y, Feng X. A novel strategy to construct a visible-light-driven Z-scheme (ZnAl-LDH with active phase/g-C_3N_4) heterojunction catalyst via polydopamine bridge (a similar "bridge" structure). J Hazard Mater 2020;386:121650.
[149] Huang L, Chu S, Wang J, Kong F, Luo L, Wang Y, Zou Z. Novel visible light driven Mg–Zn–In ternary layered materials for photocatalytic degradation of methylene blue. Catal Today 2013;212:81–8.
[150] Bharali D, Devi R, Bharali P, Deka RC. Synthesis of high surface area mixed metal oxide from the NiMgAl LDH precursor for nitro-aldol condensation reaction. New J Chem 2015;39(1):172–8.
[151] Cosano D, Esquivel D, Romero-Salguero FJ, Jiménez-Sanchidrián C, Ruiz JR. Use of Raman spectroscopy to assess nitrate uptake by calcined LDH phases. Colloids Surf. A Physicochem. Eng. Asp. 2020;602:125066.
[152] Li C, Zhao G, Zhang T, Yan T, Zhang C, Wang L, Liu L, Zhou S, Jiao F. A novel Ag@TiON/CoAl-layered double hydroxide photocatalyst with enhanced catalytic memory activity for removal of organic pollutants and Cr(VI). Appl Surf Sci 2020;504:144352.

[153] Li J-J, Zhang M, Weng B, Chen X, Chen J, Jia H-P. Oxygen vacancies mediated charge separation and collection in Pt/WO_3 nanosheets for enhanced photocatalytic performance. Appl Surf Sci 2020;507:145133.
[154] Gunjakar JL, Kim TW, Kim HN, Kim IY, Hwang SJ. Mesoporous layer-by-layer ordered nanohybrids of layered double hydroxide and layered metal oxide: highly active visible light photocatalysts with improved chemical stability. J Am Chem Soc 2011;133(38):14998–5007.
[155] Parida K, Mohapatra L. Recent progress in the development of carbonate-intercalated Zn/Cr LDH as a novel photocatalyst for hydrogen evolution aimed at the utilization of solar light. Dalton Trans 2012;41(4):1173–8.
[156] Ameur SB, Barhoumi A, Bel hadjltaief H, Mimouni R, Duponchel B, Leroy G, Amlouk M, Guermazi H. Physical investigations on undoped and Fluorine doped SnO_2 nanofilms on flexible substrate along with wettability and photocatalytic activity tests. Mater Sci Semicond Process 2017;61:17–26.
[157] Fu J, Xu Q, Low J, Jiang C, Yu J. Ultrathin 2D/2D WO_3/g-C_3N_4 step-scheme H_2-production photocatalyst. Appl Catal B 2019;243:556–65.
[158] Wang J, Zhang Q, Deng F, Luo X, Dionysiou DD. Rapid toxicity elimination of organic pollutants by the photocatalysis of environment-friendly and magnetically recoverable step-scheme $SnFe_2O_4$/$ZnFe_2O_4$ nano-heterojunctions. Chem Eng J 2020;379.
[159] Jia X, Han Q, Zheng M, Bi H. One pot milling route to fabricate step-scheme AgI/I-BiOAc photocatalyst: energy band structure optimized by the formation of solid solution. Appl Surf Sci 2019;489:409–19.
[160] He F, Meng A, Cheng B, Ho W, Yu J. Enhanced photocatalytic H_2-production activity of WO_3/TiO_2 step-scheme heterojunction by graphene modification. Chin J Catal 2020;41(1):9–20.
[161] Fan H, Zhou H, Li W, Gu S, Zhou G. Facile fabrication of 2D/2D step-scheme In_2S_3/$Bi_2O_2CO_3$ heterojunction towards enhanced photocatalytic activity. Appl Surf Sci 2020;504.
[162] Wang Y, Zhang Z, Zhang L, Luo Z, Shen J, Lin H, Long J, Wu JCS, Fu X, Wang X, Li C. Visible-light driven overall conversion of CO_2 and H_2O to CH_4 and O_2 on 3D-SiC@2D-MoS_2 heterostructure. J Am Chem Soc 2018;140(44):14595–8.
[163] Yang H, Chen Z, Guo P, Fei B, Wu R. B-doping-induced amorphization of LDH for large-current-density hydrogen evolution reaction. Appl Catal B 2020;261.
[164] Jeghan SMN, Kim N, Lee G. Mo-incorporated three-dimensional hierarchical ternary nickel-cobalt-molybdenum layer double hydroxide for high-efficiency water splitting. Int J Hydrogen Energy 2021;46(43):22463–77.
[165] Yao Z, Sun H, Sui H, Liu X. 2D/2D heterojunction of R-scheme Ti_3C_2 MXene/MoS_2 nanosheets for enhanced photocatalytic performance. Nanoscale Res. Lett. 2020;15(1):78.
[166] Tahir M, Siraj M, Tahir B, Umer M, Alias H, Othman N. Au-NPs embedded Z–scheme WO_3/TiO_2 nanocomposite for plasmon-assisted photocatalytic glycerol-water reforming towards enhanced H_2 evolution. Appl Surf Sci 2020;503:144344.
[167] Tahir B, Er PW, Tahir M, Nawawi MGM, Siraj M, Alias H, Fatehmulla A. Tailoring metal/support interaction in 0D TiO_2 NPs/MPs embedded 2D MAX composite with boosted interfacial charge carrier separation for stimulating photocatalytic H_2 production. J Environ Chem Eng 2020;8(6):104529.
[168] Fajrina N, Tahir M. Engineering approach in stimulating photocatalytic H_2 production in a slurry and monolithic photoreactor systems using Ag-bridged Z-scheme pCN/TiO_2 nanocomposite. Chem Eng J 2019;374:1076–95.
[169] Fajrina N, Tahir M. A critical review in strategies to improve photocatalytic water splitting towards hydrogen production. Int J Hydrogen Energy 2019;44(2):540–77.
[170] Wen Y, Ding H, Shan Y. Preparation and visible light photocatalytic activity of Ag/TiO_2/graphene nanocomposite. Nanoscale 2011;3(10):4411–7.
[171] Singh N, Prakash J, Gupta RK. Design and engineering of high-performance photocatalytic systems based on metal oxide–graphene–noble metal nanocomposites. Mol Syst Des Eng 2017;2(4):422–39.
[172] Prakash J, Kumar V, Kroon RE, Asokan K, Rigato V, Chae KH, Gautam S, Swart HC. Optical and surface enhanced Raman scattering properties of Au nanoparticles embedded in and located on a carbonaceous matrix. Phys Chem Chem Phys 2016;18(4):2468–80.
[173] Tung RT. Recent advances in Schottky barrier concepts. Mater Sci Eng R Rep 2001;35:1–138.
[174] Huang Z, Miseki Y, Sayama K. Solar-light-driven photocatalytic production of peroxydisulfate over noble-metal loaded WO_3. Chem Commun 2019;55(26):3813–6.
[175] Wang Z, Liu J, Chen W. Plasmonic Ag/AgBr nanohybrid: synergistic effect of SPR with photographic sensitivity for enhanced photocatalytic activity and stability. Dalton Trans 2012;41(16):4866–70.
[176] Zhang X, Chen YL, Liu RS, Tsai DP. Plasmonic photocatalysis. Rep Prog Phys 2013;76(4):046401.
[177] Li S, Cai J, Wu X, Zheng F. Sandwich-like TiO_2@ZnO-based noble metal (Ag, Au, Pt, or Pd) for better photo-oxidation performance: synergistic effect between noble metal and metal oxide phases. Appl Surf Sci 2018;443:603–12.
[178] Tonda S, Jo W-K. Plasmonic Ag nanoparticles decorated NiAl-layered double hydroxide/graphitic carbon nitride nanocomposites for efficient visible-light-driven photocatalytic removal of aqueous organic pollutants. Catal Today 2018;315:213–22.
[179] Wang T, Liu X, Ma C, Liu Y, Dong H, Ma W, Liu Z, Wei M, Li C, Yan Y. 3D Ag/NiCo-layered double hydroxide with adsorptive and photocatalytic performance. J Taiwan Inst Chem Eng 2018;93:298–305.
[180] Zhu P, Gao M, Zhang J, Wu Z, Wang R, Wang Y, Waclawik ER, Zheng Z. Synergistic interaction between Ru and MgAl-LDH support for efficient hydrogen transfer reduction of carbonyl compounds under visible light. Appl Catal B 2021;283.
[181] Carja G, Birsanu M, Okada K, Garcia H. Composite plasmonic gold/layered double hydroxides and derived mixed oxides as novel photocatalysts for hydrogen generation under solar irradiation. J Mater Chem A 2013;1(32).
[182] Wang Y, Jiang C, Le Y, Cheng B, Yu J. Hierarchical honeycomb-like Pt/NiFe-LDH/rGO nanocomposite with excellent formaldehyde decomposition activity. Chem Eng J 2019;365:378–88.
[183] Löffler T, Meyer H, Savan A, Wilde P, Garzón Manjón A, Chen Y-T, Ventosa E, Scheu C, Ludwig A, Schuhmann W. Discovery of a multinary noble metal-free oxygen reduction catalyst. Adv Energy Mater 2018;8(34).
[184] Cheng L, Chen Q, Li J, Liu H. Boosting the photocatalytic activity of $CdLa_2S_4$ for hydrogen production using Ti_3C_2 MXene as a co-catalyst. Appl Catal B 2020;267:118379.
[185] Tahir M. Investigating the influential effect of etchant time in constructing 2D/2D HCN/MXene heterojunction with controlled growth of TiO_2 NPs for stimulating photocatalytic H_2 production. Energy Fuels 2021;35(8):6807–22.
[186] Morales-Mendoza G, Tzompantzi F, García-Mendoza C, López R, De la Luz V, Lee S-W, Kim T-H, Torres-Martínez LM, Gómez R. Mn-doped Zn/Al layered double

hydroxides as photocatalysts for the 4-chlorophenol photodegradation. Appl Clay Sci 2015;118:38–47.
[187] Fan WK, Tahir M. Recent trends in developments of active metals and heterogenous materials for catalytic CO_2 hydrogenation to renewable methane: a review. J Environ Chem Eng 2021;9(4):105460.
[188] Fang X, Cui L, Pu T, Song J, Zhang X. Core-shell CdS@MnS nanorods as highly efficient photocatalysts for visible light driven hydrogen evolution. App Surf Sci 2018;457:863–9.
[189] Sadollahkhani A, Nur O, Willander M, Kazeminezhad I, Khranovskyy V, Eriksson MO, Yakimova R, Holtz P-O. A detailed optical investigation of ZnO@ZnS core–shell nanoparticles and their photocatalytic activity at different pH values. Ceram Int 2015;41(5):7174–84.
[190] Tunc I, Bruns M, Gliemann H, Grunze M, Koelsch P. Band gap determination and charge separation in Ag@TiO_2 core shell nanoparticle films. Surf Interface Anal 2010;42(6–7):835–41.
[191] Mondal K, Moitra P. Metal-semiconductor core–shell nanostructured photocatalysts for environmental applications and their recycling process. Metal Semicond Core-Shell Nanostruct Energy and Environ Appl 2017:133–57.
[192] Zhang N, Liu S, Xu YJ. Recent progress on metal core@semiconductor shell nanocomposites as a promising type of photocatalyst. Nanoscale 2012;4(7):2227–38.
[193] Thatai S, Khurana P, Boken J, Prasad S, Kumar D. Nanoparticles and core–shell nanocomposite based new generation water remediation materials and analytical techniques: a review. Micro 2014;116:62–76.
[194] Zhang J, Wang Y, Jin J, Zhang J, Lin Z, Huang F, Yu J. Efficient visible-light photocatalytic hydrogen evolution and enhanced photostability of core/shell CdS/g-C_3N_4 nanowires. ACS Appl Mater Interfaces 2013;5(20):10317–24.
[195] Ghosh Chaudhuri R, Paria S. Core/shell nanoparticles: classes, properties, synthesis mechanisms, characterization, and applications. Chem Rev 2012;112(4):2373–433.
[196] Xie X, Wang S, Zhang Y, Ding J, Liu Y, Yan Q, Lu S, Li B, Liu Y, Cai Q. Facile construction for new core-shell Z-scheme photocatalyst GO/AgI/Bi_2O_3 with enhanced visible-light photocatalytic activity. J Colloid Interface Sci 2021;581(Pt A):148–58.
[197] Ran Q, Yu Z, Jiang R, Hou Y, Huang J, Zhu H, Yang F, Li M, Li F, Sun Q. A novel, noble-metal-free core-shell structure Ni–P@C cocatalyst modified sulfur vacancy-rich $ZnIn_2S_4$ 2D ultrathin sheets for visible light-driven photocatalytic hydrogen evolution. J Alloys Compd 2021;855:157333.
[198] Wang K, Xing Z, Meng D, Zhang S, Li Z, Pan K, Zhou W. Hollow $MoSe_2$@Bi_2S_3/CdS core-shell nanostructure as dual Z-scheme heterojunctions with enhanced full spectrum photocatalytic-photothermal performance. Appl Catal B 2021;281:119482.
[199] An H, Lv Z, Zhang K, Deng C, Wang H, Xu Z, Wang M, Yin Z. Plasmonic coupling enhancement of core-shell Au@Pt assemblies on $ZnIn_2S_4$ nanosheets towards photocatalytic H_2 production. Appl Surf Sci 2021;536:147934.
[200] Mondal K, Sharma A. Recent advances in the synthesis and application of photocatalytic metal–metal oxide core–shell nanoparticles for environmental remediation and their recycling process. RSC Adv 2016;6(87):83589–612.
[201] Kim S, Fisher B, Eisler H-Jr, Bawendi M. Type-II quantum dots: CdTe/CdSe(Core/Shell) and CdSe/ZnTe(Core/Shell) heterostructures. J Am Chem Soc 2003;125:11466–7.
[202] Han L, Wei H, Tu B, Zhao D. A facile one-pot synthesis of uniform core-shell silver nanoparticle@mesoporous silica nanospheres. Chem Commun 2011;47(30):8536–8.
[203] Das S, Perez-Ramirez J, Gong J, Dewangan N, Hidajat K, Gates BC, Kawi S. Core-shell structured catalysts for thermocatalytic, photocatalytic, and electrocatalytic conversion of CO_2. Chem Soc Rev 2020;49(10):2937–3004.
[204] Khanchandani S, Kundu S, Patra A, Ganguli AK. Shell thickness dependent photocatalytic properties of ZnO/CdS core–shell nanorods. J Phys Chem C 2012;116(44):23653–62.
[205] Niu B, Xu Z. A stable Ta3N5@PANI core-shell photocatalyst: shell thickness effect, high-efficient photocatalytic performance and enhanced mechanism. J Catal 2019;371:175–84.
[206] Guo Q, Zhang Q, Wang H, Liu Z, Zhao Z. Core-shell structured ZnO@Cu-Zn–Al layered double hydroxides with enhanced photocatalytic efficiency for CO_2 reduction. Catal Commun 2016;77:118–22.
[207] Dou Y, Zhang S, Pan T, Xu S, Zhou A, Pu M, Yan H, Han J, Wei M, Evans DG, Duan X. TiO_2@Layered double hydroxide core-shell nanospheres with largely enhanced photocatalytic activity toward O_2 generation. Adv Funct Mater 2015;25(15):2243–9.
[208] Ziarati A, Badiei A, Grillo R, Burgi T. 3D Yolk@Shell TiO_{2-x}/LDH architecture: tailored structure for visible light CO_2 conversion. ACS Appl Mater Interfaces 2019;11(6):5903–10.
[209] Zhang Y-C, Li Z, Zhang L, Pan L, Zhang X, Wang L, Fazal e A, Zou J-J. Role of oxygen vacancies in photocatalytic water oxidation on ceria oxide: experiment and DFT studies. Appl Catal B 2018;224:101–8.
[210] Li M, Yu Z, Hou Y, Liu Q, Qian L, Lian C, Rao X, Yang X. Charge trapping and transfer mechanisms of noble metals and metal oxides deposited Ga_2O_3 toward typical contaminant degradation. Chem Eng J 2019;370:1119–27.
[211] Li Z, Zhang Q, Liu X, Wu L, Hu H, Zhao Y. One-step mechanochemical synthesis of plasmonic Ag/Zn–Al LDH with excellent photocatalytic activity. J Mater Sci 2018;53(18):12795–806.
[212] Yang C, Zhang G, Meng Y, Pan G, Ni Z, Xia S. Direct Z-scheme CeO_2@LDH core-shell heterostructure for photodegradation of Rhodamine B by synergistic persulfate activation. J Hazard Mater 2020;408:124908.
[213] Maeda K, Domen K. Photocatalytic water splitting: recent progress and future challenges. J Phys Chem Lett 2010;1(18):2655–61.
[214] Yang M, Zhang Z, Wu L, Li P, Jiang W, Men X. Enhancing interfacial and tribological properties of self-lubricating liner composites via Layer-by-Layer self-assembly MgAl-LDH/PAMPA multilayers film on fibers surface. Tribol Int 2019;140:105887.
[215] Guo X, Zhang F, Evans DG, Duan X. Layered double hydroxide films: synthesis, properties and applications. Chem Commun 2010;46(29):5197–210.
[216] Liu Z, Ma R, Osada M, Iyi N, Ebina Y, Takada K, Sasaki T. Synthesis, anion exchange, and delamination of Co-Al layered double hydroxide: assembly of the exfoliated nanosheet/polyanion composite films and magneto-optical studies. J Am Chem Soc 2006;128:4872–80.
[217] Zhang D, Lu J, Shi C, Zhang K, Li J, Gao L. Anti-corrosion performance of covalent layer-by-layer assembled films via click chemistry reaction on the copper surface. Corrosion Sci 2021;178:109063.
[218] Joseph N, Mees MA, Vergaelen M, Valley B, Marien H, Hoogenboom R, Vankelecom IFJ. Layer-by-Layer assembled hydrogen-bonded multilayer poly(2-oxazoline) membranes for aqueous separations. ACS Appl Polym Mater 2020;2(12):5398–405.
[219] Pan L, Liu YT, Zhong M, Xie XM. Coordination-driven hierarchical assembly of hybrid nanostructures based on 2D materials. Small 2020;16(15):1902779.

[220] Lipton J, Weng G-M, Röhr JA, Wang H, Taylor AD. Layer-by-Layer assembly of two-dimensional materials: meticulous control on the nanoscale. Matter 2020;2(5):1148–65.
[221] Nunes BN, Paula LF, Costa ÍA, Machado AEH, Paterno LG, Patrocinio AOT. Layer-by-layer assembled photocatalysts for environmental remediation and solar energy conversion. J Photochem Photobiol, C 2017;32:1–20.
[222] Szekeres M, Széchenyi A, Stépán K, Haraszti T, Dékány I. Layer-by-layer self-assembly preparation of layered double hydroxide/polyelectrolyte nanofilms monitored by surface plasmon resonance spectroscopy. Colloid Polym Sci 2005;283(9):937–45.
[223] Dong X, Zhang Y, Ding B, Hao X, Dou H, Zhang X. Layer-by-layer self-assembled two-dimensional MXene/layered double hydroxide composites as cathode for alkaline hybrid batteries. J Power Sources 2018;390:208–14.